

FLUORESCENT CHEMOSENSORS FOR THE DETECTION  
OF BIOLOGICAL AMINES

---

A Dissertation  
presented to  
the Faculty of the Graduate School  
at the University of Missouri-Columbia

---

In Partial Fulfillment  
of the Requirements for the Degree  
Doctor of Philosophy

---

by  
JESSICA L. KLOCKOW  
Dr. Timothy E. Glass, Dissertation Supervisor

The undersigned, appointed by the dean of the Graduate School, have examined the dissertation entitled

FLUORESCENT CHEMOSENSORS FOR THE DETECTION OF  
BIOLOGICAL AMINES

presented by Jessica L. Klockow,

a candidate for the degree of doctor of philosophy

and hereby certify that, in their opinion, it is worthy of acceptance.

---

Professor Timothy E. Glass

---

Professor Kent S. Gates

---

Professor Michael A. Harmata

---

Professor Kevin D. Gillis

## ACKNOWLEDGEMENTS

There are numerous people that I need to thank for support and guidance throughout my tenure as a graduate student.

Thank you to my group members: Jae Lee, Shaohui Zhang, Chun Ren, Yuksel Alan, Chad Cooley, Xiaole Shao, Patrick Cavins, Nicholas Cooley, Wanjun Zhou, C.W. Littlefield, Kang Han, Tam Tran, and Le Zhang. I appreciate your talents, unfailing humor, and above all, your friendship for the past many years. I wish you only the best in the years to come, whatever they may hold.

Thank you to Drs. Lever, Gates, Harmata, and Gillis for your thoughtful direction in matters of teaching, chemistry, and professional development. You lead by example showing enthusiasm for your craft and compassion for your students. You have inspired me to work hard, do what I love, and pay it forward. Please know how valued you are.

I owe a debt of gratitude to Dr. Tim Glass who mentored me on laboratory techniques, data analysis, academia politics, personal adversities, and more. Thank you for every meeting in which you ignored the ringing phone and for every bout of failure that you met with optimism. Given my professional and personal circumstances, I am very glad to have had you as an adviser.

Most importantly, thank you to my family and to my husband, Ken, for believing in me and encouraging me to push the limits of my abilities. Thank you for motivating during the slumps and celebrating the victories.

## TABLE OF CONTENTS

<b>ACKNOWLEDGEMENTS</b> .....	ii
<b>LIST OF FIGURES</b> .....	vi
<b>LIST OF TABLES</b> .....	xi
<b>ABSTRACT</b> .....	xii
<b>CHAPTER ONE: Introduction</b> .....	1
1.1 Fluorescence Sensing.....	1
1.1.1 Molecular Recognition.....	1
1.1.2 Fluorescence Basics.....	3
1.1.3 Mechanisms of Fluorescence Modulation.....	5
1.2 Detection of Amino Acids.....	11
1.3 Detection of Neurotransmitters.....	14
1.4 Monitoring Exocytosis.....	20
1.4.1 FM Dyes.....	21
1.4.2 SynaptopHluorins.....	22
1.4.3 False Fluorescent Neurotransmitters (FFNs).....	23
<b>CHAPTER TWO: A Fluorescent Chemosensor for Kynurenine</b> .....	26
2.1 Overview.....	26
2.2 Coumarin Dimers .....	28
2.3 Coumarin Monomer .....	30
<b>CHAPTER THREE: Visualizing Exocytosis with Sulfonamide Coumarins</b> .....	36
3.1 Background.....	36
3.2 Molecular Logic Gates.....	37

3.3 NeuroSensors.....	38
3.4 ExoSensors.....	41
3.5 Design of ExoSensors.....	42
3.6 Synthesis of ExoSensors.....	46
3.7 Spectroscopic Results.....	52
3.7.1 pH Titrations.....	52
3.7.2 Analyte Titrations.....	54
3.7.3 Response to Exocytosis.....	58
3.8 Cellular Analysis.....	59
<b>CHAPTER FOUR: Three-Input Molecular Logic Gates for Glutamate &amp; Zinc Corelease.....</b>	<b>63</b>
4.1 Background.....	63
4.2 Previous Work.....	65
4.3 Sensor Design.....	66
4.4 Synthesis.....	67
4.5 Titrations.....	69
<b>APPENDIX: Experimental Procedures and Characterization Data.....</b>	<b>76</b>
Part I. General Information.....	76
Part II. Spectroscopic Studies.....	76
Part III. Binding Constant Determination.....	97
Part IV. $pK_a$ Determination.....	99
Part V. Cellular Analyses.....	100
Part VI. Synthetic Procedures and Characterization Data.....	102

<b>REFERENCES</b> .....	142
<b>VITA</b> .....	150

## LIST OF FIGURES

<b>Figure 1-1:</b> Reversible host-guest interactions.....	1
<b>Figure 1-2:</b> Covalent analyte recognition motifs.....	2
<b>Figure 1-3:</b> Jablonski diagram.....	3
<b>Figure 1-4:</b> Stokes shift.....	4
<b>Figure 1-5:</b> Extrinsic fluorophores.....	5
<b>Figure 1-6:</b> Spectral overlap of FRET pairs.....	6
<b>Figure 1-7:</b> FRET sensor for nucleoside polyphosphates.....	8
<b>Figure 1-8:</b> Acceptor- and donor-excited PET.....	9
<b>Figure 1-9:</b> PET sensor for mercury.....	9
<b>Figure 1-10:</b> Effect of EDGs and EWGs on absorption.....	10
<b>Figure 1-11:</b> ICT BODIPY-based sensor for cadmium.....	11
<b>Figure 1-12:</b> Examples of amino acid detection.....	12
<b>Figure 1-13:</b> Covalent interaction of coumarin aldehydes with amino acids.....	13
<b>Figure 1-14:</b> UV/Vis & fluorescence spectra of sensor <b>1</b> with glycine.....	14
<b>Figure 1-15:</b> Neurotransmitter uptake into synaptic vesicles.....	15
<b>Figure 1-16:</b> Molecular structures of amine neurotransmitters.....	15
<b>Figure 1-17:</b> Detection of dopamine using cyclic voltammetry.....	16
<b>Figure 1-18:</b> GluSnFR biosensor.....	17
<b>Figure 1-19:</b> Snifit biosensor.....	18
<b>Figure 1-20:</b> Chemical sensors for neurotransmitters.....	19
<b>Figure 1-21:</b> Quenching ability of neurotransmitters.....	19
<b>Figure 1-22:</b> Coumarin aldehyde catecholamine sensors.....	20

<b>Figure 1-23:</b> Structure and mechanism of FM dyes.....	21
<b>Figure 1-24:</b> Amino acid sequences for GFP and phluorin.....	22
<b>Figure 1-25:</b> Structures of FFN dyes.....	23
<b>Figure 1-26:</b> Summary of indirect methods for monitor exo- & endocytosis.....	24
***	
<b>Figure 2-1:</b> The kynurenine pathway.....	27
<b>Figure 2-2:</b> Binding of glycine to coumarin aldehydes.....	28
<b>Figure 2-3:</b> Synthesis of O-linked dimers.....	29
<b>Figure 2-4:</b> Synthesis of N-linked dimers.....	30
<b>Figure 2-5:</b> Synthesis of coumarin monomer.....	30
<b>Figure 2-6:</b> UV/vis & fluorescence spectra of sensor <b>14</b> with kynurenine.....	31
<b>Figure 2-7:</b> UV/vis spectra of sensor <b>14</b> with various analytes.....	32
<b>Figure 2-8:</b> UV/vis spectra & regression curve of sensor <b>14</b> pH titration.....	33
<b>Figure 2-9:</b> Competitive binding study of sensor <b>14</b> .....	35
***	
<b>Figure 3-1:</b> Symbols & truth tables for various logic operations.....	38
<b>Figure 3-2:</b> Logic gate and truth table for NeuroSensors.....	39
<b>Figure 3-3:</b> Confocal fluorescence microscopy of NeuroSensor 521.....	40
<b>Figure 3-4:</b> Pictorial representation of selective binding of NeuroSensor 521.....	41
<b>Figure 3-5:</b> Logic gate and truth table for two-input ExoSensors.....	42
<b>Figure 3-6:</b> Sensing mechanism of ExoSensors.....	44
<b>Figure 3-7:</b> Neurotransmitter binding and deprotonation of ExoSensors.....	45
<b>Figure 3-8:</b> Synthesis using carbamate protecting groups.....	46



<b>Figure 3-9:</b> The carbamate-protected coumarin is deactivated.....	47
<b>Figure 3-10:</b> Synthesis using allyl protecting groups.....	47
<b>Figure 3-11:</b> Rearranged products from the Pechmann cyclization.....	48
<b>Figure 3-12:</b> Formylation of the allyl-protected aminocoumarin.....	49
<b>Figure 3-13:</b> Claisen condensation of an aryl sulfonamide.....	50
<b>Figure 3-14:</b> Synthesis by oxidizing to the aldehyde.....	50
<b>Figure 3-15:</b> Synthesis using Buchwald-Hartwig coupling.....	51
<b>Figure 3-16:</b> UV/vis & fluorescence spectra of ES517 pH titration .....	53
<b>Figure 3-17:</b> UV/vis & fluorescence spectra of ES517-glutamate pH titration.....	54
<b>Figure 3-18:</b> UV/vis & fluorescence spectra of ES517 adding glutamate.....	56
<b>Figure 3-19:</b> Fluorescence enhancements of ES517 simulating exocytosis.....	57
<b>Figure 3-20:</b> Relationship between sensor $pK_a$ and fluorescence upon exocytosis.....	59
<b>Figure 3-21:</b> ES517 in live cells.....	61

\*\*\*

<b>Figure 4-1:</b> $Zn^{2+}$ -mediated amyloid- $\beta$ oligomerization.....	64
<b>Figure 4-2:</b> Molecular logic gates for neuronal imaging.....	66
<b>Figure 4-3:</b> Logic gate & truth table for three-input AND gates.....	67
<b>Figure 4-4:</b> Synthesis of hydroxysalicylaldehyde starting material.....	68
<b>Figure 4-5:</b> Second part of synthesis for three-input AND gates.....	69
<b>Figure 4-6:</b> UV/vis & fluorescence spectra of ES470 adding glutamate.....	70
<b>Figure 4-7:</b> UV/vis & fluorescence spectra of ES470-glutamate adding $Zn^{2+}$ .....	71
<b>Figure 4-8:</b> Relative fluorescence intensities & truth table for ES470.....	73

\*\*\*

<b>Figure A-1:</b> UV/vis & fluorescence spectra of compound <b>41</b> adding glutamate.....	77
<b>Figure A-2:</b> UV/vis & fluorescence spectra of compound <b>41</b> adding norepinephrine.....	77
<b>Figure A-3:</b> UV/vis & fluorescence spectra of compound <b>41</b> adding dopamine.....	78
<b>Figure A-4:</b> UV/vis & fluorescence spectra of compound <b>41</b> adding serotonin.....	78
<b>Figure A-5:</b> Fluorescence spectra of ES517 adding GABA.....	79
<b>Figure A-6:</b> Fluorescence spectra of ES517 adding glycine.....	79
<b>Figure A-7:</b> Fluorescence spectra of ES517 adding norepinephrine.....	80
<b>Figure A-8:</b> Fluorescence spectra of ES517 adding dopamine.....	80
<b>Figure A-9:</b> Fluorescence spectra of ES517 adding serotonin.....	81
<b>Figure A-10:</b> UV/vis & fluorescence spectra of compound <b>28</b> adding glutamate.....	81
<b>Figure A-11:</b> UV/vis & fluorescence spectra of compound <b>28</b> adding norepinephrine...	82
<b>Figure A-12:</b> UV/vis & fluorescence spectra of compound <b>28</b> adding dopamine.....	82
<b>Figure A-13:</b> UV/vis & fluorescence spectra of compound <b>28</b> adding serotonin.....	83
<b>Figure A-14:</b> UV/vis & fluorescence spectra of compound <b>43</b> adding glutamate.....	83
<b>Figure A-15:</b> UV/vis & fluorescence spectra of compound <b>43</b> adding norepinephrine...	84
<b>Figure A-16:</b> UV/vis & fluorescence spectra of compound <b>43</b> adding dopamine.....	84
<b>Figure A-17:</b> UV/vis & fluorescence spectra of compound <b>43</b> adding serotonin.....	85
<b>Figure A-18:</b> UV/vis & fluorescence spectra of compound <b>44</b> adding glutamate.....	85
<b>Figure A-19:</b> UV/vis & fluorescence spectra of compound <b>44</b> adding norepinephrine...	86
<b>Figure A-20:</b> UV/vis & fluorescence spectra of compound <b>44</b> adding dopamine.....	86
<b>Figure A-21:</b> UV/vis & fluorescence spectra of compound <b>44</b> adding serotonin.....	87
<b>Figure A-22:</b> UV/vis & fluorescence spectra of compound <b>56a</b> adding glutamate.....	87
<b>Figure A-23:</b> UV/vis & fluorescence spectra of compound <b>56b</b> adding glutamate.....	88

<b>Figure A-24:</b> UV/vis & fluorescence spectra of compound <b>56d</b> adding glutamate.....	88
<b>Figure A-25:</b> Fluorescence spectra of <b>56a</b> -glutamate adding zinc.....	89
<b>Figure A-26:</b> Fluorescence spectra of <b>56b</b> -glutamate adding zinc.....	89
<b>Figure A-27:</b> Fluorescence spectra of <b>56d</b> -glutamate adding zinc.....	90
<b>Figure A-28:</b> Fluorescence spectra of ES470-glutamate adding zinc.....	90
<b>Figure A-29:</b> Fluorescence spectra of ES470 adding glycine.....	91
<b>Figure A-30:</b> Fluorescence spectra of ES470 adding aspartate.....	91
<b>Figure A-31:</b> Fluorescence spectra of ES470 adding GABA.....	92
<b>Figure A-32:</b> Fluorescence spectra of ES470 adding butylamine.....	92
<b>Figure A-33:</b> UV/vis & fluorescence spectra of compound <b>28</b> pH titration.....	93
<b>Figure A-34:</b> UV/vis & fluorescence spectra of compound <b>43</b> pH titration.....	93
<b>Figure A-35:</b> UV/vis & fluorescence spectra of compound <b>44</b> pH titration.....	94
<b>Figure A-36:</b> UV/vis & fluorescence spectra of compound <b>41</b> pH titration.....	94
<b>Figure A-37:</b> UV/vis & fluorescence spectra of compound <b>56a</b> pH titration.....	95
<b>Figure A-38:</b> UV/vis & fluorescence spectra of compound <b>56b</b> pH titration.....	95
<b>Figure A-39:</b> UV/vis & fluorescence spectra of ES470 pH titration.....	96
<b>Figure A-40:</b> UV/vis & fluorescence spectra of compound <b>56d</b> pH titration.....	96
<b>Figure A-41:</b> UV/vis spectra & regression curve for compound <b>40</b> .....	97
<b>Figure A-42:</b> Sample binding isotherm .....	98
<b>Figure A-43:</b> Sample regression curve from a pH titration.....	99

## LIST OF TABLES

<b>Table 1-1:</b> Spectroscopic & binding results of sensor <b>1</b> .....	14
***	
<b>Table 2-1:</b> Spectroscopic & binding results of sensor <b>14</b> .....	34
***	
<b>Table 3-1:</b> Absorbance & $pK_a$ values of two-input ExoSensors.....	54
<b>Table 3-2:</b> Spectroscopic & binding results of two-input ExoSensors.....	55
<b>Table 3-3:</b> Spectroscopic & binding results of ES517 with various amines.....	57
***	
<b>Table 4-1:</b> Spectroscopic & binding results of three-input ExoSensors.....	72
<b>Table 4-2:</b> Spectroscopic & binding results of ES470 with various amines.....	74

## ABSTRACT

Chemical sensing has become an important field for the study of bioanalytes and provides key information pertaining to disease pathogenesis, and the physiological mechanisms underlying cellular processes. Discussed herein is a brief introduction to fluorescence methods for bioanalyte detection along with the design and synthesis of novel chemical sensors for important bioamines.

First, we report a chemical sensor for kynurenine, a molecule known to contribute to tumor growth and the development of neurodegenerative diseases. Several coumarin dimers were developed for the two-point binding of kynurenine, but showed poor solubility in aqueous media. Later, a coumarin monomer was developed that showed high selectivity for kynurenine and a pronounced fluorescence response at low pH.

Next, we produced pH-sensitive chemical sensors for neurotransmitters. The sensors are designed to produce a turn-on fluorescence response upon exocytosis. Secretion from the acidic vesicle into the neutral synaptic cleft deprotonates the sensor and makes it highly fluorescent. The sensor's fluorescence response is easily tuned by altering the  $pK_a$  of the pH-sensitive group through a single coupling reaction.

By slightly altering the coumarin core, we then achieved a three-input sensor for pH, glutamate, and zinc as the latter two molecules are copackaged in high concentrations in glutamatergic boutons. An 11-fold fluorescence enhancement of the sensor-glutamate-zinc bound complex was observed at the pH values germane to exocytosis.

# CHAPTER ONE

## Introduction

### 1.1 Fluorescence Sensing

#### 1.1.1 Molecular Recognition

Molecular recognition is a wide field that involves the interaction of a host molecule with a guest through a reversible interaction which may include hydrogen bonding, dipole-dipole interactions, van der Waals forces, metal coordination, hydrophobic interactions, electrostatic effects, or covalent bonding.<sup>1</sup> The host possesses an optical reporter and a recognition unit that associates with the analyte (Figure 1-1).

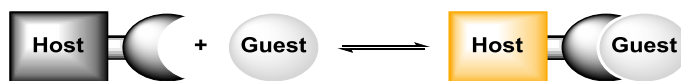


**Figure 1-1.** Reversible host-guest interaction

The label “chemodosimeter” or “probe” is used if the equilibrium constant between the host and guest is strong enough to be irreversible.<sup>2</sup> However, for continuous monitoring, a reversible “chemosensor” is desired which exhibits a binding constant comparable to the dissociation constant of the host-guest complex.

Equation 1 depicts the reversible binding of a host with a guest. Because the interaction between host and guest is reversible, there exists an equilibrium between

the unbound and bound species. The stronger the binding between the host and guest, the higher the equilibrium constant, also known as the binding or association constant ( $K_a$ ) (eq. 2).



$$K_a = \frac{[\text{Host:Guest}]}{[\text{Host}] [\text{Guest}]} \quad (\text{eq. 2})$$

The projects described herein use covalent bonding interactions for analyte detection. There are many known reversible covalent interactions that are commonly employed for analyte recognition. Our research has largely exploited the reversible reaction between aldehydes and primary amines to form iminium ions (Figure 1-2, f). Later, we will discuss how covalent bond formation can alter the optical response of the host.

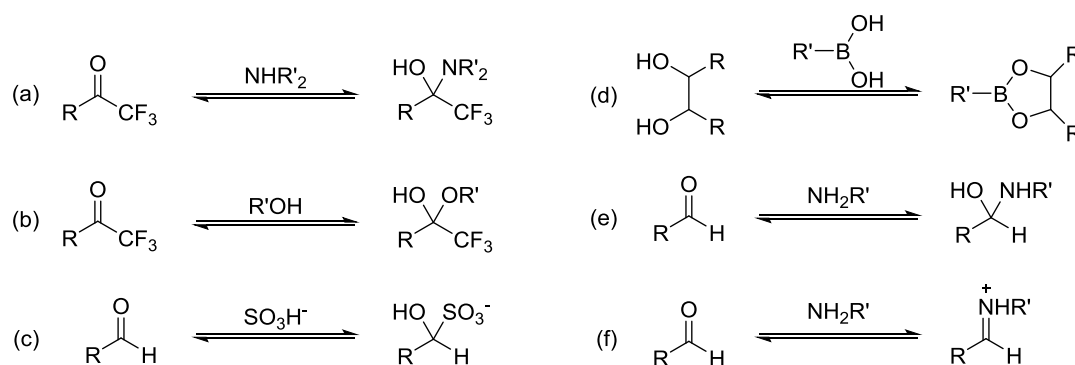


**Figure 1-2.** Covalent analyte recognition motifs<sup>2</sup>

### 1.1.2 Fluorescence Basics

Luminescence, or the emission of light from a substance, includes both phosphorescence and fluorescence phenomena.<sup>3</sup> Phosphorescence is the process by which an electron is excited into a higher energy level, undergoes intersystem crossing (ISC), and relaxes from the triplet state (Figure 1-3). The emission process may take  $10^{-3}$ - $10^2$  seconds. Fluorescence, on the other hand, is the direct relaxation of an excited electron to its ground state and subsequent emission of a photon which occurs on a much faster nanosecond timescale. Fluorescence is an incredibly sensitive technique that has garnered interest in the fields of biology, pharmaceuticals, and medicine for the purpose of investigating processes in living systems.<sup>4</sup>

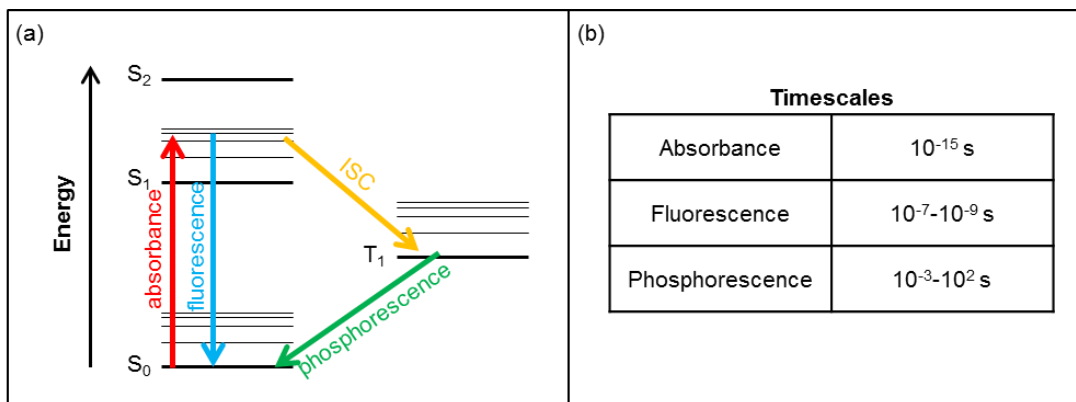


**Figure 1-3.** (a) Jablonski diagram and (b) photophysical timescales

After a fluorophore is excited at a given wavelength, the electron relaxes, emitting a photon at a longer and lower energy wavelength. The difference between the absorption maxima and the emission maxima of the fluorophore is called the Stokes shift (Figure 1-4). This loss in energy can be attributed to: (1) the rapid decay of the electron to the lowest vibrational energy level of the  $S_1$  excited state; (2) the



thermalization of the excess vibrational energy; or (3) other effects due to excited state complex formation, solvent, or energy transfers.<sup>3</sup> The shape of the absorbance and emission curves are almost always mirror images of each other as the absorption transitions from  $S_0 \rightarrow S_1$  are generally the same for the emission and because  $S_0$  and  $S_1$  have similar vibrational energy levels.

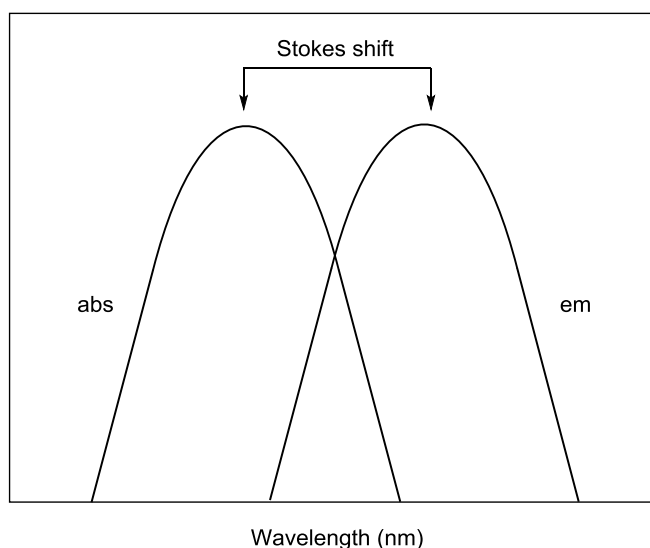


**Figure 1-4.** Stokes shift

There are several environmental factors that affect the fluorescence of a fluorophore including solvent, temperature, viscosity, and pH. The influences of pH will be discussed further in Chapters 3 & 4.

Fluorophores can be intrinsic (naturally fluorescent molecules) or extrinsic (synthetic molecules) in nature. Intrinsic fluorophores include proteins containing aromatic amino acids, hemoglobin, NADH, collagen, flavins, etc.<sup>3, 5</sup> Many extrinsic fluorophores have also been developed and are useful tools in biological imaging and chemical sensing (Figure 1-5). Their fluorescence properties can be altered with

organic synthesis and functionalization with recognition handles permits interaction with various functional groups found on bioanalytes.

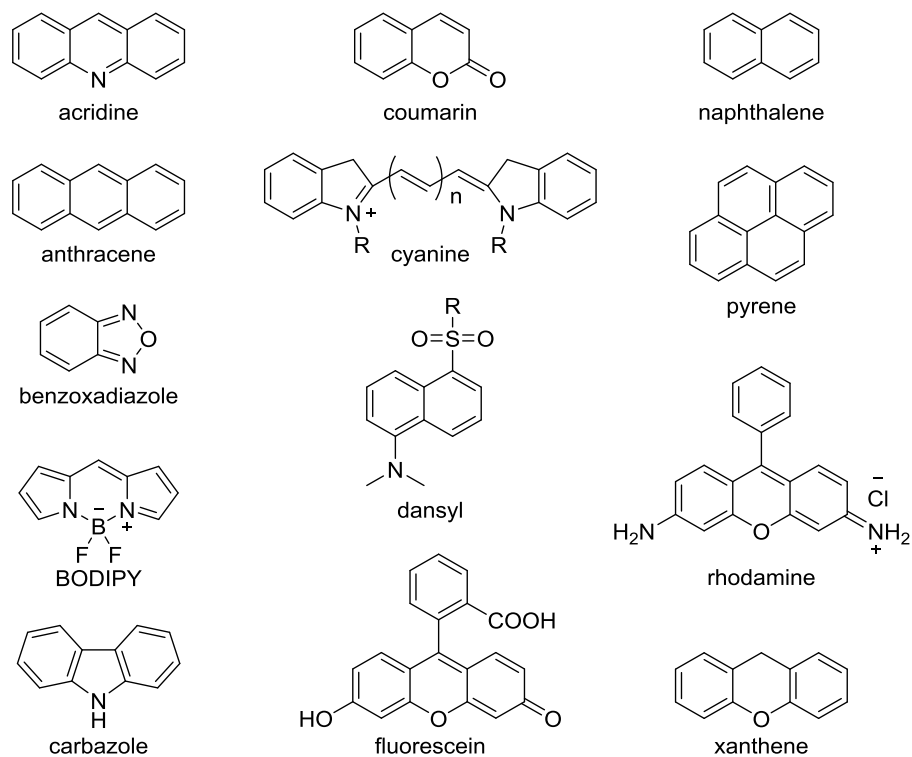


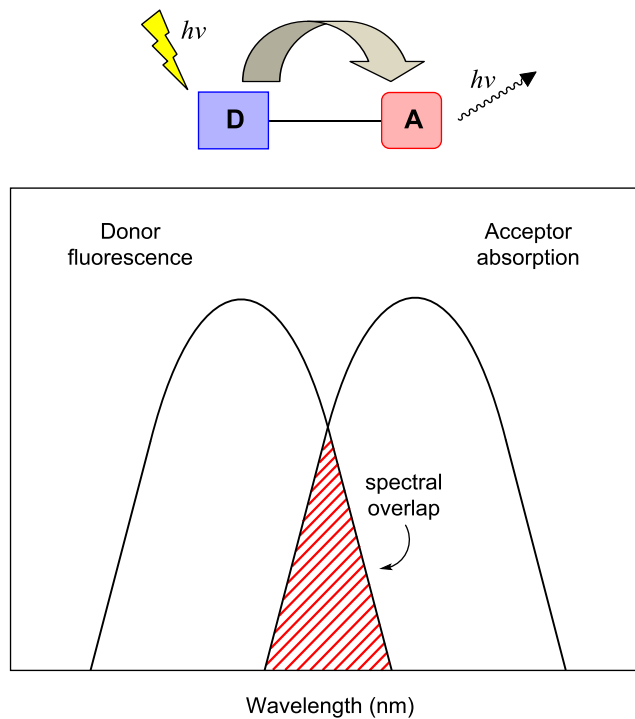
**Figure 1-5.** Common extrinsic fluorophores in chemical sensing

### 1.1.3 Mechanisms of Fluorescence Modulation

There are several signal transduction mechanisms by which fluorescence phenomena can be exploited for the purposes of bioimaging and sensing. This synopsis will include Förster resonance energy transfer (FRET), photoinduced electron transfer (PET), and internal charge transfer (ICT).

## FRET

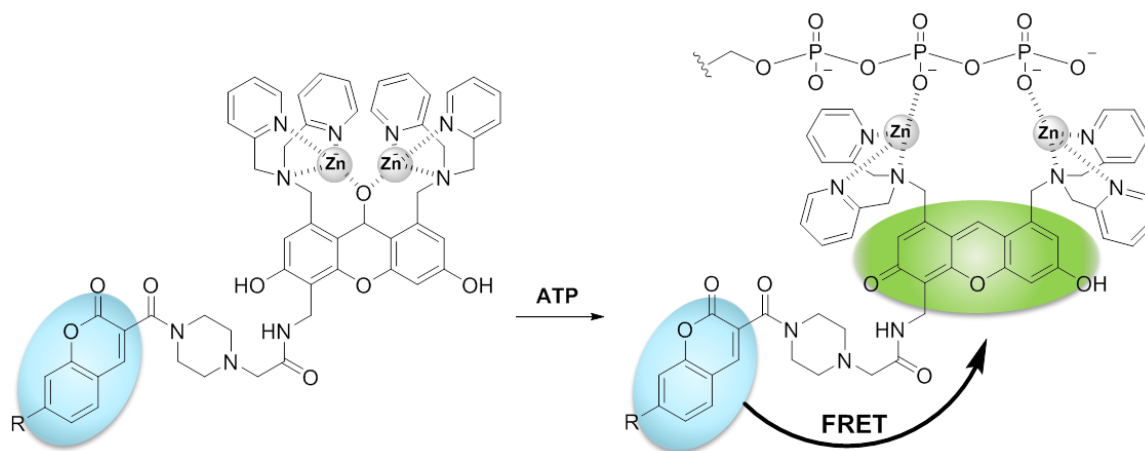
FRET requires the presence of two tethered fluorophores: a donor and an acceptor.<sup>6</sup> The emission spectrum of the donor chromophore must have sufficient overlap with the acceptor absorbance spectrum (Figure 1-6). The donor is excited with a laser and because its fluorescence emission band overlaps with the acceptor's absorbance band, the acceptor is excited and emits at a longer wavelength. This phenomenon depends on the distance between the donor-acceptor pair. The distance at which the resonance energy transfer is 50% efficient is called the Förster distance and generally ranges from 20-60 Å.<sup>3</sup>



**Figure 1-6.** Spectral overlap of donor (D) and acceptor (A) FRET pairs

FRET pairs have been used extensively in biology for studying conformational changes in proteins,<sup>7</sup> visualizing gene expression,<sup>8</sup> investigating protein activation,<sup>9</sup> and monitoring cellular levels of calcium,<sup>10</sup> mercury,<sup>11</sup> and thiols.<sup>12</sup> This method has benefits in providing a ratiometric response allowing for analyte quantification.<sup>13</sup> However, FRET sensors sometimes suffer from formation of nonfluorescent dimers when the hydrophobic fluorophores stack on top of each other and poor cellular uptake due to the large size of many FRET complexes.

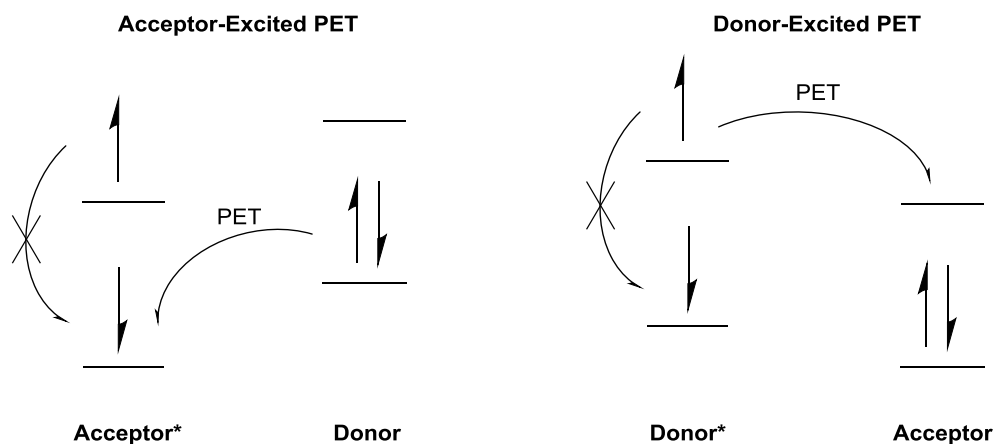
One recent example of a FRET sensor for bioanalytes comes from the Hamachi lab and is for the turn-on fluorescent detection of nucleoside polyphosphates (Figure 1-7).<sup>14</sup> Prior to phosphate addition, only blue fluorescence is exhibited by the coumarin fluorophore. The unconjugated xanthene absorbs at very low wavelengths. However, the addition of nucleotide polyphosphates promotes elimination of the zinc-bound water to yield the fully-conjugated fluorescein product whose absorbance has good overlap with the coumarin emission. Upon excitation, FRET occurs and green emission from the fluorescein is visualized. This sensor was used to monitor enzymatic reactions *in vitro* such as saccharide synthesis and phosphorylation that involve nucleoside polyphosphates as substrates, which further substantiates small molecular systems as simple yet powerful tools for monitoring biological processes.



**Figure 1-7.** A molecular sensor that uses a turn-on FRET response for the visualization of nucleoside polyphosphates

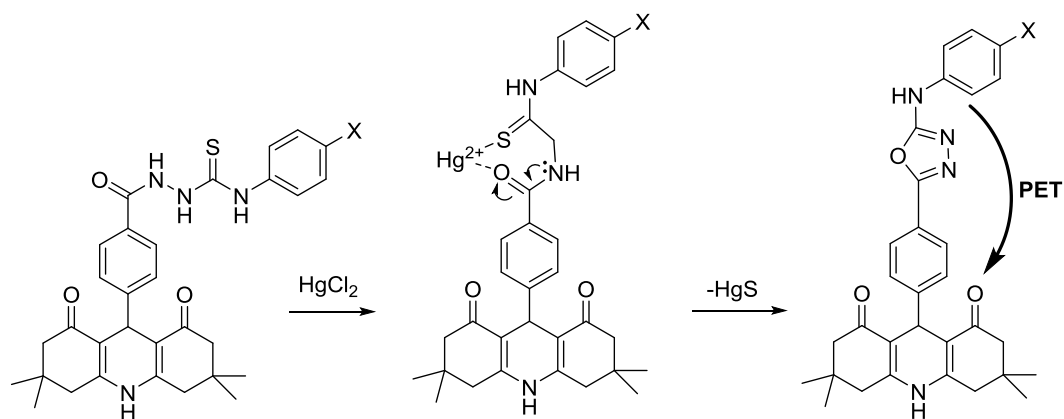
### PET

PET quenching occurs when the excited electron of a fluorophore is unable to relax and emit a photon (fluoresce) due to the presence of a nearby electron-donating or -accepting species.<sup>3</sup> There are two forms of PET quenching (Figure 1-8). Acceptor-excited PET occurs when the fluorophore (acceptor) is excited and an electron from the quencher (donor) fills the ground state of the acceptor.<sup>15</sup> Fluorescence is prohibited and the excited electron must relax via some non-radiative process. Donor-excited PET occurs when the fluorophore (donor) is excited and instead of relaxing to emit a photon, the excited electron transfers into the LUMO of a nearby quencher (acceptor). PET sensors have been employed for the intracellular measurement of pH<sup>16,17</sup> and for many bioanalytes such as nitric oxide,<sup>18</sup> mercury,<sup>19</sup> copper,<sup>20</sup> zinc,<sup>21,22</sup> and thiols.<sup>23,24</sup>



**Figure 1-8.** Acceptor- and donor-excited PET quenching

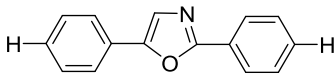
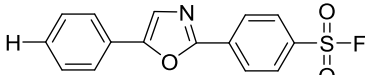
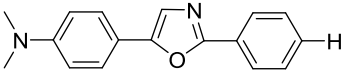
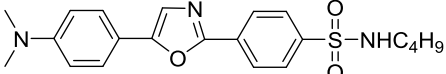
Here is a recent chemosensor developed for the aqueous detection of mercury uses a turn-off acceptor-excited PET mechanism (Figure 1-9).<sup>19</sup> The addition of mercury promotes desulfurization and the formation of a 1,3,4-oxadiazole derivative. Removal of the thiocarbonyl group increases the electron density of the aniline which can then donate an electron to the fluorophore and quench fluorescence.



**Figure 1-9.** Molecular sensor for mercury that uses an acceptor-excited PET mechanism.

## ICT

A fluorophore can form an ICT state if it contains both an electron-donating group (EDG) and an electron-withdrawing group (EWG).<sup>3</sup> The two substituents are in conjugation with each other and are separated by the extended  $\pi$ -system. Excitation can increase the charge transfer across the fluorophore and this charge separation may become the lowest energy state, especially if stabilized by a polar solvent. Fluorophores exhibiting these characteristics often produce a bathochromic shift with stronger electron donor-acceptor pairs (Figure 1-10).<sup>25</sup>

<u>EDGs</u>	<u>EWGs</u>	<u>Absorbance</u>
	H	303 nm
	$\text{SO}_2\text{F}$	332 nm
	H	348 nm
	$\text{SO}_2\text{NHC}_4\text{H}_9$	382 nm

**Figure 1-10.** The effect of EDGs and EWGs on the absorption of several 2,5-diphenyloxazole (DPO) derivatives.<sup>25</sup>

Shown below is a representative example of a chemosensor that uses an ICT mechanism and uses a BODIPY core with extended conjugation (Figure 1-11).<sup>26</sup> When no metal is present, the tertiary nitrogen from the dipicolylamine (DPA) donates its lone pair into the  $\pi$ -system of the fluorophore leading to a strong ICT state. Upon the addition of cadmium, the metal coordinates with all three nitrogens of

the DPA which reduces the ICT across the fluorophore and results in a blue-shifted emission.

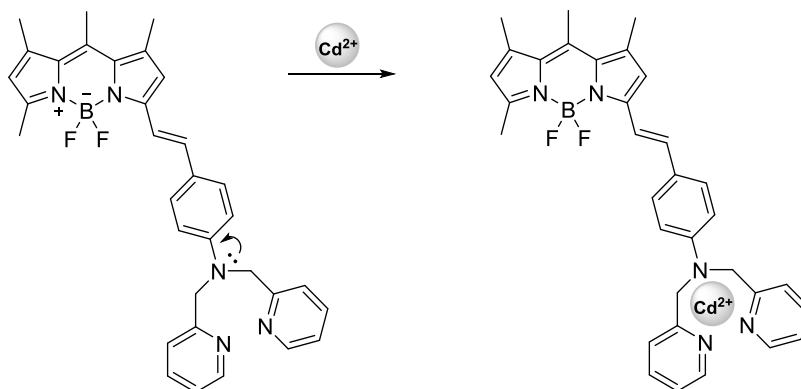


**Figure 1-11.** BODIPY-based chemosensor that detects cadmium through the reduction in the ICT state.

## 1.2 Detection of Amino Acids

Amines are ubiquitous in biology and are important components to amino acids, the subunits of proteins, and key neurotransmitters such as dopamine, norepinephrine, epinephrine, and serotonin. Amino acids play a multitude of roles in physiological processes including protein and enzyme synthesis, metabolic pathway regulation, hormone production, muscular structure, and neurotransmission.<sup>27,28</sup> Due to their biological importance, the development of optical probes for their facile and continuous detection has garnered much interest in recent years. Fluorescent and colorimetric chemosensors have detected AAs is through indicator displacement assays (IDA),<sup>29,30,31,32,33</sup> hydrogen-bonding,<sup>34,35,36,37,38</sup> covalent cleavage of fluorescence quenchers,<sup>39,40</sup> metal ion coordination,<sup>41</sup> Michael additions,<sup>42,43,44</sup> thiazinane and thiazolidine formation,<sup>39,40</sup> and imine formation.<sup>45,46,47,48</sup> Only a select few of these are highlighted below (Figure 1-12).



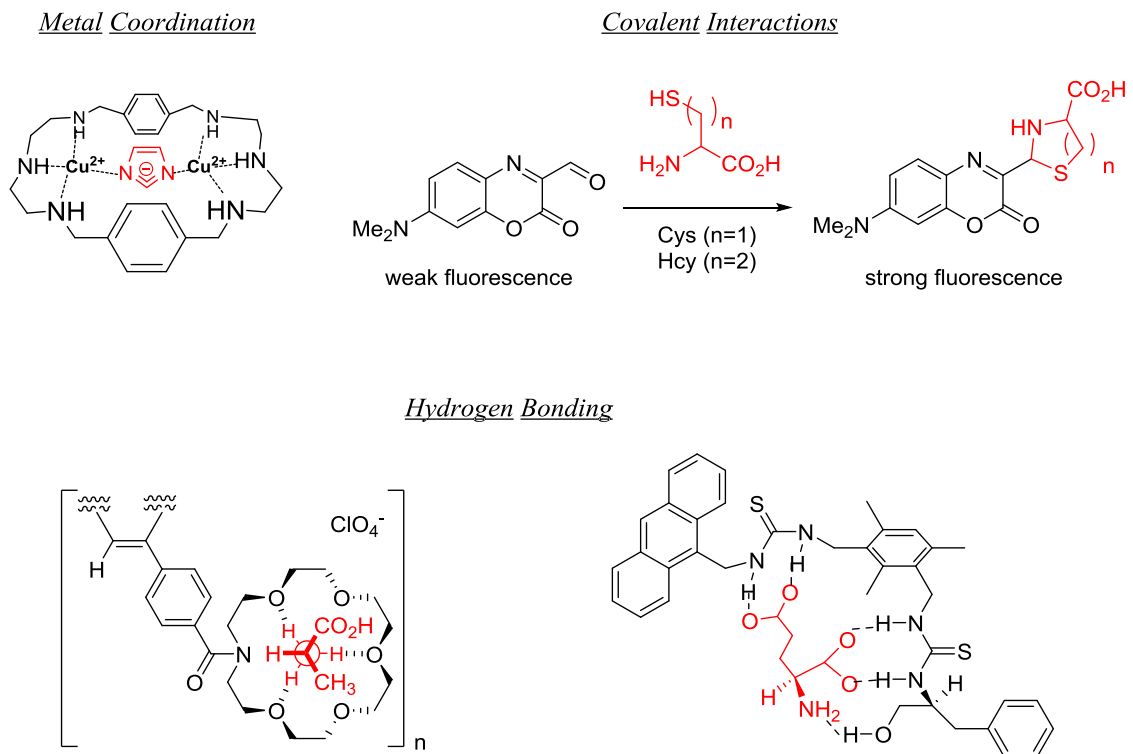


**Figure 1-12.** Examples of amino acid detection using metal coordination, covalent interactions, and hydrogen bonding<sup>41, 49</sup>

Our research group has focused on the reversible formation of iminium ions due to the covalent bonding between aldehydes and amines. In 2003, the group published compound **1**, the first chemosensor for amino acids where a turn-on fluorescence response was noted due to the formation of an iminium ion in high salt aqueous conditions (Figure 1-13).<sup>48</sup> Binding of the sensor to the amino acid induced a bathochromic shift of 34 nm and by exciting the bound complex at 495 nm, a fluorescence increase to analyte addition was noted (Figure 1-14).

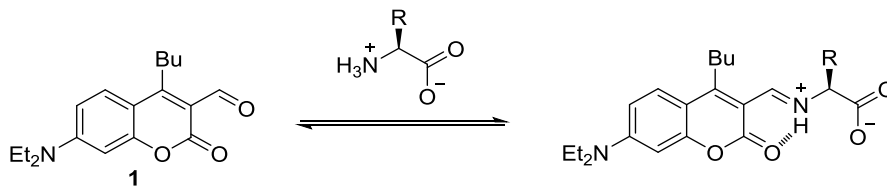


**Figure 1-13.** Reversible covalent interaction of a coumarin aldehyde to an amino acid

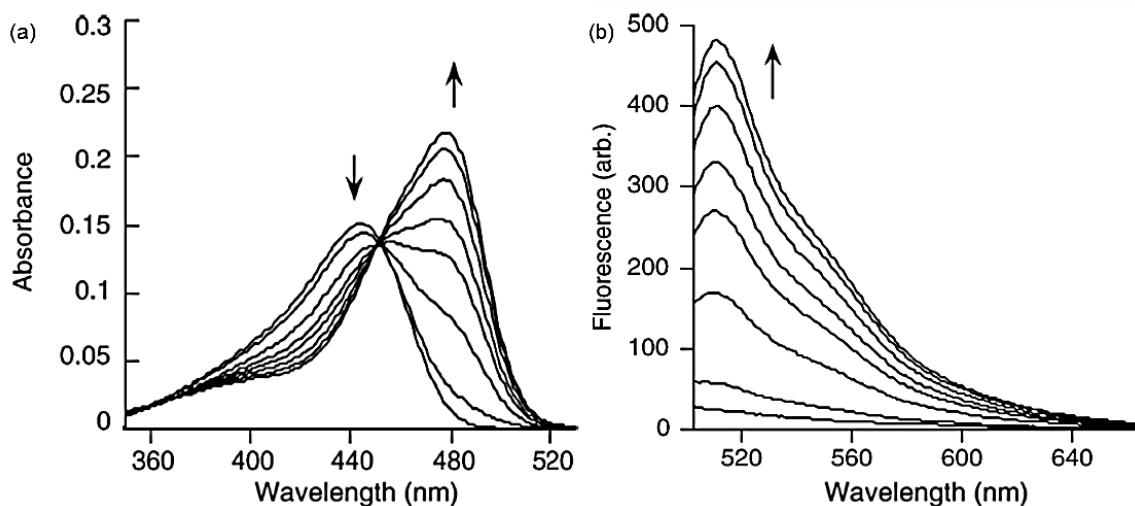


**Figure 1-14.** (a) UV/Vis and (b) fluorescence spectra of sensor **1** (10  $\mu\text{M}$ ) adding aliquots of glycine in buffer (100 mM NaCl, 50 mM HEPES, pH 7.4, 37  $^{\circ}\text{C}$ ).  $\lambda_{\text{ex}} = 495$  nm.<sup>48</sup>

The sensor was then examined with a variety of analytes (Table 1-1). The sensor was selective for amino acids and did not bind to secondary amines or hydroxyacids. All amino acids gave single-digit binding constants with the butylated diethylaminocoumarin aldehyde, the highest tested being lysine ( $6.5 \text{ M}^{-1}$ ). Fluorescence enhancements to analyte addition, on the other hand, were very impressive and ranged between 23- and 45-fold.

**Table 1-1.** Equilibrium constants ( $K_{\text{eq}}$ ) and fluorescence enhancements of sensor **1** with various analytes.<sup>a</sup>

Analyte	$K_{\text{eq}}$ ( $\text{M}^{-1}$ )	$I_{\text{max}}/I_0$ <sup>b</sup>
glycine	4.0	26
aspartate	2.3	40
glutamate	2.4	45
lysine	6.5	29
serine	5.2	23
,8-alanine	2.5	23
alanine	1.4	29
ethanolamine	6.7	15
1,3-diamino-propane	12.5	22
lactic acid	-	-
diethylamine	-	-

<sup>a</sup>Measured by fluorescent titration of **1** with amines at 37 °C;  $\lambda_{\text{ex}} = 495$  nm; 100 mM NaCl; 50 mM HEPES; pH 7.4. <sup>b</sup> $I_{\text{max}}$  is the maximum intensity at saturation taken from the fit of the titration data.

### 1.3 Detection of Neurotransmitters

Neurotransmitters are a very important class of biomolecules as they regulate numerous behavioral and cellular processes. These chemicals are taken up into vesicles using either an electrochemical gradient or a proton pump (Figure 1-15).<sup>50</sup> In the latter case, protons are exchanged for neurotransmitters using a neurotransmitter transporter until a very high concentration has accumulated within the vesicle (0.2-1.0 M).<sup>51,52,53,54</sup> An excess of protons also leaves the vesicle acidic at ~pH 5.<sup>55,56</sup> These two characteristics will be very important to understanding the function of our sensors. Many neurotransmitters possess amine functional groups, that can serve as a handle for molecular recognition (Figure 1-16).

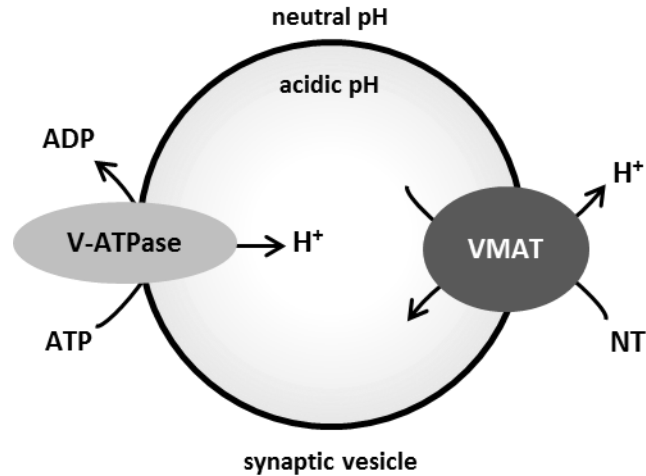


**Figure 1-15.** Neurotransmitter (NT) uptake into synaptic vesicles. A proton pump uses the hydrolysis of ATP to pump protons into the vesicle. The vesicular monoamine transporter (VMAT) exchanges protons for neurotransmitters. The end result is an acidic vesicle (pH ~5) that is highly concentrated with neurotransmitters (0.3-1.0 M).

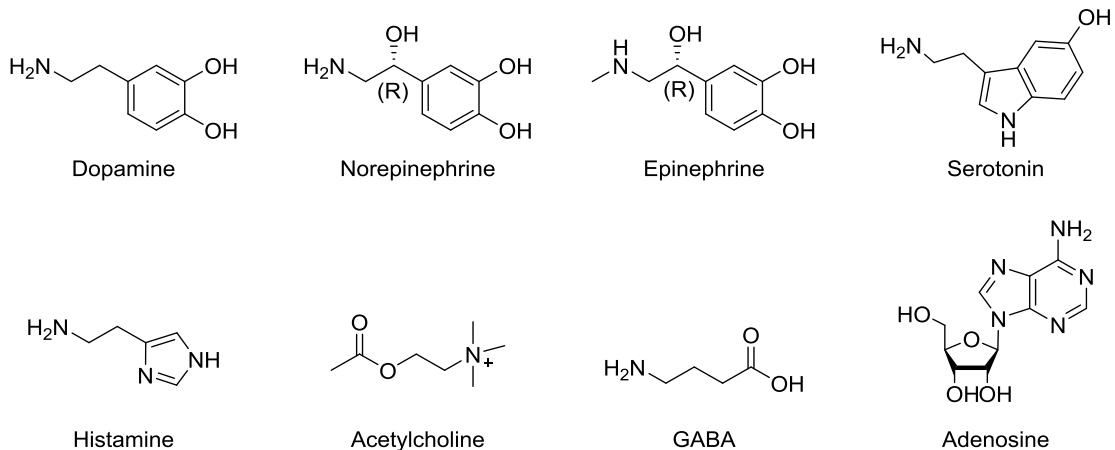


**Figure 1-16.** Molecular structures of select amine neurotransmitters

Scientists have many tools with which to study the brain, however, there are a limited number of strategies that will detect the neurotransmitter itself. Indirect techniques that do not specifically detect neurotransmitters, but do provide information regarding brain structure and function include heavy metal staining (uranium, lead, osmium) followed by electron microscopy,<sup>57,58</sup> immunofluorescence,<sup>59,60</sup> membrane

probes (FM dyes, <sup>61</sup> pHluorins<sup>62</sup>), and fluorescent tracers (FFNs).<sup>63</sup> On the other hand, techniques for direct detection of neurotransmitters including separation/analysis methods (HPLC-MS,<sup>64</sup> CE-LIF<sup>65</sup>), electrochemistry (cyclic voltammetry,<sup>66</sup> amperometry<sup>67,68</sup>), biosensors,<sup>69</sup> and small chemical sensors.<sup>70,71</sup>

The standard method for detecting neurotransmitters has been through electrochemical processes (Figure 1-17).<sup>72</sup> Catecholamines are easily oxidized to quinones which can be detected by an electrode. However, in order to achieve spatial resolution and/or monitor multiple vesicles at once, we have chosen to use fluorescent sensors which will be described in more detail.

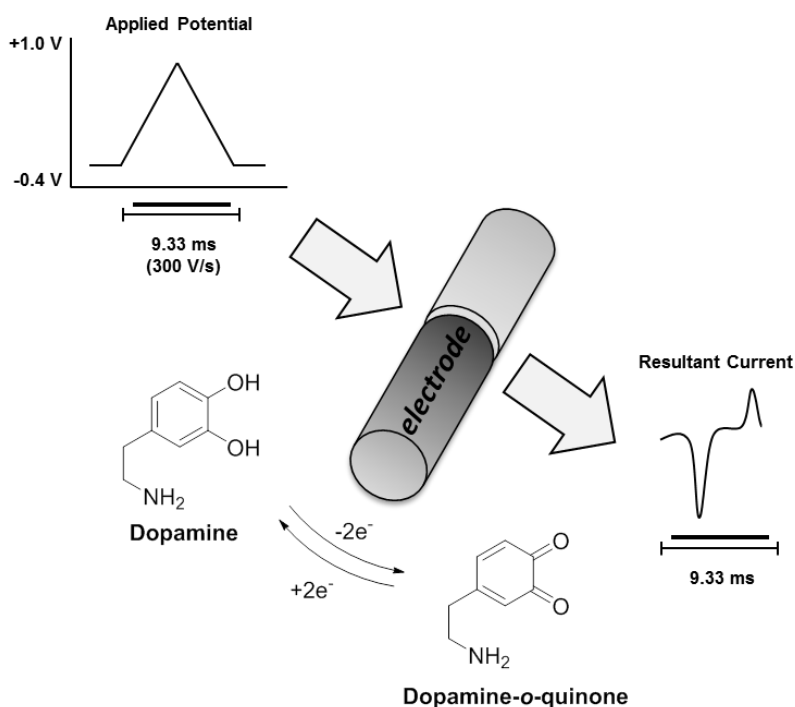


**Figure 1-17.** Detection of dopamine through an electrode using cyclic voltammetry.<sup>72</sup> Potential is applied to an electrode, dopamine becomes oxidized to the quinone, and the two lost electrons are detected as current which is proportional to the number of molecules electrolyzed.

## Biosensors

Biosensors have been a popular method used to monitor exocytosis by directly binding to the neurotransmitters typically using neurotransmitter-specific binding proteins. Tsien and colleagues have developed several FRET-based tools for glutamate imaging including glutamate-sensing fluorescent reporters (GluSnFRs & SuperGluSnFRs) and fluorescent indicator proteins for glutamate (FLIPES) (Figure 1-18).<sup>73,74,69a</sup> For SuperGluSnFRs, the surface of hippocampal neurons were linearly fused with glutamate periplasmic binding protein (GltI), cyan fluorescent protein (CFP) and yellow fluorescent protein (YFP). When glutamate is bound to GltI, there is a change in the distance between the two fluorescent proteins and consequently the FRET. In *in vitro* studies, the sensor displayed a 44% change in FRET emission ratio upon glutamate binding ( $K_a = 400,000 \text{ M}^{-1}$ ).<sup>69a</sup>

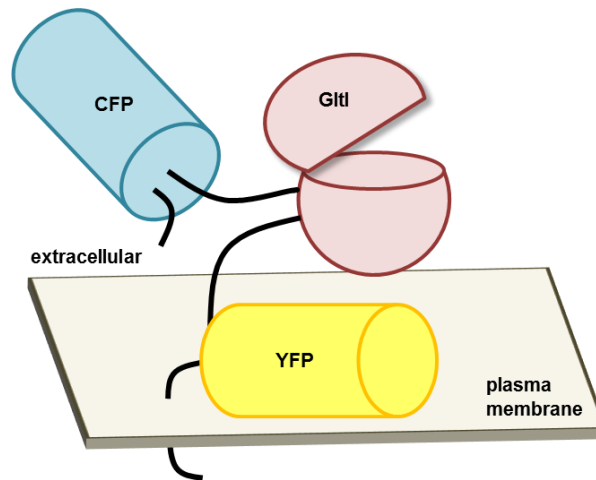


**Figure 1-18.** Graphic of surface-displaced GluSnFR in a ligand-free state

Researchers from the Johnsson group have developed FRET-based probes for both glutamate and GABA.<sup>69b, 69c</sup> The semisynthetic fluorescent sensor proteins (Snifits)

are fused to the extracellular surface of the cell and contain a SNAP-tag, CLIP-tag, and a protein that binds to the specific analyte (Figure 1-19). The semisynthetic glutamate sensor (Snifit-iGluR5) was used to label the outer membrane of human embryonic cells (HEK 293) in hopes of monitoring only secreted glutamate. When glutamate is present, it displaces a bound antagonist and changes the FRET ratio. A binding constant of  $K_a = 67,000 \text{ M}^{-1}$  was obtained for glutamate. This biosensor had a better ratiometric change than previously discussed sensor by Tsien (156% vs. 44%).

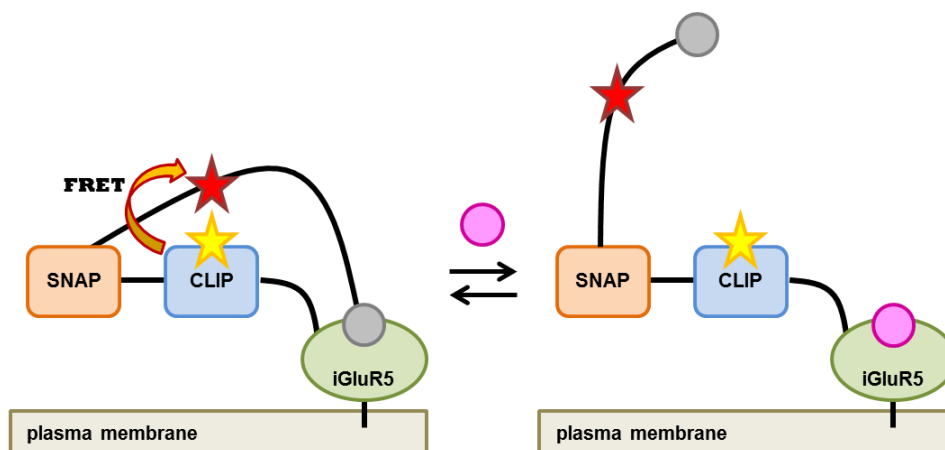


**Figure 1-19.** Snifit sensor for sensing glutamate. The glutamate analog (gray ball) is bound to the receptor (iGluR5) and FRET occurs between the two fluorophores (stars). The addition of glutamate (pink ball) displaces the intramolecular ligand which separates the fluorophores so that no FRET occurs.

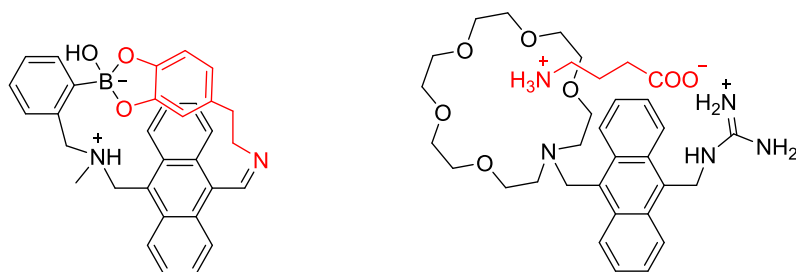


**Figure 1-20.** Examples of chemical sensors for neurotransmitters (dopamine and GABA shown).

Only a few chemical sensors for the direct detection of neurotransmitters have been developed (Figure 1-20).<sup>70b,71,48, 70a</sup> The key challenges in developing such sensors include achieving water-solubility, using the recognition motifs of electrostatic interactions and hydrogen bonding in water, and overcoming the strong fluorescence quenching properties of catecholamine and indoleamine neurotransmitters. Aromatic neurotransmitters tend to quench fluorescence as they are easily oxidized and can donate an electron into the ground state of the excited fluorophore leading to acceptor-excited PET quenching (Figure 1-21).

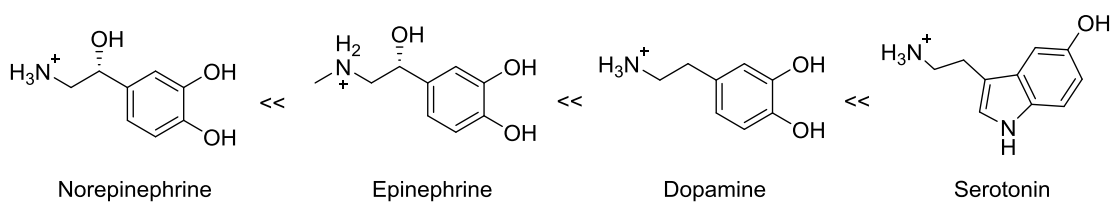


**Figure 1-21.** Quenching ability of aromatic neurotransmitters



Our group has developed a series of sensors for the detection of primary amine neurotransmitters (Figure 1-22).<sup>46, 70a</sup> The first generation sensor was intended to bind to catecholamine neurotransmitters with high affinity. It bound to dopamine with an affinity of  $3400 \text{ M}^{-1}$  due to a strong two-point binding interaction but gave a turn-off fluorescence response due to quenching from the analyte catechol. The second generation sensor was designed to give a turn-on response due to fluorescence-modulating effects of an added *p*-methoxyphenyl substituent. The one-point binding strategy resulted in lower binding affinities to the neurotransmitters but to no adverse effect in practical applications as will be explained in later chapters.

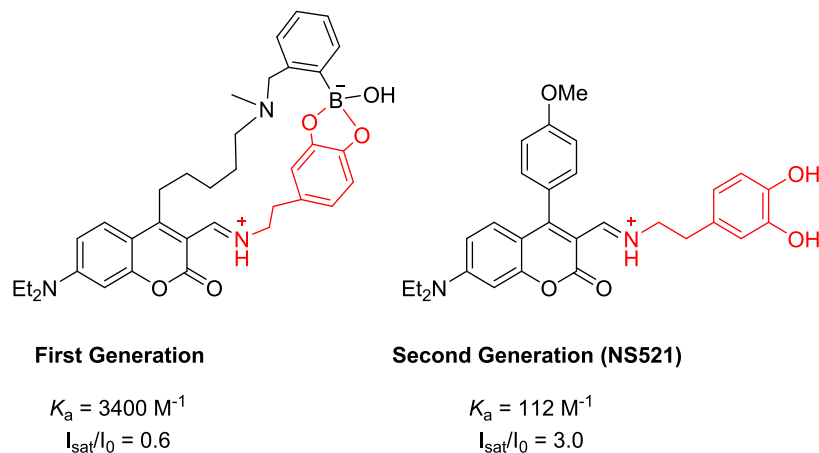


**Figure 1-22.** First- and second-generation catecholamine sensors based on the coumarin aldehyde scaffold shown bound to dopamine.

#### 1.4 Monitoring Exocytosis

While the static imaging of neurotransmitters is important, researchers would also like to monitor exocytosis and the detailed mechanics behind neurotransmission. Several methods have been developed to do so, namely, through the use of FM dyes, synaptopHluorins, and fluorescent false neurotransmitters (FFNs).<sup>75</sup>

### 1.4.1 FM Dyes

FM dyes are amphiphilic styryl pyridinium molecules that have been used to monitor exocytosis (Figure 1-23).<sup>76,61a, 61b</sup> The dye has a charged polar head and a lipophilic tail. The fluorescence is environment-dependent and only turns on when the lipophilic tail inserts into a hydrophobic medium, such as a lipid membrane. In neuroscience, the dye is added to the extracellular space surrounding neurons. Stimulation is applied which causes the vesicles to release neurotransmitters and upon subsequent endocytosis, the dye is taken up and inserts into the intravesicular membrane. All remaining dye is washed away, and the vesicles can be clearly visualized. Exocytosis is monitored as a measure of fluorescence decrease. After the dye has been internalized, the cell can be stimulated again, the dye is released and dispersed, and the fluorescence signal disappears.

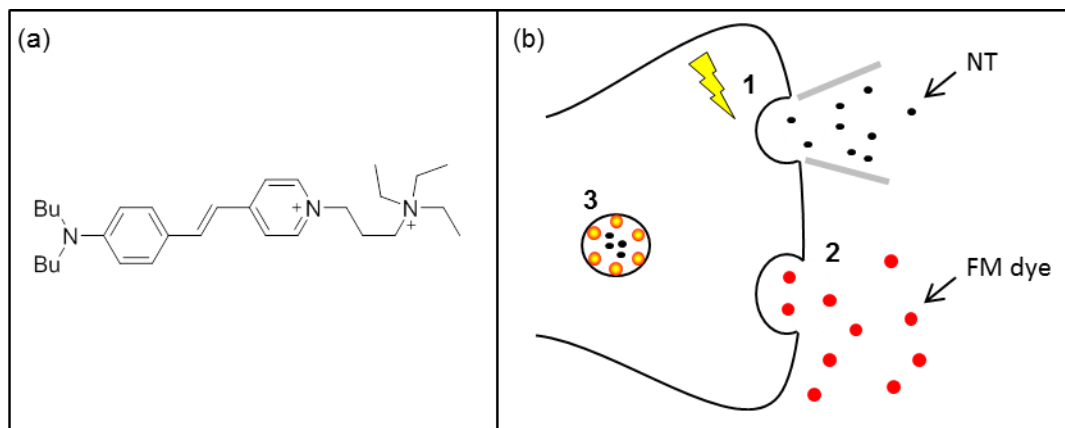


**Figure 1-23.** Structure and mechanism of FM dyes. (a) Molecular structure of FM 1-43, and (b) FM dye uptake into the axonal terminus of a neuron: 1) An action potential stimulates exocytosis of the vesicle. Neurotransmitters (NTs) are released. 2) Dye from the extracellular space is taken up into the vesicle upon endocytosis. 3) The dye partially inserts into the hydrophobic intravesicular membrane which causes a fluorescence increase.

### 1.4.2 SynaptopHluorins

pH-sensitive proteins called “pHluorins” were developed to respond to the difference in pH between the synaptic vesicle (pH ~5) and the synaptic cleft (pH~7.4).<sup>62b, 77,78,62a,79</sup> The pHluorins are fused to the intravesicular membrane and have been genetically-engineered to incorporate green fluorescent protein (GFP) mutant which has had key residues replaced with pH-sensitive amino acids (Figure 1-24). The mutant is fluorescent at pH > 6 but not in more acidic media.

	151				200
GFP2	YIMADKQKNG	IKVNFKIRHN	IEDGSVQLAD	HYQQNTPIGD	GPVLLPDNHY
pHluorin	YIMADKQKNG	<b>TKAIFQV</b> HHN	IEDGGVQLAD	HYQQNTPIGD	GPVLLPDNHY
	201			239	
GFP2	LSTQSALSKD	PNEKRDHML	LEFVTAAGIT	LGMDELYK*	
pHluorin	<b>L</b> HTQSALSKD	PNEKRDHML	LEFVTAAGIT	<b>H</b> GMDELYK*	

**Figure 1-24.** Segment of the amino acid sequences for GFP and pHluorin with key differences highlighted.<sup>80</sup>

The GFP mutant is fused to the luminal vesicular membrane and has low fluorescence when the vesicle is closed due to being protonated in the acidic environment. However, when the vesicle docks and undergoes exocytosis, the pHluorins are exposed to the pH 7.4 cytosol which causes deprotonation and a fluorescence turn-on response.

Ratiometric pHluorins have been used to measure intravesicular pH as well as to identify a readily releasable pool of vesicles in the axonal terminal.<sup>79</sup> FM dyes and synaptopHluorins have been used in concert to study localization of both endocytosis and exocytosis. Such studies have found that that fluorescence signals from the two dyes colocalize when stimulated with high frequency, though

the events of exo- and endocytosis appear to occur on different time scales.<sup>81</sup> The researchers concluded that the exocytotic pathway (visualized with synaptopHluorins) and the endocytotic pathway (visualized with FM dyes) are important to the synaptic vesicle cycle when stimulated at high frequencies.

### 1.4.3 False Fluorescent Neurotransmitters (FFNs)

Fluorescent false neurotransmitters (FFNs) have been developed as neurotransmitter mimics to help monitor vesicular events (Figure 1-25).<sup>63, 82</sup> Their structure includes a coumarin fluorophore with a donor group at the 7-position and an ethylamine moiety at either the 3- or 4-positions. FFNs are taken up into synaptic vesicles via the VMAT2 monoamine transporter protein and give punctate fluorescence as they are copackaged with neurotransmitters in high concentration within secretory vesicles.

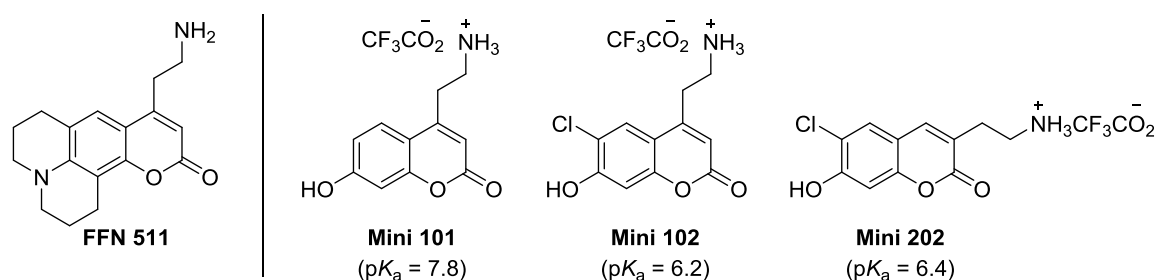


**Figure 1-25.** Structures of FFN dyes

The pH-sensitive versions of FFNs have hydroxyl donors at the 7-position that can become deprotonated upon exocytosis. Chlorines were appended and the 6-position of the ethylamine moiety altered to modify the pK<sub>a</sub> value of the hydroxyl

proton. These FFNs can monitor pH within the vesicle and are shown to increase the background fluorescence within mouse brain striatal slices upon addition of amphetamine, addition of high  $K^+$ , or electrical stimulation.

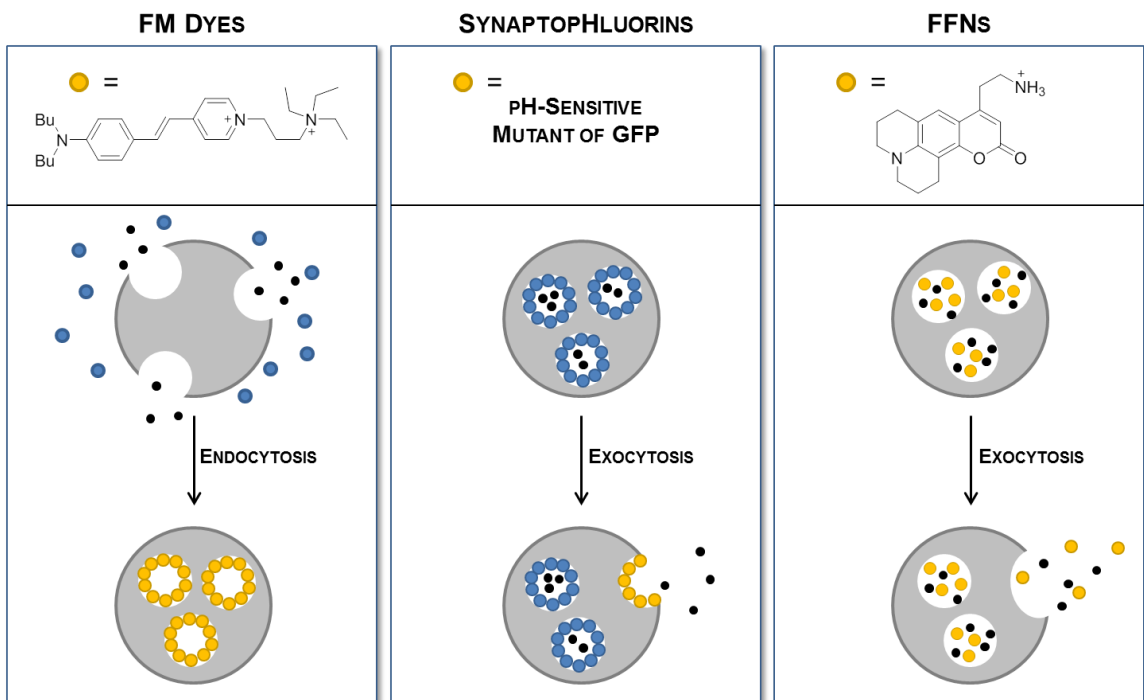


**Figure 1-26.** Summary of indirect methods to monitor neurotransmitter uptake and release. Yellow and blue circles are fluorescent and nonfluorescent dyes, respectively. Black dots are neurotransmitters. FM dyes fluoresce only after being taken up into the synaptic vesicle upon endocytosis and embedding in the intravesicular membrane. Synaptophluorins, become deprotonated and fluoresce when exposed to the cytosol upon exocytosis. FFNs are neurotransmitter mimics and show punctate fluorescence when accumulated within vesicles alongside neurotransmitters.

The aforementioned methods consist of probes that monitor the event of exocytosis, but do not monitor the neurotransmitters, themselves, and may require laborious genetic modification of the vesicle (Figure 1-26). There are as of now, no molecular sensors that directly bind to and visualize the release of neurotransmitters in live cells. We will describe in Chapters 3 and 4 the

development of chemosensors for the direct detection of neurotransmitter release from secretory vesicles.

## CHAPTER TWO

### A Fluorescent Sensor for Kynurenine

#### 2.1 Overview

Kynurenine, a metabolite of tryptophan, is a precursor to the biological production of picolinic acid and NAD (Figure 2-1).<sup>83</sup> Abnormally high concentrations have been associated with coronary heart disease, invasive tumor growth, Huntington's, Alzheimer's, and other neurological diseases.<sup>84,85,86</sup> Kynurenine acts as an endogenous ligand for the aryl hydrocarbon receptor (AHR) that inhibits antitumor immunological responses by suppressing allogenic T-cell proliferation. As a result, elevated levels of kynurenine allow for unhindered invasive tumor growth.<sup>87,88</sup> As the first stable intermediate in the kynurenine pathway, kynurenine is generated when the indoleamine 2,3-dioxygenase (IDO) or tryptophan dioxygenase (TDO) enzymes are activated. The ratio of kynurenine to tryptophan is often used as an index of IDO and TDO activity. Both increased IDO/TDO activity and high AHR levels have been correlated with poor prognosis in cancer patients further tying kynurenine and its known functions to cancer progression.

The selective detection of kynurenine is material in the ongoing study of cancer progression. Current detection methods include HPLC, GCMS, biosensors, and various electrochemical techniques that entail costly or time-consuming preparations.<sup>89,90,91,92,93</sup> Fluorescent sensors, by contrast represent a convenient and sensitive method for analyte

detection. We sought to develop a fluorescent sensor for kynurenine by binding to its primary amine functional groups.

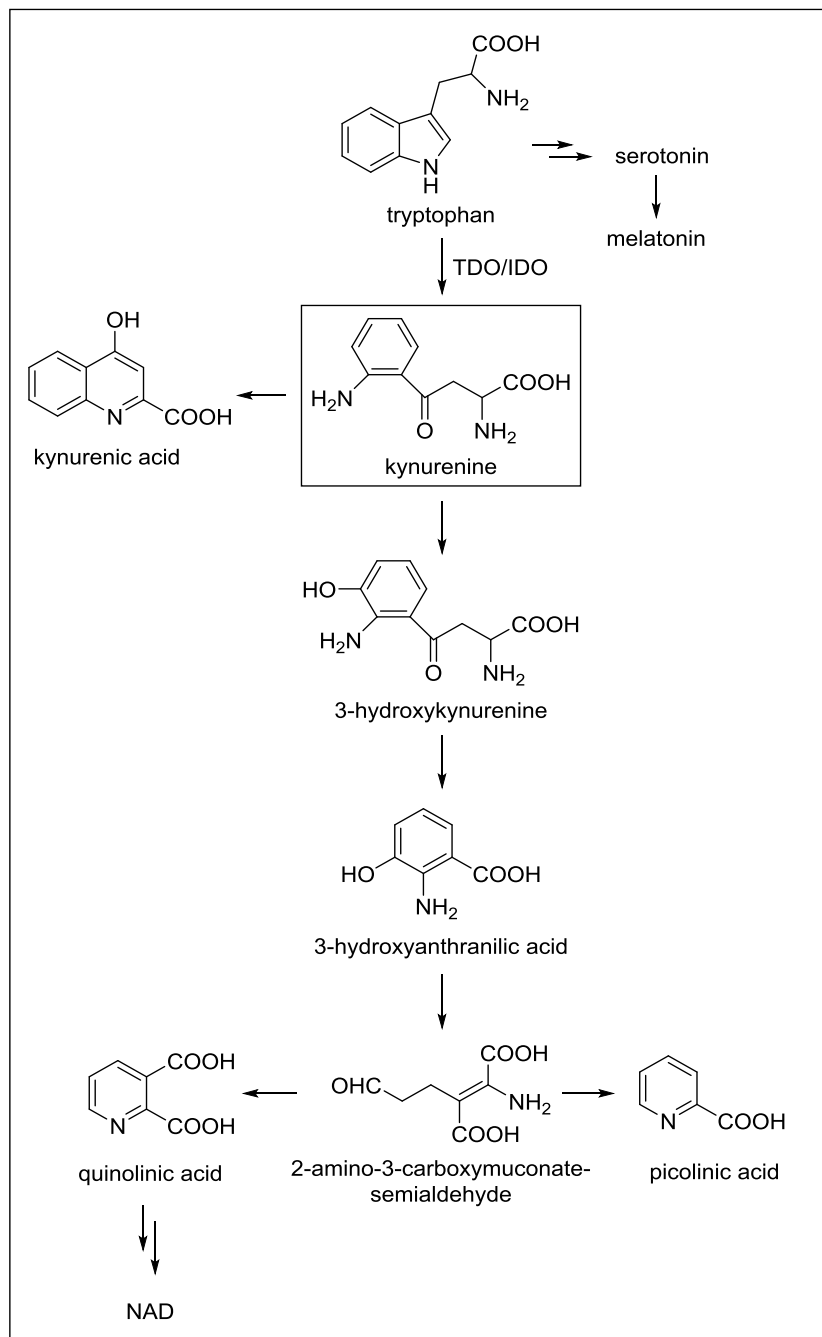


**Figure 2-1.** The kynurenine pathway



Our group has previously demonstrated that coumarin aldehydes reversibly bind to primary amines which induces a bathochromic shift in absorbance (Figure 2-2).<sup>48</sup> Sensor **1** functions through an internal charge transfer (ICT) mechanism whereby the tertiary nitrogen serves as the electron donor and the aldehyde acts as the electron acceptor. The aldehyde of the sensor reversibly binds to primary amines to form a positively charged iminium ion that enhances the ICT and modulates both the absorbance and fluorescence. The red shift in absorption upon analyte binding permits excitation and monitoring of the sensor in both its unbound and bound states.

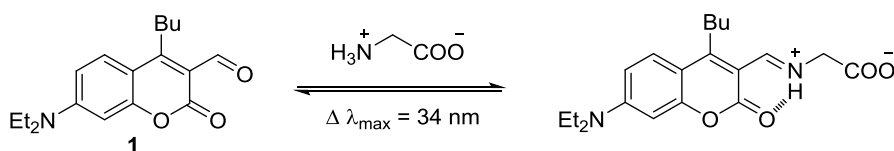


**Figure 2-2.** Binding of glycine to sensor **1** induces a bathochromic shift in absorbance

## 2.2 Coumarin Dimers

Kynurenine is unusual in that it possesses both an aliphatic and an aromatic primary amine, and until now we had not examined the interaction of aromatic amines with our sensor system. Therefore, coumarin aldehyde dimers were developed for two-point binding which would theoretically increase the sensitivity of the sensor to kynurenine. Two dimers with varying linker lengths were designed with the hope that one would better assume the geometry necessary for two-point binding with kynurenine.

Dimers **7** and **8** were synthesized from the commercially available 7-diethylamino-4-hydroxycoumarin core (**2**) by first doing an *in situ* tosylation and Suzuki

coupling reaction to afford compound **3** (Figure 2-3). Demethylation using  $\text{BBr}_3$  was followed by dimerization using potassium carbonate and dibromoalkanes. Subsequent formylation rendered the final sensors **7** and **8**.

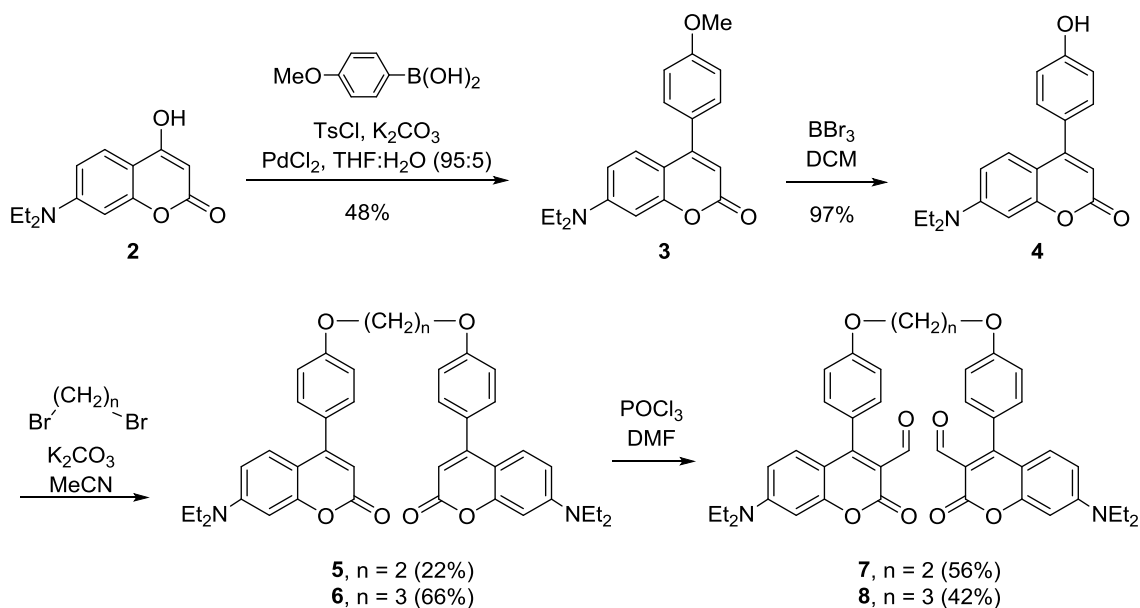


**Figure 2-3.** Synthesis of oxygen-linked coumarin dimers for kynurenine detection

It was noted that **7** and **8** were not water soluble likely due to the planarity of the molecules' aromatic rings as well as the hydrophobicity of the alkyl linker. Therefore, to achieve higher water solubility we designed amine-based linkers that would be protonated in solution (Figure 2-4). However, the last dimerization step would only return starting material.

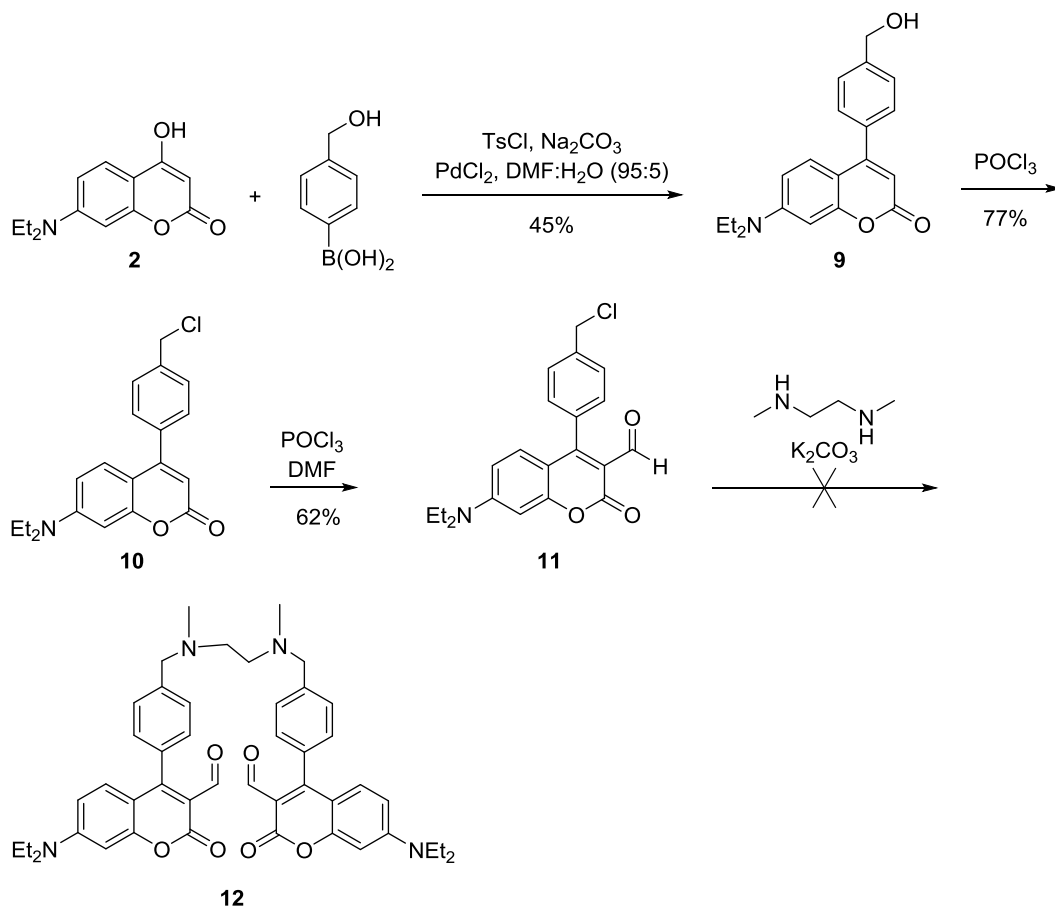


**Figure 2-4.** Synthesis of amine-linked coumarin aldehyde dimers for kynurenine detection

### 2.3 Coumarin Monomer

Due to difficulties with synthesis and solubility of the coumarin dimers, the coumarin monomer model was pursued (Figure 2-5). We functionalized the coumarin core with alkyl thiols in a similar fashion to previously reported quinolone aldehydes.<sup>47</sup>

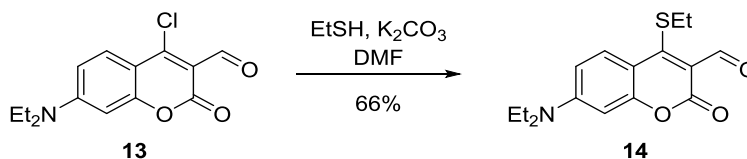


**Figure 2-5.** Synthesis of coumarin aldehyde monomer for kynurenine detection

Initial efforts to test sensor binding to kynurenine were hampered by its low solubility in neutral aqueous media. Therefore, the solution pH was lowered to 1.0 to enhance kynurenine solubility and the absorbance and fluorescence spectra were monitored (Figure 2-6). Sensor **14** has an absorption band at 468 nm. This wavelength of absorption is typical for the coumarin aldehydes and indicates that the diethylamino donor group is not protonated even at this low pH. Upon the addition of kynurenine, two new absorption bands were observed at 525 and 555 nm at pH 1. This represents an unprecedented bathochromic shift of 87 nm compared to the ~35 nm shift that is typical for the coumarin aldehyde class of sensors.<sup>48</sup>

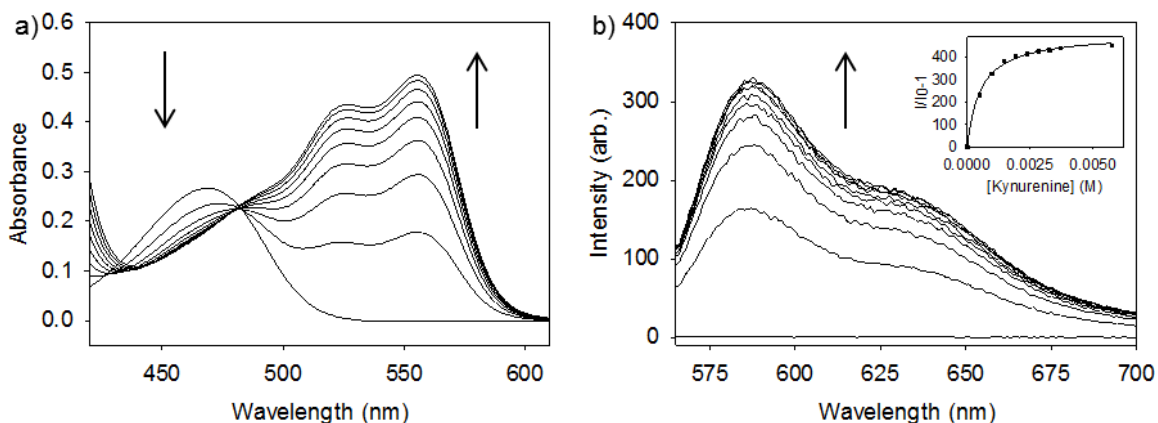
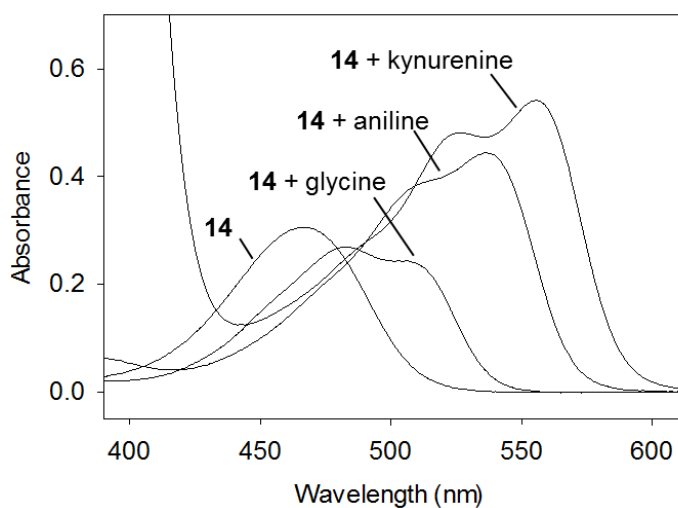


**Figure 2-6.** (a) UV/vis and (b) fluorescence spectra ( $\lambda_{\text{ex}} = 555$  nm) of sensor **14** (10  $\mu\text{M}$ ) in buffer (50mM  $\text{H}_3\text{PO}_4$ , 120 mM NaCl, pH 1, 1% DMSO) adding aliquots of 50 mM kynurenine. Inset is the fit to a one-site binding isotherm.

The fluorescence emission spectrum mirrors the absorbance spectrum revealing two bands at 586 and 632 nm upon excitation at 555 nm. Because sensor **14** does not absorb above 530 nm in its unbound form, exciting at 555 nm realizes the fluorescence emission from the bound sensor only. Binding to kynurenine provides a pronounced 390-

fold fluorescence enhancement. Furthermore, the binding constant with kynurenine was  $1880 \text{ M}^{-1}$ , which is nearly three orders of magnitude higher than the binding of an aliphatic primary amine to the coumarin aldehyde sensors.<sup>48</sup>

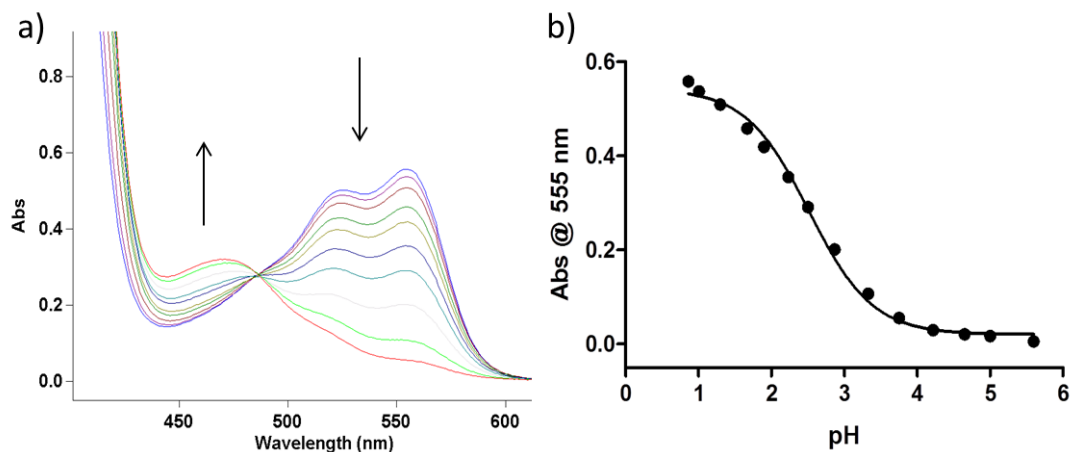
We surmised that the aromatic amine must be involved in extending the conjugation of the chromophore. To test this hypothesis, we titrated sensor **14** with aniline which gave a similar, though smaller, bathochromic shift with two distinct bands (Figure 2-7). The larger shift and higher binding constant of kynurenine is attributed to the *ortho*-carbonyl group, which extends the conjugation of the chromophore with an additional electron-withdrawing group.



**Figure 2-7.** UV/vis spectrum of sensor **14** (10 μM) with various analytes (5 mM kynurenine; 16 mM aniline; 360 mM glycine) in buffer (50 mM H<sub>3</sub>PO<sub>4</sub>, 120 mM NaCl, pH 1, 1% DMSO).

A pH titration of the sensor-kynurenine bound complex gave a pK<sub>a</sub> of 2.5 that is consistent with the pK<sub>a</sub> of an aniline Schiff base (Figure 2-8).<sup>94</sup> Upon raising the pH of the solution, the long wavelength absorption is lost. The sensor response requires that the imine be protonated, thus the sensor only operates at low pH. It should be noted that a

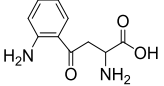
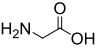
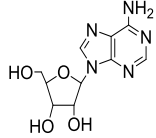
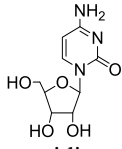
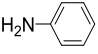
Schiff base from an aliphatic amine has  $pK_a$  values of  $\sim 6-8$ .<sup>95</sup> This supports the notion that it is the aromatic amine of kynurenine that binds to the sensor.



**Figure 2-8.** (a) UV-vis spectra and (b) binding isotherm of the pH titration of the **14** -kynurenine complex with 4 M NaOH. The sensor (10  $\mu$ M) was saturated with kynurenine (8 mM) and the absorbance at 555 nm monitored over a pH range (0.9-5.6). A  $pK_a$  of 2.5 was obtained from the best-fit curve.

To test for selectivity, sensor **14** was titrated with other biological amines and the fluorescence was monitored. The various analytes bound to sensor **14** weakly and provided only modest bathochromic shifts. In turn, no fluorescence response was observed when excited at 555 nm (Table 2-1). Even aromatic primary amines such as adenosine provided no response. Thus, sensor **14** is highly selective for kynurenine.

**Table 2-1.** Association constants and spectroscopic results from the binding of sensor **14** (10  $\mu$ M) with various bioanalytes (50-500 mM)

Analyte	$K_a$ ( $M^{-1}$ ) <sup>a</sup>	$\lambda_{max1}$ (nm)	$\lambda_{max2}$ (nm)	$I_{sat}/I_0$ <sup>b</sup>
 kynurenine	1880	525	555	390
 glycine	8.0	483	507	n.d.
 adenosine	5.3	470	-	n.d.
 cytidine	1.6	470	-	n.d.
 aniline	600	510	536	220

<sup>a</sup>Error in  $K_a$  is  $\pm 5\%$  based on triplicate titrations; <sup>b</sup> $\lambda_{ex} = 555$  nm; n.d. = not determinable

A competitive binding study was performed to investigate the effect of competing analytes on the binding of sensor **14** to kynurenine (Figure 2-9). Sensor **14**, kynurenine (10 mM), and various competing analytes (100 mM) were combined and the fluorescence intensities observed with an excitation of 555 nm. The relative fluorescence intensity did not change when competing analytes were added in 10-fold excess. These data indicate that sensor **14** can selectively sense kynurenine in complex mixtures containing other biological aromatic and aliphatic primary amines.

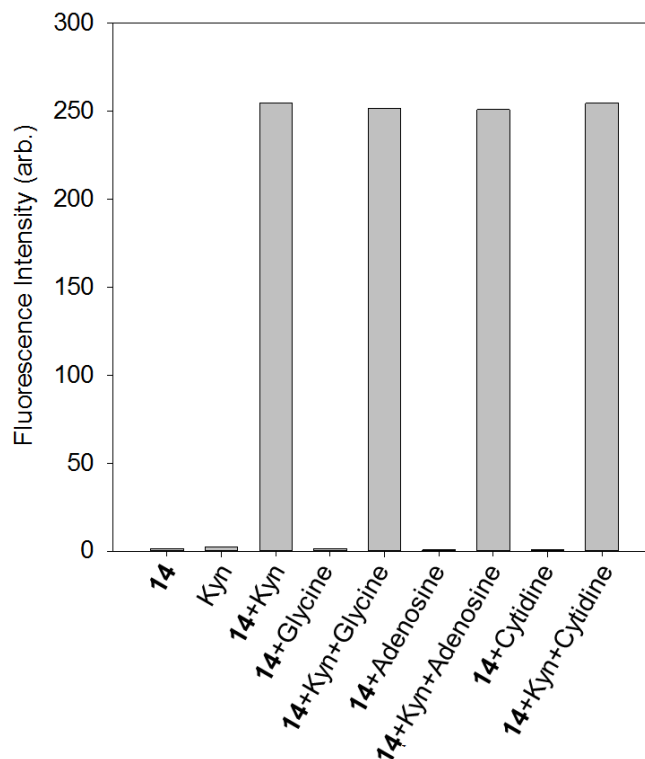


**Figure 2-9.** Fluorescence emissions of sensor **14** (10  $\mu$ M) at  $\lambda_{em} = 586$  nm with kynurenine (10 mM) in the presence of various analytes (100 mM) in buffer (50 mM  $H_3PO_4$ , 120 mM NaCl, pH 1, 1% DMSO).

In conclusion, we have developed sensor **14** as a tool for the selective detection of kynurenine. The coumarin aldehyde confers a turn-on fluorescence response upon binding due to an enhanced charge transfer. This method is unique in that kynurenine is incorporated as part of the fluorophore thus giving exquisite selectivity for the target analyte due to an unprecedented bathochromic shift. Other biological amines form bound complexes that do not absorb at such high wavelengths. The considerable fluorescence enhancement seen upon binding to kynurenine is unperturbed by the presence of excess competing analytes and further substantiates sensor **14** as a means to monitor kynurenine in order to facilitate studies of cancer initiation and progression.



## CHAPTER THREE

### Visualizing Exocytosis with Sulfonamide Coumarins

#### 3.1 Background

Neurotransmitters are critical to the regulation of the central and peripheral nervous systems and command a number of functions such as learning, memory, sleep, and movement.<sup>96,65</sup> Discerning the machinery involved in vesicular fusion, the spatiotemporal mechanisms of synaptic release, and the chemical activity of neurotransmitters is vital to understanding both normal and atypical cellular processes. The ability to effectively monitor exocytotic operations bolsters research in neuroscience, serving as a useful tool in the study of neurophysiology and neuropsychiatric disorders. Methods to evaluate exocytosis include fluorescence imaging,<sup>79,63a,97,98,99</sup> capillary electrophoresis,<sup>100,101,102,103</sup> microelectrochemistry,<sup>104,105</sup> and mass spectrometry<sup>106</sup>. Non-optical techniques are limited by poor throughput and a lack of spatial resolution.<sup>107</sup> Conversely, fluorescence methods offer a sensitive means to elucidate the spatial distribution of neuronal vesicles and chemical messengers.

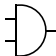
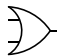
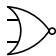
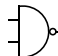
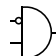

Fluorescence imaging of secretion was studied early on by loading chromaffin cells with acridine orange and observing a loss in fluorescence upon exocytosis.<sup>99</sup> More recently, exocytosis has been visualized using the genetically-encoded synapto-pHluorins, wherein a pH-sensitive GFP construct is expressed on the inner membrane of secretory vesicles.<sup>79</sup> The engineered vesicles fluoresce upon exocytosis due to a change

in pH from the acidic synaptic vesicle (~5) to the neutral synaptic cleft (~7.4). These methods solely monitor the process of vesicle membrane fusion during an exocytotic event but do not directly image active neurotransmitters released upon exocytosis. In recent years, a genetically-encoded CFP/YFP FRET biosensor was developed to monitor glutamate release, spillover, and reuptake by fluorescence.<sup>69a</sup> However, these protein-based biosensors require genetic manipulation and display high, irreversible affinity for glutamate with limited dynamic range and overall small changes in fluorescence. To avoid the use of protein-based fluorophores, a pH sensitive fluorescent false neurotransmitter (FFN) has been developed to monitor exocytosis. This fluorescent tracer is loaded into vesicles expressing VMAT and fluoresces upon exocytosis similar to the synapto-pHluorins.<sup>63c</sup> We wanted to develop a *direct* method of visualizing neurotransmitter exocytosis that would not interfere with native cell behavior and so we turned to fluorescent molecular logic gates.

### 3.2 Molecular Logic Gates

A molecular logic gate represents a chemical system with two or more semi-stable states that possess distinct chemical or physical properties and can be reversibly interconverted.<sup>108</sup> The device has one or more inputs that provide a logical output depending on their presence (“1”) or absence (“0”). Fluorescent chemical sensors can be considered a type of logic gate as the presence of an analyte (input) can either switch the fluorescence (output) on or off. When analyte addition switches the fluorescence on, the sensor is termed a “YES” logic gate. If the fluorescence turns off, it is termed a “NOT” logic gate.<sup>109</sup> Depending on the number of inputs, a host of logic functions may exist

including YES, NOT, AND, OR, NOR, NAND, INHIBIT, and XOR (Figure 3-1).<sup>110</sup> The number of potential outputs and overall complexity of the system grows exponentially with increasing inputs.

Input 1	Input 2	Output					
0	0	0	0	1	1	0	0
0	1	0	1	0	1	1	1
1	0	0	1	0	1	0	1
1	1	1	1	0	0	0	0
		AND	OR	NOR	NAND	INHIBIT	XOR
							

**Figure 3-1.** Symbols and truth tables for several logic operations

### 3.3 NeuroSensors

Our group has developed a series of molecular logic gates for neurotransmitters that rely on one, two, or three inputs. The first sensors in the series are single-input YES logic gates called “NeuroSensors.”<sup>46</sup> NeuroSensors are designed to image neurotransmitters within vesicles and only rely on the presence of the neurotransmitter to provide a fluorescence response (Figure 3-2). They consist of a coumarin scaffold with an electron-donating group at the 7-position, an aryl group at the 4-position to modify the fluorescence response, and the analyte-sensitive aldehyde at the 3-position. As discussed in Chapter 1, the sensors fluoresce through an internal charge transfer (ICT) signal transduction mechanism. Upon neurotransmitter binding, the charge transfer increases which both red-shifts the absorption and increases the fluorescence response due to selective excitation at the longer absorption wavelength of the bound species.

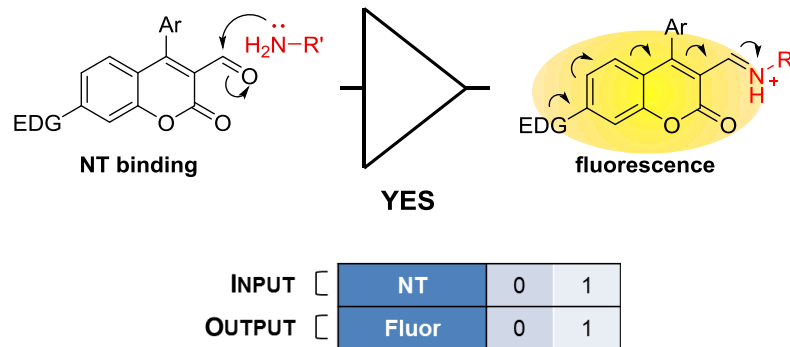


**Figure 3-2.** Logic gate and truth table for NeuroSensors. The molecular logic gates fluoresce upon neurotransmitter (NT) binding. EDG = electron-donating group. Ar = aryl group.

The practical application of NeuroSensors was tested using NeuroSensor 521 in norepinephrine- and epinephrine-secreting chromaffin cells which serve as a standard model for monitoring neurotransmitter secretion.<sup>46</sup> Upon incubation within the cells, punctate fluorescence was observed only when exciting at 488 nm, the sensor's bound wavelength (as opposed to the unbound wavelength of 440 nm) and only with norepinephrine, a primary amine neurotransmitter (as opposed to epinephrine, a secondary amine). These results indicate that the sensor is only present in its bound state within norepinephrine-secreting vesicles where the neurotransmitter is highly concentrated (Figure 3-3).<sup>54</sup>

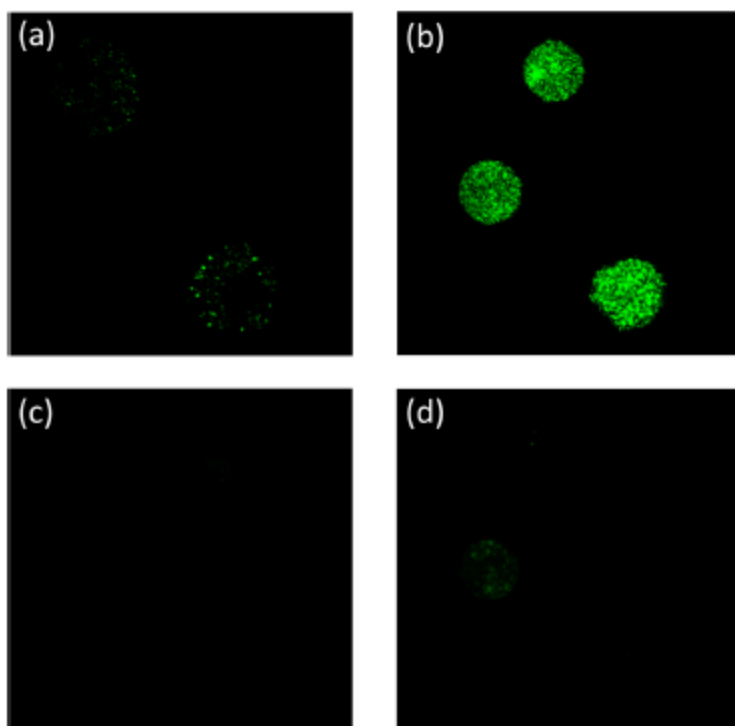
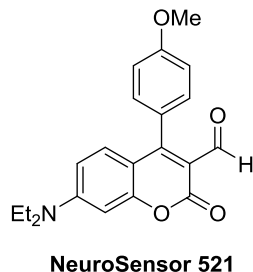


**Figure 3-3.** Confocal fluorescence microscopy of NeuroSensor 521 (0.1  $\mu\text{M}$ ) incubated with epinephrine- (a & c) and norepinephrine-secreting (b & d) chromaffin cells. Excitation at 488 nm (a & b) images the sensor in its bound state, while excitation at 440 nm (c & d) images the sensor in its unbound state. Punctate fluorescence pattern is indicative of the sensor binding within secretory vesicles.

The noted accumulation within vesicles and selective binding can be explained using Figure 3-4. We hypothesize that the sensor diffuses into the vesicle in its neutral form, binds to norepinephrine, and becomes trapped because the positively-charged iminium ion formed upon binding cannot cross the vesicular membrane. Please note that this property of becoming trapped once bound is also an important feature for the

subsequent logic gates. The sensor cannot bind to epinephrine because it is a secondary amine. Therefore, it is free to diffuse back *out* of the vesicle in its neutral form and be washed away in pre-imaging cellular preparations.

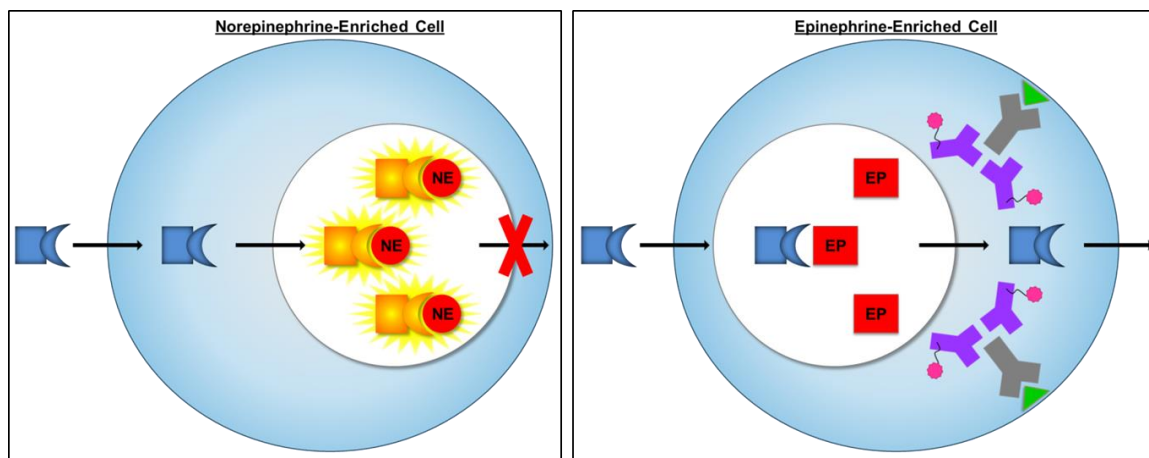


**Figure 3-4.** Pictorial representation of selective binding for NeuroSensor 521. NeuroSensor 521 (blue) can diffuse into the vesicle, bind to norepinephrine (NE) and become trapped due to the formation of a positively-charged bound complex. However, the sensor cannot bind to epinephrine (EP) and hence, diffuses out of the vesicle in its neutral unbound form. Epinephrine cells contain a specific enzyme (green triangle) that can be used to verify the selectivity of the sensor for norepinephrine over epinephrine cells using an immunofluorescence assay that tags only the EP cells with a Cy3 dye (pink ball).

### 3.4 ExoSensors

The second class of molecular logic gates that we developed are called “ExoSensors.” They were developed to monitor primary amine neurotransmitters only upon *release* from the secretory vesicle. ExoSensors are two-input AND gates that produce a fluorescence response only upon neurotransmitter binding *and* the pH change associated with exocytosis (pH 5  $\rightarrow$  7.4). They require both inputs to be present in order to produce a fluorescence output (Figure 3-5). The molecular logic gate design strategy allows for direct imaging of released neurotransmitters while minimizing interference

with native neurotransmitter trafficking due to the reversible recognition motif and small size of the sensor.

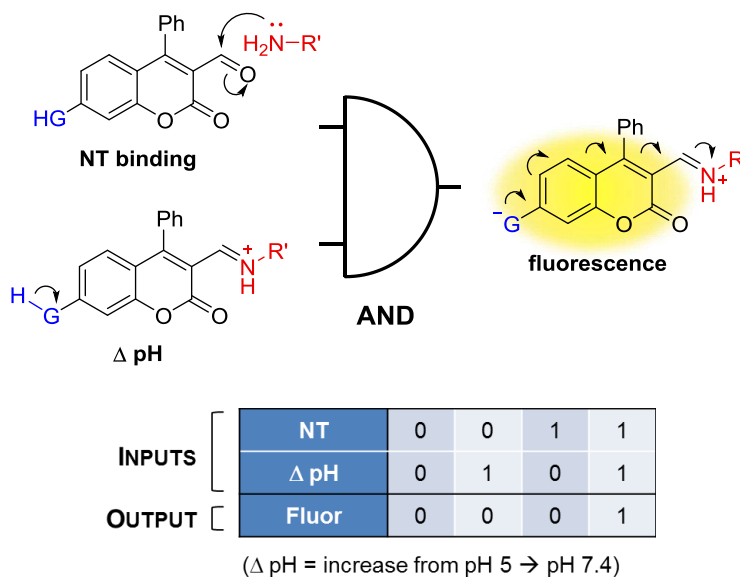


**Figure 3-5.** Logic gate and truth table for ExoSensors. The molecular logic gates respond only upon concomitant neurotransmitter (NT) binding and the pH change associated with exocytosis.  $\Delta$  pH = pH increases from 5 to 7.4.

### 3.5 Design of ExoSensors

We built our design using the NeuroSensor 521 model as it was shown to be effective at binding norepinephrine, a primary amine neurotransmitter, in live secretory cells (Figure 3-3).<sup>46</sup> While the coumarin aldehyde could technically bind to any primary amine analyte present in the cell, “specialized” neurons (e.g., glutamatergic, dopaminergic, serotonergic, etc.) package only one specific neurotransmitter at very high concentrations, and would therefore be the only amine visualized, especially given the relatively weak binding constant. To image the *exocytosis* of these specially packaged neurotransmitters, we sought to create a pH-sensitive analog of NS521 that would have

weak fluorescence in the synaptic vesicle (pH 5) but strong fluorescence in the synaptic cleft (pH 7.4).

As depicted in Figure 3-6, the dual-analyte sensor can enter the vesicle and selectively bind to the highly concentrated primary amine neurotransmitter, yet remain fluorescently “off” due to the acidic environment. Formation of a positively-charged complex causes the bound sensor to become trapped within the vesicle, encouraging sensor accumulation. Exocytosis releases the bound sensor complex into the synaptic cleft and the change in environmental pH switches the fluorescence “on” for only the released sensor in its bound state.

It is imperative that the sensor enters the vesicle and binds to the neurotransmitter *before* release. The reason is that binding may take seconds to occur, whereas exocytosis occurs on a millisecond timescale.<sup>111,112</sup> The sensor would not be able to keep up with synaptic firing. Our strategy allows the sensor to bind to the neurotransmitter and lay in wait until vesicular release. The turn-on fluorescence response is switched on by *deprotonation* of the bound complex which occurs on a much faster microsecond timescale.



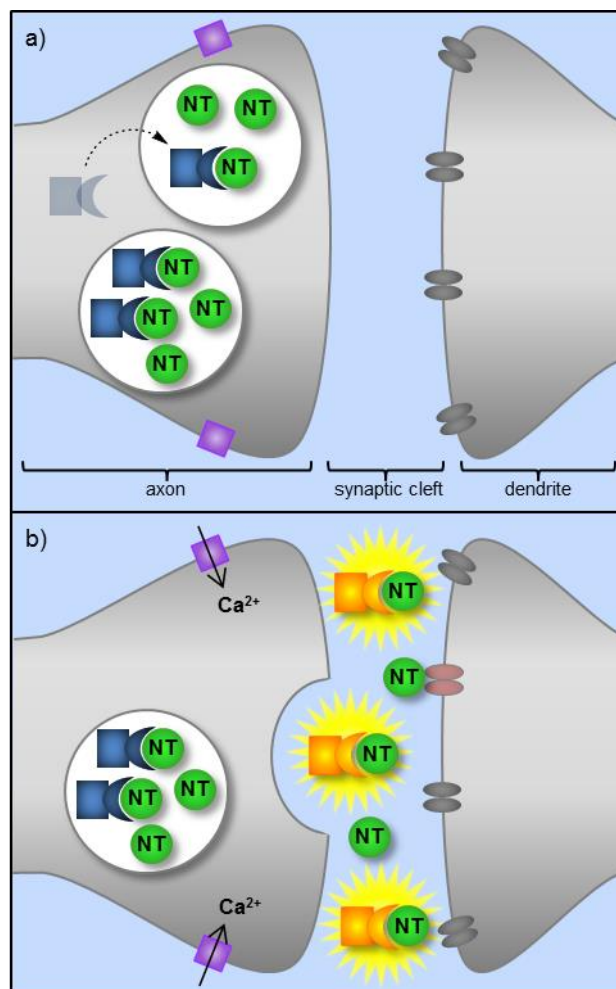


**Figure 3-6.** Sensing mechanism of ExoSensors. a) Sensor enters vesicle and selectively labels the neurotransmitter (NT). The bound complex accumulates but fluorescence is “off” due to low pH (~5). b) Influx of Ca<sup>2+</sup> triggers exocytosis. The increase in environmental pH in the synaptic cleft (7.4) switches the fluorescence “on.”

To create a sensor that would respond in this way, the diethyl amino group of NS521 was exchanged for an electron-poor sulfonamide that can be deprotonated at neutral pH to become electron-rich (Figure 3-7). The sensor fluoresces via an intramolecular charge transfer (ICT) state in which the deprotonated sulfonamide acts as an electron donor and the iminium ion acts as an electron acceptor. Both analyte binding and sulfonamide deprotonation enhance the charge transfer across the fluorophore. In addition, both binding to the analyte and deprotonation of the sensor produce large

bathochromic shifts which means exciting at the highest possible wavelength of absorption permits visualization of only the active neurotransmitters in the synapse. Any unbound sensor would not be visualized as it absorbs at a much lower wavelength.

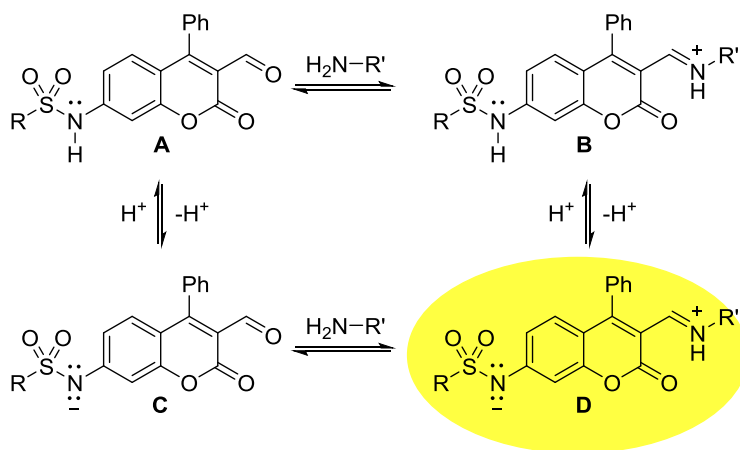


**Figure 3-7.** Neurotransmitter binding and deprotonation of ExoSensors

In the cytosol, the sensor (**A**) will exist largely in the deprotonated and unbound form (**C**) due to the neutral pH and relatively low concentration of amines, respectively. Both forms **A** and **C** would have weak fluorescence as they lack the iminium ion as a strong electron acceptor. When the sensor enters the vesicle, it binds to the highly concentrated neurotransmitters and produces the iminium ion **B**. Form **B** would have marginal electron transfer and weak fluorescence since the protonated sulfonamide is a weak electron donor. Upon exocytosis, the bound complex enters the synaptic cleft, becomes deprotonated (structure **D**), and produces a marked fluorescence increase due to the enhanced ICT. To obtain the maximum fluorescence increase upon exocytosis, the sensor  $pK_a$  must be between the pH of the vesicle (5) and the synaptic cleft (7.4). The

sulfonamide functional group was chosen as literature precedent indicated the  $pK_a$  would be approximately 6.<sup>113</sup>

### 3.6 Synthesis of ExoSensors

A series of synthetic schemes were devised in order to achieve a coumarin aldehyde sensor with a sulfonamide appended at the 7-position. The first attempt to synthesize the sensor was made using nitrogen protecting groups (Figure 3-8).

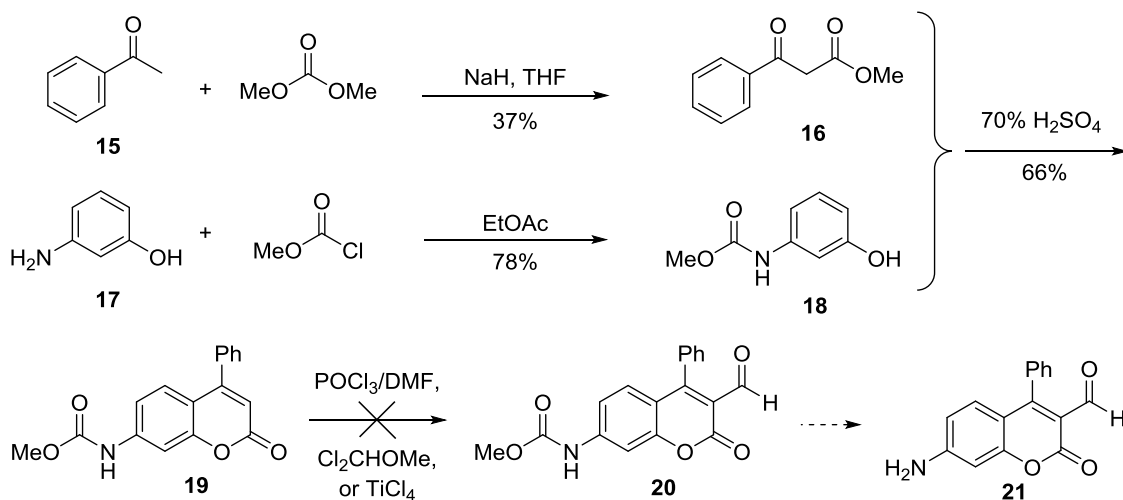


**Figure 3-8.** Synthetic strategy using carbamate protecting groups

The strategy was to take 3-aminophenol (**17**) and protect the nitrogen so that a Pechmann reaction with compound **16** would cause cyclization to preferentially occur on the oxygen of **17** which is inherently less nucleophilic than the nitrogen. After cyclization, we would formylate **19** to make compound **20**. Deprotection of the nitrogen to make compound **21** would then allow us to do a substitution reaction with a sulfonyl chloride to afford the final product. The Pechmann cyclization occurred using 70%

H<sub>2</sub>SO<sub>4</sub> at room temperature but would not formylate under either Vilsmeier or Reiche conditions. We believe the reasoning was because the electron-withdrawing carbamate on **19** reduced the nucleophilicity of the alkene (Figure 3-9).

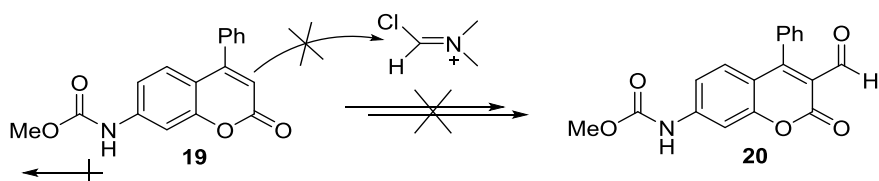


**Figure 3-9.** The carbamate-protected aminocoumarin is deactivated toward Vilsmeier formylation

The next strategy was to use a more electron-donating allyl protecting group based on literature precedent (Figure 3-10).<sup>82</sup> The nitrogen of 3-aminophenol would be protected using allyl bromide so that the Pechmann cyclization would occur off of the oxygen to form the coumarin body. The sensor would then be formylated, the allyl groups removed, and the sulfonyl group appended via a substitution reaction.

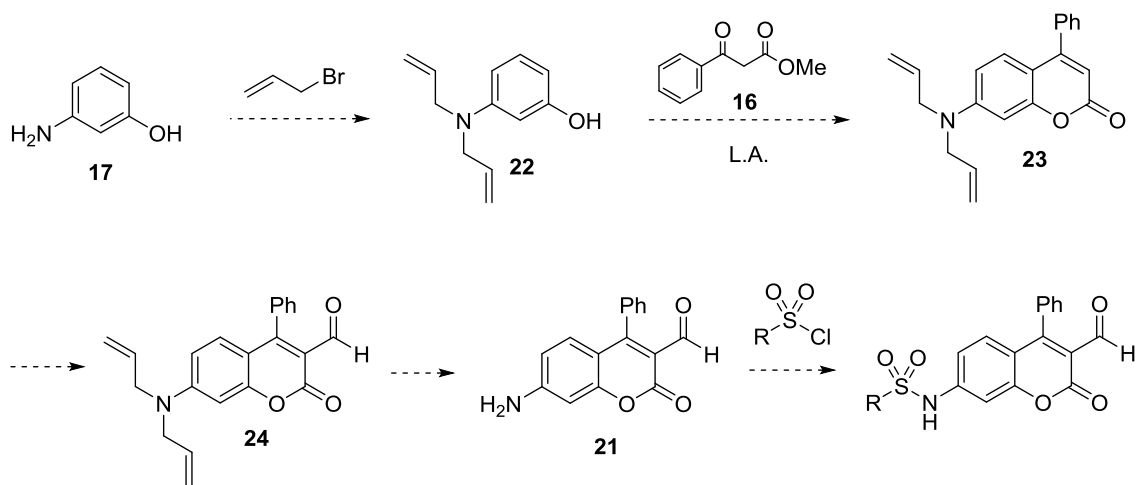


**Figure 3-10.** Synthesis strategy using allyl protecting groups

The allyl groups were placed on the nitrogen in good yield, however, the Pechmann cyclization did not go smoothly and provided several unwanted byproducts (Figure 3-11).

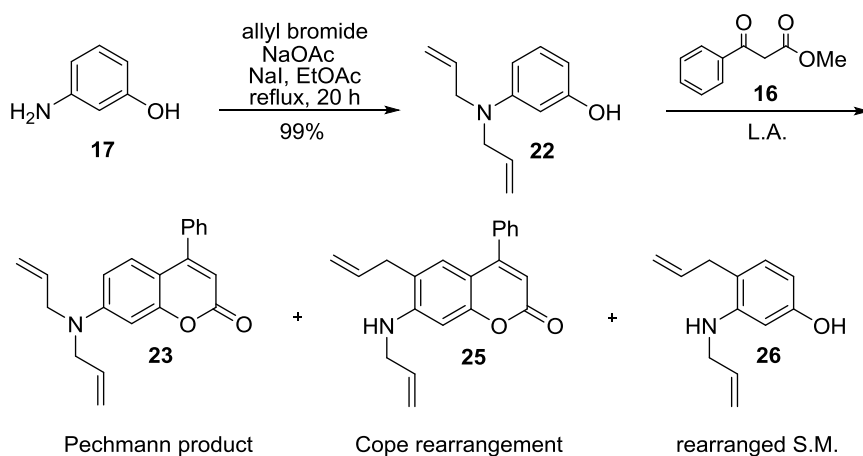


**Figure 3-11.** Rearranged products from the Pechmann cyclization

We then chose to add allyl groups to a 7-aminocoumarin (27) that had already been cyclized. We would then formylate, deprotect, and append a sulfonyl group (Figure 3-12). The difficulty arose in removing the allyl protecting groups. After several tries using barbituric acid and methane sulfonyl chloride, only small amounts of the mono-allylated coumarin were isolated.

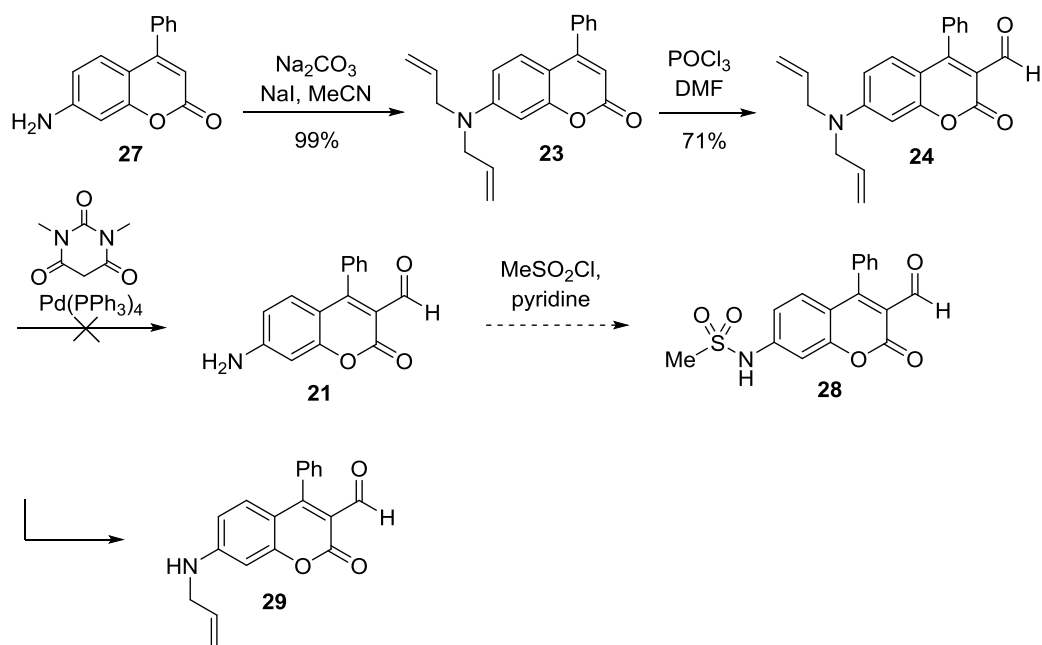


**Figure 3-12.** Formylation of allyl-protected aminocoumarin

Given the inefficiency of protecting groups and our difficulties with both cyclization and formylation, we decided on a different strategy which was formation of the coumarin body using a Claisen condensation which would eliminate the need to protect the nitrogen. Therefore, we took 3-aminophenol and acylated using acyl chloride to give compound **30** (Figure 3-13). After deacylation of the nitrogen and sulfonation, we attempted to do a Claisen condensation, however, only starting material was isolated. The reaction mechanism requires that the ketone be deprotonated for the reaction to go forward, but we believe that the phenol and sulfonamide were deprotonated first. Additional deprotonation of the acyl group (as is necessary to create the enolate nucleophile), would cause the molecule to become trianionic which is very unfavorable.

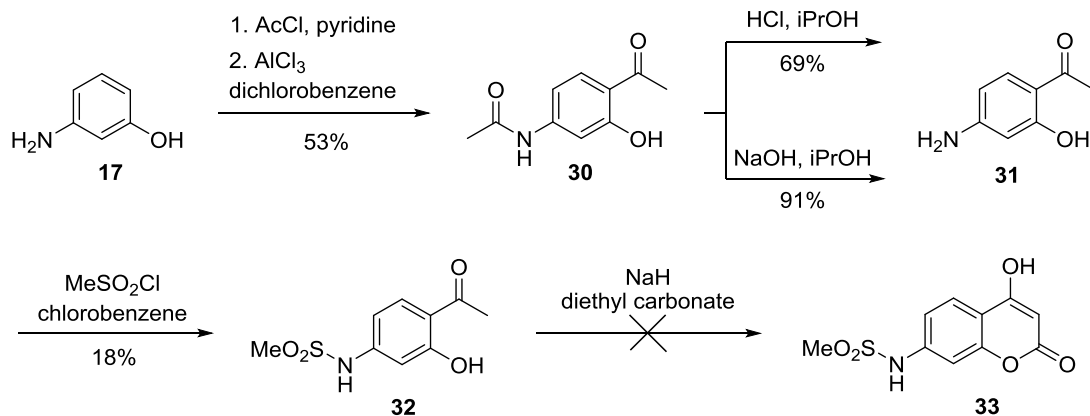


**Figure 3-13.** Claisen condensation of an aryl sulfonamide

Another synthetic method that doesn't use protecting groups involved purchasing compound **34** which we could triflate, couple to, and then oxidize to the aldehyde (Figure 3-14). The first two steps worked smoothly, however the oxidation reaction only returned starting material. The reaction was successively heated hotter until the starting material decomposed.

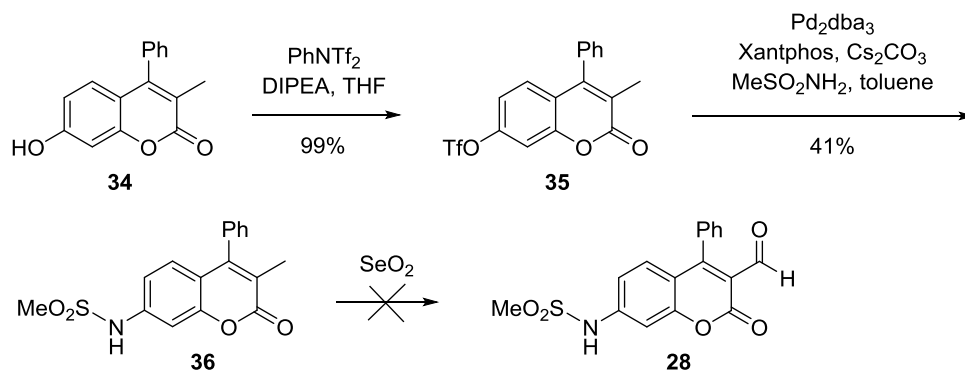


**Figure 3-14.** Synthesis by oxidizing to the aldehyde

The final ExoSensors were ultimately prepared by combining several of the aforementioned strategies (Figure 3-15). First, a Claisen condensation of compound **37**

formed the coumarin core. Vilsmeier conditions both chlorinated and formylated the ring which was then functionalized with a benzene ring via Suzuki coupling. Demethylation of the methoxy group followed by triflation of the phenol yielded compound **42**. Lastly, various sulfonamide substituents were appended using Buchwald-Hartwig coupling conditions to produce the final sensors. Both aliphatic and aromatic sulfonamides were coupled in hopes of optimizing the fluorescence response produced. It should be noted that several amides were also coupled to the coumarin 7-position in case we wrongly predicted the  $pK_a$  of a 7-sulfonamide coumarin. They were not used further, however, due to poor water-solubility.

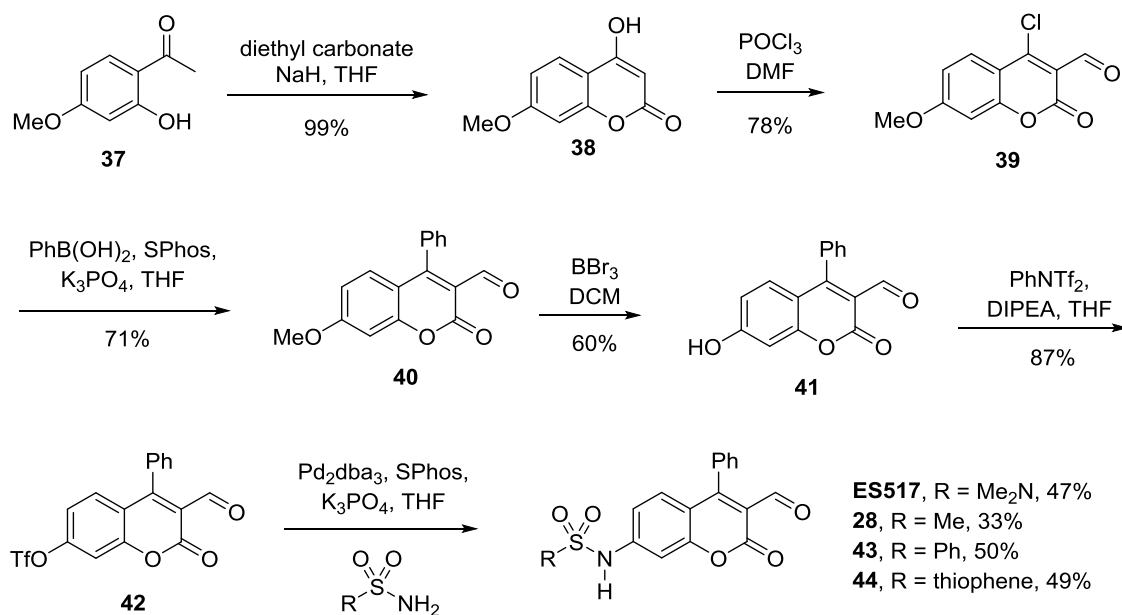


**Figure 3-15.** Synthesis of ExoSensors using a Buchwald-Hartwig coupling strategy



## 3.7 Spectroscopic Results

### 3.7.1 pH Titrations

As mentioned earlier, the  $pK_a$  of the sensor needs to be between 5.0 and 7.4 in order to be protonated in the synaptic vesicle and deprotonated in the synaptic cleft. The acidity of the sensor was determined by titrating in aliquots of aqueous HCl or NaOH and monitoring the absorbance or fluorescence intensity over a wide pH range. Figure 3-16 is a representative example of a pH titration using ExoSensor 517 (ES517) and monitoring both absorbance and fluorescence. The protonated sensors absorb at  $\sim 370$  nm and deprotonation causes an approximate 50 nm bathochromic shift due to the increased charge transfer across the pi-system of the fluorophore. The pH was plotted against the absorbance or fluorescence to produce a sigmoidal curve where the inflection point represents the  $pK_a$ . ES517 had the highest  $pK_a$  of 6.3 and the remaining  $pK_a$  values decreased along with the donating ability of the sulfonyl substituent.

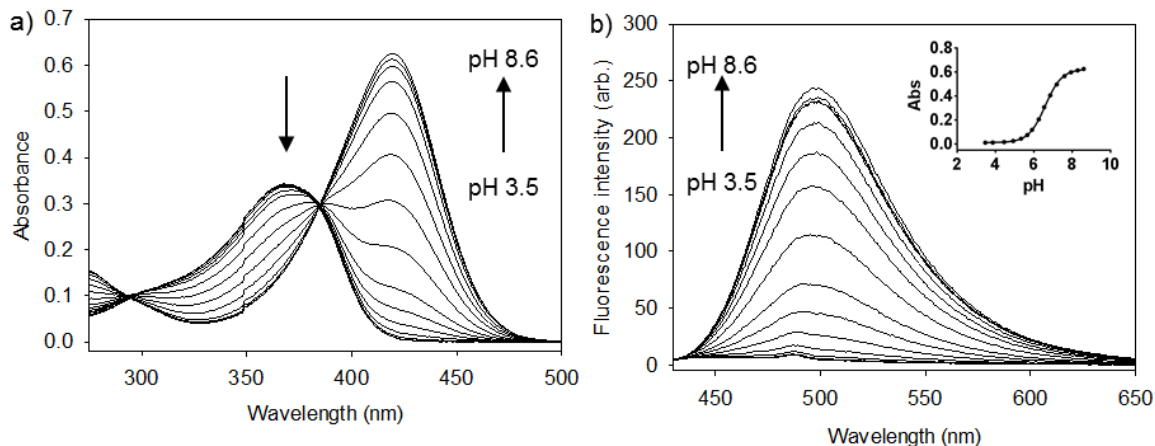


**Figure 3-16.** a) UV/vis and b) fluorescence pH titration of ES517 (20  $\mu\text{M}$ ) in buffer (50 mM bis tris propane, 120 mM NaCl, 1% DMSO) adjusting the pH from 3.5 to 8.6. Inset is the fit to a sigmoidal regression curve where the inflection point represents the  $\text{p}K_a$ .

To test the  $\text{p}K_a$  of the bound sensors, as they would be in the vesicle, ES517 was saturated with glutamate and the spectroscopic properties measured over a pH range (Figure 3-17). The protonated form of the bound sensor (Figure 3-7, structure **B**) absorbed at 368 nm. Upon deprotonation, two bands were observed at 428 and 458 nm. The 428 nm band was assigned to the unbound deprotonated form of the sensor (structure **C**). The 458 nm band therefore represents the bound, deprotonated sensor (structure **D**). The plot of pH vs. intensity was fit to a pH isotherm and the  $\text{p}K_a$  determined to be 6.3, the same  $\text{p}K_a$  as the unbound sensor. This result indicates that binding to the analyte does not affect the acidity of the sensor. All absorption wavelengths of the bound and unbound sensors in addition to bound and unbound  $\text{p}K_a$  values are reported in Table 3-1.

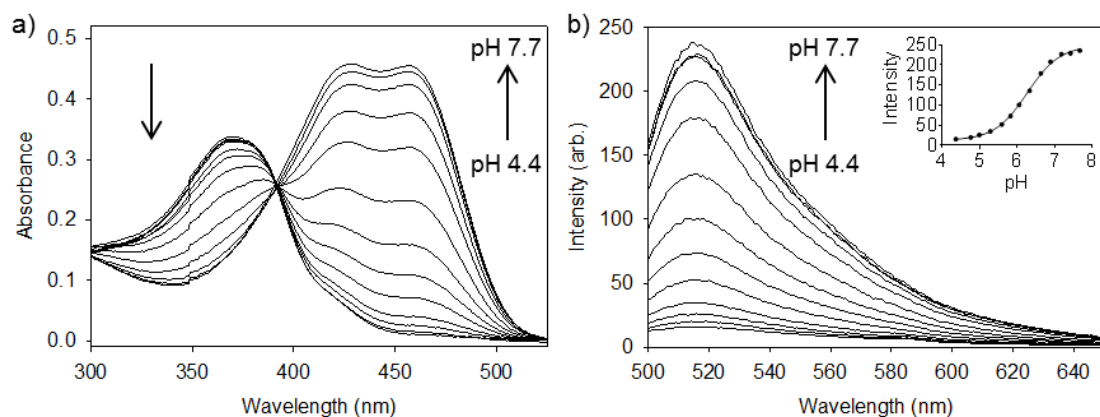


**Figure 3-17.** a) UV/vis and b) fluorescence pH titration of ES517 (20  $\mu$ M) with 300 mM glutamate in buffer (50 mM bis-tris propane, 120 mM NaCl, 1% DMSO) adjusting the pH from 4.4-7.7.  $\lambda_{\text{ex}} = 488$  nm. Inset is the fit to a sigmoidal regression curve where the inflection point represents the  $pK_a$ .

**Table 3-1.** Absorption Wavelengths and  $pK_a$  Values of ExoSensors

Sensor	$\lambda_{\text{max}}$ (nm) <sup>a</sup> GH/G-	Unbound $pK_a$ <sup>b</sup>	Bound $pK_a$ <sup>c</sup>
ES517	368/419	6.3	6.3
28	365/420	5.9	6.0
43	373/418	5.7	5.7
44	366/416	5.2	5.3

<sup>a</sup>Absorption maxima of the protonated and deprotonated forms of the sensor. <sup>b</sup> $pK_a$  values were determined by adding aliquots of aq. HCl or NaOH to 20  $\mu$ M sensor in buffer (50 mM bis-tris propane, 120 mM NaCl, 1% DMSO). <sup>c</sup>Glutamate was added (300 mM) to force the sensor into the bound state. The complex was monitored over a pH range.

### 3.7.2 Analyte Titrations

The ExoSensors were titrated with primary amine neurotransmitters (glutamate, norepinephrine, dopamine, and serotonin) and monitored using UV/Vis and fluorescence spectroscopy. Summarized in Table 3-2 are the association constants ( $K_a$ ), fluorescent enhancements to analyte addition ( $I_{\text{sat}}/I_0$ ), and fluorescent

enhancements of the neurotransmitter-bound ExoSensors to pH conditions simulating exocytosis ( $I_{\text{pH } 7.4}/I_{\text{pH } 5.0}$ ).

**Table 3-2.** Binding Affinities and Fluorescence Enhancements of ExoSensors with Various Primary Amine Neurotransmitters

Sensor	$K_a$ ( $M^{-1}$ ) <sup>a</sup>				$I_{\text{sat}} / I_0$ <sup>b</sup>				$I_{\text{pH } 7.4} / I_{\text{pH } 5.0}$ <sup>c</sup>			
	Glu	Nor	Dop	Ser	Glu	Nor	Dop	Ser	Glu	Nor	Dop	Ser
<b>ES517</b>	8.6	49	55	54	12	14	10	0.4	12	5.3	5.5	1.5
<b>28</b>	3.7	58	76	57	64	8.7	3.3	0.3	5.5	4.2	2.4	0.7
<b>43</b>	2.8	156	105	110	150	10	4.7	0.7	3.6	2.2	2.1	1.4
<b>44</b>	3.8	75	11	46	14	2.3	0.5	0.1	1.9	1.3	1.3	1.1

<sup>a</sup>Binding constant of sensor (10  $\mu\text{M}$ ) with analyte (1.5 M Glu or 100 mM Nor, Dop, Ser) in buffer (50 mM bis-tris propane, 50 mM  $\text{Na}_2\text{S}_2\text{O}_3$ , 1% DMSO, pH 7.4);  $\lambda_{\text{ex}} = 488$  nm.

<sup>b</sup>Fluorescent enhancement upon binding to the analyte.  $I_{\text{sat}}$  is taken from the theoretical maximum of the binding isotherm. <sup>c</sup>Fluorescent enhancement of sensor (10  $\mu\text{M}$ ) saturated with analyte (300 mM Glu or 100 mM Nor, Dop, Ser) mimicking exocytosis from pH 5.0 to pH 7.4;  $\lambda_{\text{ex}} = 488$  nm. Glu = glutamate, Nor = norepinephrine, Dop = dopamine, Ser = serotonin.

Addition of all amine analytes induced a bathochromic shift of  $\sim 40$  nm in the absorbance indicating formation of the iminium ion from the coumarin aldehyde (Figure 3-18). The sensors bound to all amine analytes, however, with varying degrees of affinity. Glutamate, the only amino acid, bound to all sensors with weak affinity ( $<10 M^{-1}$ ) while the remaining biogenic amines bound with double- or triple-digit association constants. The weaker binding of glutamate is likely due to the reduced nucleophilicity of nitrogen and intramolecular electrostatic interaction with the alpha carboxylate. Lower binding constants, however, are actually preferred to allow continuous monitoring of vesicular glutamate concentrations which have been measured from 50-210 mM.<sup>51-52</sup>

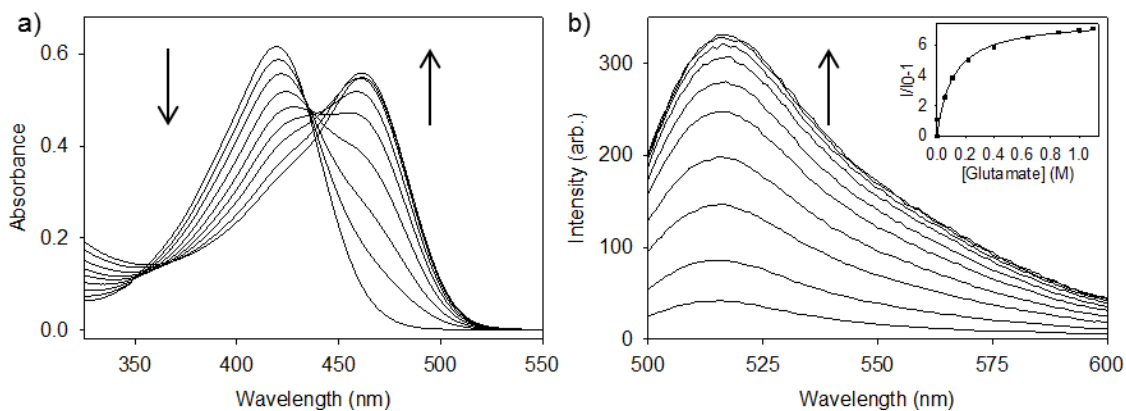


**Figure 3-18.** a) UV/vis and b) fluorescence titration of ES517 (20  $\mu\text{M}$ ) in buffer (50 mM bis-tris propane, 50 mM  $\text{Na}_2\text{S}_2\text{O}_3$ , 1% DMSO, pH 7.4) adding 20-800  $\mu\text{L}$  aliquots of 1.5 M glutamate.  $\lambda_{\text{ex}} = 488$  nm. Inset is the fit to a one-site binding isotherm.

The fluorescence intensity increased with the addition of most amine analytes when excited at 488 nm, a wavelength that is commonly available with standard microscopy setups and long enough to excite only the bound deprotonated sensor. The only analyte exception was serotonin, which possesses an electron-rich indole that tends to quench fluorescence through photoinduced electron transfer (PET). The fluorescence enhancements upon analyte addition trend such that glutamate > norepinephrine > dopamine > serotonin.

Given that ES517 possessed the most optimal spectroscopic properties, it was monitored with additional analytes and the key results are presented in Table 3-3. As with the non-pH-sensitive NS521, all primary amine neurotransmitters bound relatively weakly with a preference for aromatic neurotransmitters. By contrast, the non-aromatic neurotransmitters produced the largest change in fluorescence upon binding at pH 7.4 due to PET quenching effects from the electron-rich aromatic groups. Importantly, all non-aromatic neurotransmitters produced large fluorescence increases upon pH change from 5.0 to 7.4. The catecholamines gave smaller, but still

significant fluorescence increases and serotonin was unique in that it gave little fluorescence change (Figure 3-19). Taken together, our results suggest that ES517 is the best candidate to directly visualize glutamate release as it would provide the greatest turn-on fluorescence response to exocytosis.

**Table 3-3.** Binding and spectroscopic properties of ES517 with various primary amine neurotransmitters

Neurotransmitter <sup>a</sup>	$K_a$ ( $M^{-1}$ )	$I_{sat}/I_0$ <sup>b</sup>	$I_{pH7.4}/I_{pH5}$ <sup>c</sup>
glutamate	8.6	12	12 <sup>d</sup>
GABA	8.3	27	11 <sup>d</sup>
glycine	9.2	25	10 <sup>d</sup>
norepinephrine	49	14	5.3 <sup>e</sup>
dopamine	55	10	5.5 <sup>e</sup>
serotonin	54	0.5	1.5 <sup>e</sup>

<sup>a</sup>Binding studies of ES517 (20  $\mu$ M) with saturating amounts of analyte in buffered conditions (50 mM bis-tris propane, 50 mM  $Na_2S_2O_3$ , 1% DMSO, pH 7.4) with  $\pm 10\%$  error based on triplicate titration. <sup>b</sup>Fluorescence enhancement upon binding analyte at pH 7.4 ( $I_{sat}$  taken from the theoretical max of the binding isotherm).  $\lambda_{em} = 517$  nm. <sup>c</sup>Ratio of fluorescence at pH 7.4 vs. 5.0 of ES517 (20  $\mu$ M) saturated with analyte. <sup>d</sup>Saturated with 300 mM analyte. <sup>e</sup>Saturated with 100 mM analyte.

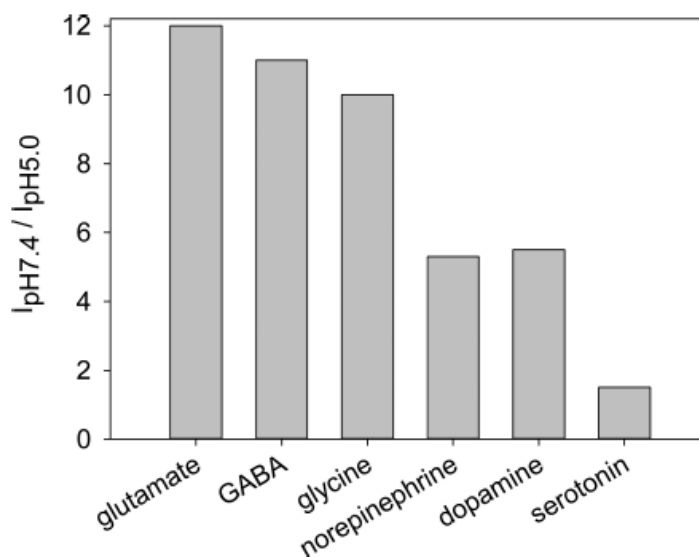


**Figure 3-19.** Fluorescence enhancements of ES517 saturated with various amine analytes under pH conditions simulating exocytosis.

### 3.7.3 Response to Exocytosis

The most important parameter tested was the fluorescence increase of the analyte-bound sensor when changing the pH from 5 to 7.4 ( $I_{\text{pH } 7.4} / I_{\text{pH } 5.0}$ ) which mimics neurotransmitter release from the acidic vesicle to the neutral synapse. The glutamate-bound ES517 gave the greatest fluorescence enhancement over the pH range than did all other sensor-amine combinations. There was a clear correlation between the  $\text{p}K_{\text{a}}$  of the sensor and the pH jump from 5 to 7.4 that mimics the release of the neurotransmitter from the vesicle to the synaptic cleft (Figure 3-20).

The ratio of  $I_{\text{pH } 7.4} / I_{\text{pH } 5.0}$  is the greatest for ES517 because it has the highest  $\text{p}K_{\text{a}}$ . The fluorescence intensity at pH 5.0 is much lower due to the majority of the sensor molecules being protonated. Therefore, when you divide by a smaller denominator, the result is a greater fluorescence enhancement. The thiophene-substituted sensor, on the other hand, has a  $\text{p}K_{\text{a}}$  of  $\sim 5$  which means that in the vesicle, approximately half of the sensor molecules are already deprotonated and contributing to higher background fluorescence.

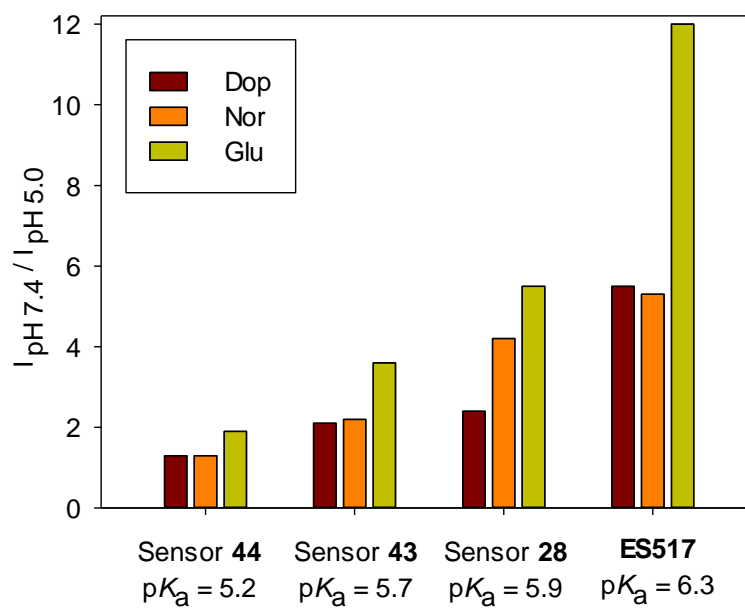


**Figure 3-20.** Relationship between the sensor  $pK_a$  and the fluorescence change of the bound sensor under conditions mimicking exocytosis ( $I_{\text{pH } 7.4} / I_{\text{pH } 5.0}$ ). Dop = dopamine, Nor = norepinephrine, Glu = glutamate. Serotonin quenches fluorescence and is therefore not shown in the comparison.

### 3.8 Cellular Analysis

The practical use of this method was evaluated by incubating ES517 with live norepinephrine-secreting chromaffin cells. Chromaffin cells are taken from the adrenal glands but remain one of the standard models used to study cellular exocytosis of norepinephrine and epinephrine because they function similar to neuronal cells and are easily obtained. The cells were imaged using both confocal and total internal reflection fluorescence (TIRF) microscopies (Figure 3-21). In confocal microscopy, light from a laser is passed through a pinhole, reflected by a mirror, and focused on a small spot on the specimen. This technique allows for the depth of field to be tightly controlled during imaging. On the other hand, TIRF directs the laser light at a critical incident angle so that nearly all of the light is reflected back. This critical angle is achieved by considering the



refractive indices of the materials at the interface (i.e. aqueous media and a glass slide). When total internal reflection occurs, an evanescent wave is produced which illuminates only fluorophores within ~100 nm of the interface. This technique provides low background as only a shallow slice of the sample is imaged and we believed it would aid in visualizing events occurring at individual vesicles within a secretory cell.

Confocal fluorescence microscopy of the cells revealed punctate fluorescence, similar to that seen for NS521 (Figure 3-21a,b). We believe this is due to the accumulation of ES517 within secretory vesicles. TIRF imaging also shows punctate fluorescence with very low background. These preliminary studies are promising and future work will include excitation of the cells to induce exocytosis. We would first have to confirm that ES517 has accumulated within the secretory vesicles, then reduce the laser power so that a turn-on fluorescence response could be visualized upon stimulation. A variety of reagents could be used either to stimulate exocytosis or collapse the pH gradient of the vesicle including potassium chloride, chloroquine, nicotine, and reserpine. Electrical stimulation could also be used. If these studies go as expected, we will have produced the first fluorescent molecular logic gate that directly detects the release of neurotransmitters.

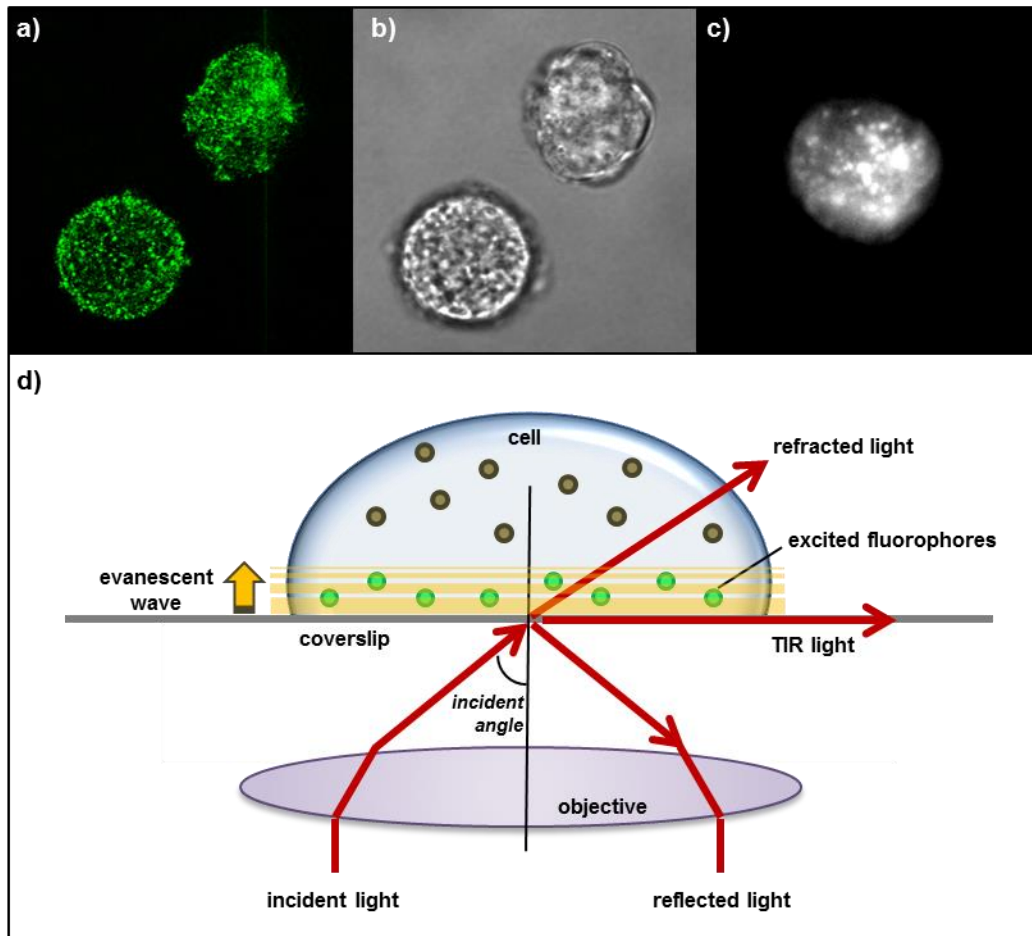


**Figure 3-21.** ES517 in live norepinephrine-secreting chromaffin cells viewed by a) confocal fluorescence microscopy, b) brightfield, and. c) total internal reflection fluorescence (TIRF) microscopy. d) Explanation of TIRF. A critical incident angle of light must be directed at the sample in order to achieve total internal reflection. This produces an evanescent wave that excites only the fluorophores within ~100 nm of the interface.

In summary, a series of two-input fluorescent molecular logic gates were developed for the visualization of neurotransmitters released upon exocytosis. The design strategy exploits high vesicular neurotransmitter concentrations and the pH gradient between the vesicle and synaptic cleft. When bound to glutamate, ES517 afforded a 12-fold fluorescence enhancement to conditions mimicking synaptic release and further studies are underway to optimize the fluorescence response to quenching analytes. ES517

serves as a potential research tool for studying the mechanisms underlying neurotransmission. Preliminary *in vitro* tests in chromaffin cells show potential and we hope to further investigate the utility of these sensors in neurons and brain slices.

## CHAPTER FOUR

### Three-Input Molecular Logic Gates for Glutamate & Zinc Corelease

#### 4.1 Background

Glutamate, the primary excitatory neurotransmitter, mediates roughly half of all synaptic transmissions in the central nervous system and affects learning, memory, motor control, and cognition.<sup>114</sup> There exists a subset of glutamatergic neurons in the forebrain (~10%) that contain high concentrations of glutamate *and* zinc which are coreleased into the synaptic cleft.<sup>115,116,117</sup> Zinc, also an important neuromodulator, affects enzyme catalysis, gene expression regulation, neural tissue growth and development, and modulation of brain excitability through effects on voltage-gated calcium channels<sup>118,116b,115</sup> Moreover, researchers have recently observed correlations between synaptically released zinc and increased concentrations of hyperphosphorylated tau, the chief component of neurofibrillary tangles in Alzheimer's disease (AD).<sup>119</sup> It also promotes oligomerization of amyloid- $\beta$ , also a known contributor to AD (Figure 4-1).<sup>120</sup> Therefore, understanding the specific contributions of zinc in the neuronal synapse could elucidate disease-causing mechanisms.

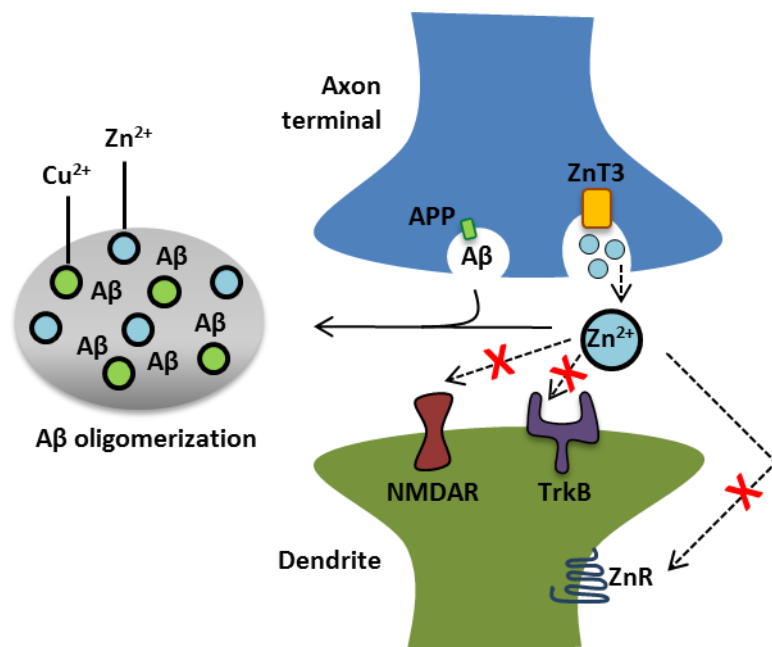


**Figure 4-1.**  $Zn^{2+}$ -mediated amyloid- $\beta$  oligomerization and disruption of physiology by formation of amyloid- $\beta$ - $Zn^{2+}$  complexes. Zinc can encounter amyloid- $\beta$  upon glutamatergic neurotransmission and form oligomers. The greater the zinc concentration, the more insoluble the oligomer. Sequestration of zinc from its normal targets can disrupt physiology necessary for memory events among other things. APP =  $\beta$ -amyloid precursor protein; ZnR = metabotropic  $Zn^{2+}$ -sensing receptor, ZnT3 =  $Zn^{2+}$  transporter 3.

However, much is still unknown as to zinc accumulation and release from synaptic vesicles. Zinc-containing glutamatergic neurons are heavily studied, particularly with respect to the fate of the zinc ions post-exocytosis. To selectively image transmitter release from these neurons, in the presence of zinc-independent glutamatergic neurons, it would be necessary to build a sensor that not only responds to both zinc and glutamate, but also to the change in pH upon exocytosis. Here, we report a series of three-input AND fluorescent molecular logic gates that serve as a proof-of-concept for directly imaging the corelease of glutamate and zinc from glutamatergic secretory vesicles. The molecular logic gates described here are designed to exploit the copackaging of highly concentrated glutamate and zinc in glutamatergic boutons in order to directly visualize

their corelease upon exocytosis. Information about glutamate and zinc corelease would offer significant insight into the mechanisms underlying neurotransmitter dysregulation and the progression of neurodegenerative diseases without altering transmission activity.

## 4.2 Previous Work

Recently, we have developed a series of increasingly-sophisticated fluorescent molecular logic gates for the direct visualization of primary amine neurotransmitters (Figure 4-2).<sup>46, 121</sup> The sensors consist of a coumarin core with functionalities integrated into the fluorophore  $\pi$ -system. The sensor aldehyde reversibly binds to primary amine neurotransmitters under physiological conditions to create a positively-charged iminium ion which induces a large bathochromic shift in absorbance. By exciting at the new, longer wavelength, a fluorescence increase is observed due to the enhanced internal charge transfer (ICT) across the  $\pi$ -system.

NS521 was developed as a single-input YES fluorescent molecular logic gate for the direct visualization of norepinephrine and dopamine.<sup>46</sup> The sensor capitalizes on the high concentrations of catecholamines (0.5 – 1.0 M) and acidic environment within secretory vesicles of specialized cells in order to afford selective labeling over typical cellular amines which are present at significantly lower concentrations.<sup>52,122,123,51,56</sup> We extended the utility of this method to sense neurotransmitter release by developing ES517, a dual-input AND molecular logic gate.<sup>121</sup> ES517 incorporates a pH-sensitive functionality into the coumarin-3-aldehyde scaffold and only fluoresces upon concomitant neurotransmitter binding and the pH change associated with exocytosis.

Release of the bound complex from the acidic vesicle (pH 5) into the neutral synaptic cleft (pH 7.4) would allow for direct visualization of *only* released neurotransmitters.

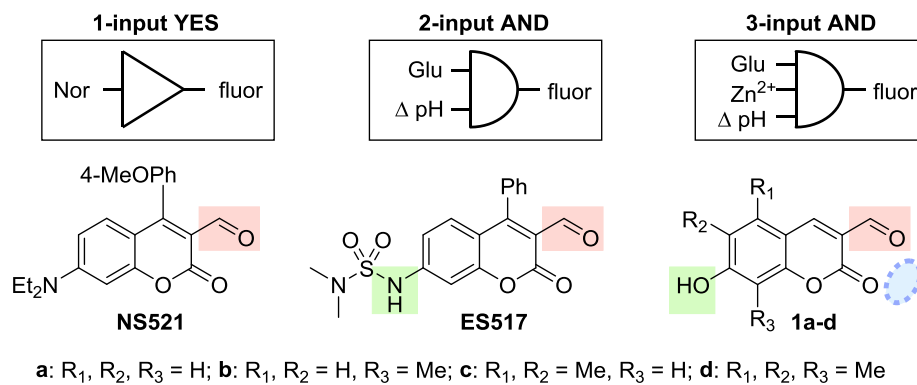


**Figure 4-2.** a) Molecular logic gates for neuronal imaging. Nor = norepinephrine, Glu = glutamate, fluor = fluorescence output, Δ pH = increase in pH from 5.0 to 7.4 (mimics exocytosis from the acidic vesicle to the synaptic cleft).

### 4.3 Sensor Design

The three-input AND gates (**56a-d**) respond to glutamate, zinc, and pH through functional groups that are integrated into the  $\pi$ -system of the fluorophore (Figure 4-3). The aldehyde at the coumarin 3-position reversibly forms imines with glutamate and thereby, creates a multi-point binding pocket with the lactone carbonyl oxygen with which zinc can coordinate in a cooperative fashion.<sup>124</sup> The hydroxyl group at the 7-position imparts pH-sensitivity which acts as the final switch for a turn-on fluorescence response. Deprotonation of the hydroxyl group increases the absorbance ~45 nm, permitting selective visualization of only the deprotonated species. The sensor-glutamate-zinc bound complex would be weakly fluorescent until exocytosis when the increase in pH would switch the fluorescence on. Methyl groups were appended to the coumarin

body to increase absorption wavelengths and therefore optimize the fluorescence response when using a specific laser wavelength.

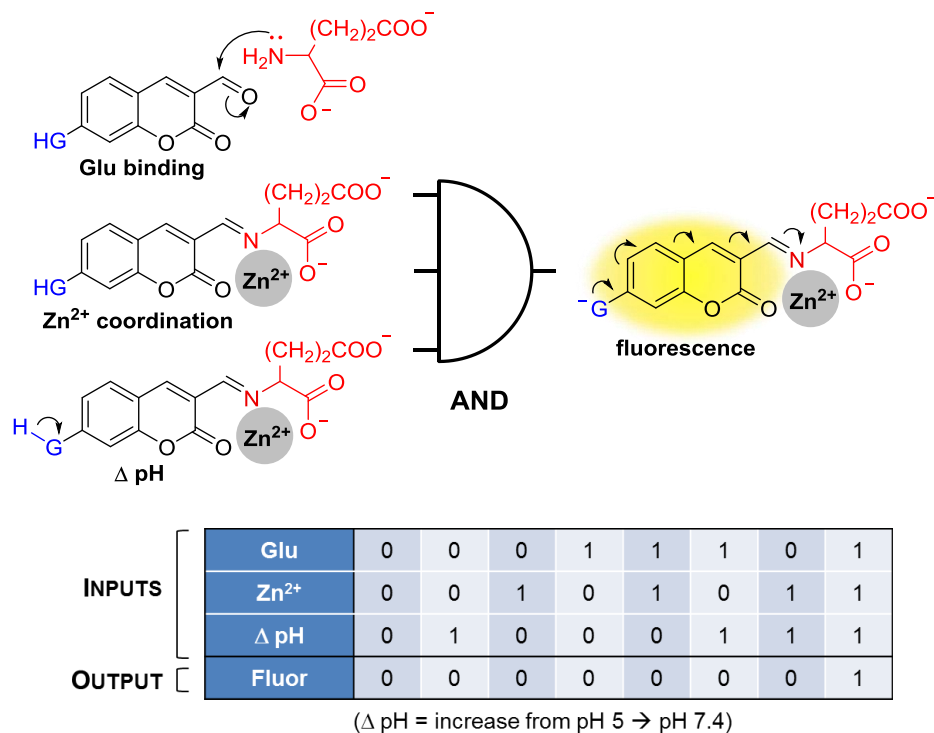


**Figure 4-3.** Logic gate and truth table for three-input AND gates. The molecular logic gates respond only upon concomitant neurotransmitter (NT) binding, Zn<sup>2+</sup> coordination, and the pH change associated with exocytosis. Δ pH = pH increases from 5 to 7.4.

#### 4.4 Synthesis

The hydroxysalicylaldehyde starting materials (**52a-d**) for the 3-input AND gates were synthesized following literature precedent (Figure 4-4).<sup>125</sup> Methylation of this aromatic core was achieved through a simple series of straightforward formylation and reduction steps until the desired number of methyls were appended. Again, the purpose of the methyl groups is to shift the absorption of the sensors for optimization toward specific microscope wavelengths.



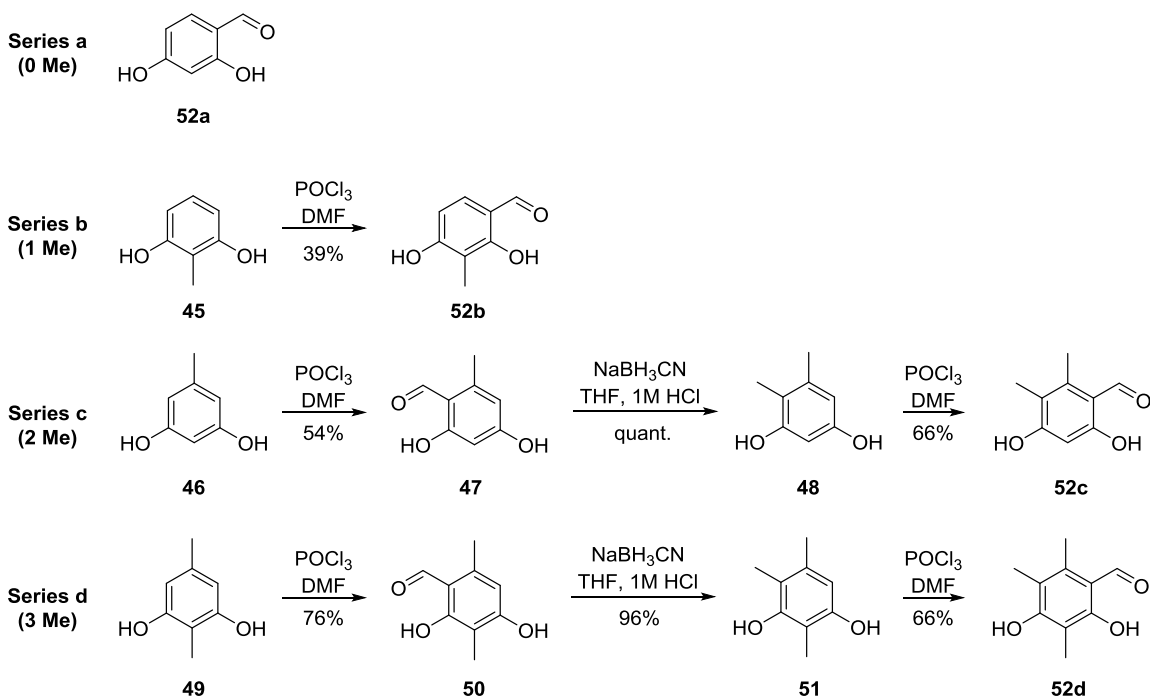


**Figure 4-4.** Synthesis of hydroxysalicylaldehyde starting materials for 3-input AND molecular logic gates.

Subsequent treatment of **52a-d** with diethylglutaconate and base induced an Aldol reaction followed by intramolecular transesterification to produce the coumarin body (Figure 4-5). Protection of the phenolic oxygen was achieved using acetic anhydride which allowed for oxidative cleavage of the alkene using osmium tetroxide and sodium periodate. Deprotection of the phenol was achieved using ammonium acetate and methanol/water (4:1) to yield the final products (**56a-d**).

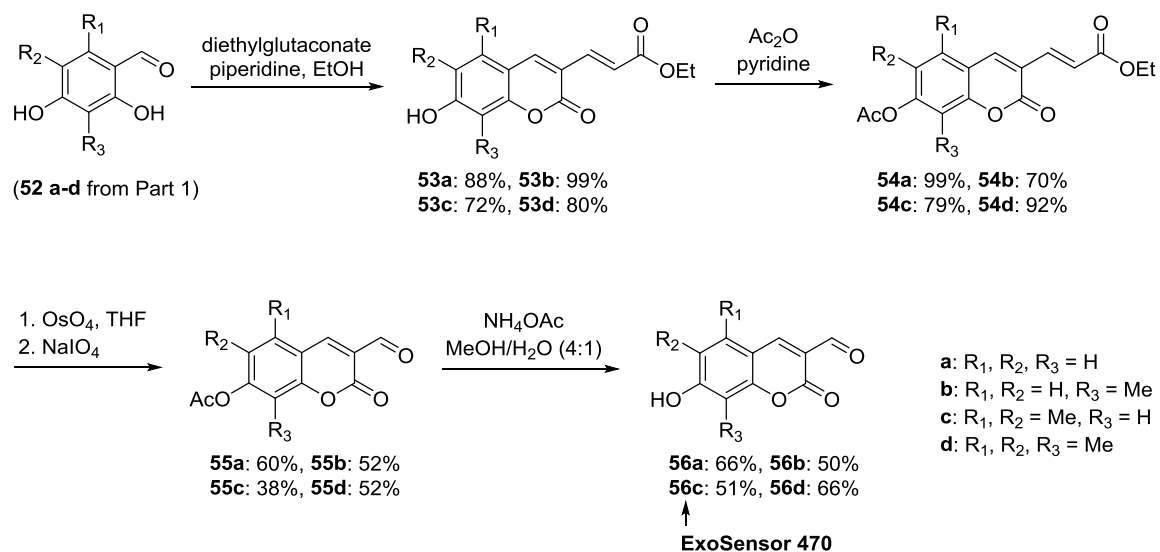


**Figure 4-5.** Second part of synthesis for the 3-input molecular AND logic gates.

#### 4.5 Titrations

pH and analyte titrations were conducted and the representative spectra of ExoSensor 470 (ES470, **56c**) are shown. Deprotonation of the sensors caused a large bathochromic shift in the absorbance and a concomitant increase in fluorescence when excited at the deprotonated wavelength. Each additional methyl group added ~10 nm to the excitation maximum and proved to be an effective method for tailoring the sensors toward a specific excitation wavelength. In this case, we optimize the sensors for the 440 nm laser line as it is one of the standard wavelengths in many microscopy setups.

The titration of ES470 with glutamate gave an absorbance increase at 452 nm; however, the fluorescence emission decreases which is opposite of the response obtained for coumarin aldehydes containing substituents at the 4-position (Figure 4-6).<sup>46,48</sup> Coumarin aldehydes with C4 substituents (structure **A**) lead to a rigid iminium ion with a high quantum yield, resulting in strong fluorescence.<sup>126</sup> However, ES470 lacks a

substituent at the 4-position (structure **B**) which results in free rotation of the imine and weak fluorescence.

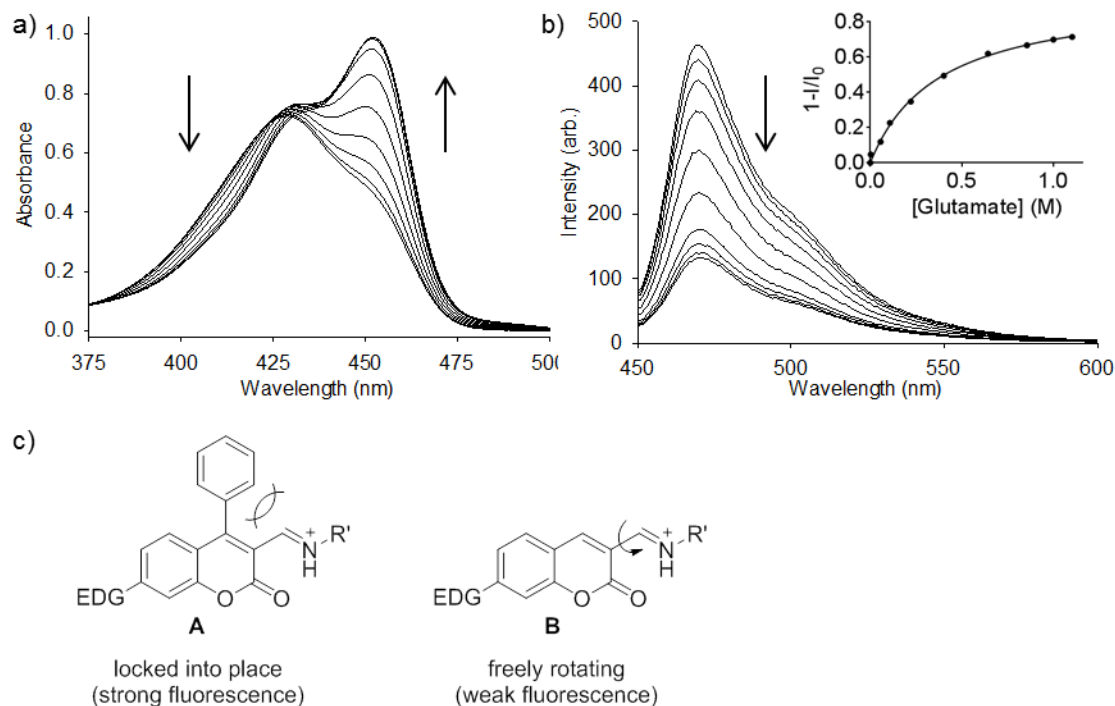


**Figure 4-6.** a) UV/vis (20 μM) and b) fluorescence (1 μM) titration of ES470 in buffer (50 mM bis-tris propane, 120 mM NaCl, 1% DMSO, pH 7.4) adding 20-800 μL aliquots of 1.5 M glutamate.  $\lambda_{\text{ex}} = 440$  nm. Inset is the fit to a one-site binding isotherm. c) Substituents at the coumarin 4-position inhibit free rotation of the imine. EDG = electron-donating group.

Adding aliquots of zinc acetate to the ES470-glutamate complex induces a hypsochromic shift in both the absorption and fluorescence maxima as well as a modest fluorescence increase (Figure 4-7). Addition of zinc rigidifies the fluorophore and locks the  $\pi$ -system into place, resulting in the fluorescence increase. The presence of zinc in the binding pocket prevents protonation of the imine which is otherwise protonated at physiological pH. We hypothesize that this change in protonation state mitigates the electron transfer across the fluorophore and induces the small blue shift in the spectra. A

control experiment was performed in which zinc was added to ES470 alone and no fluorescence change was observed.

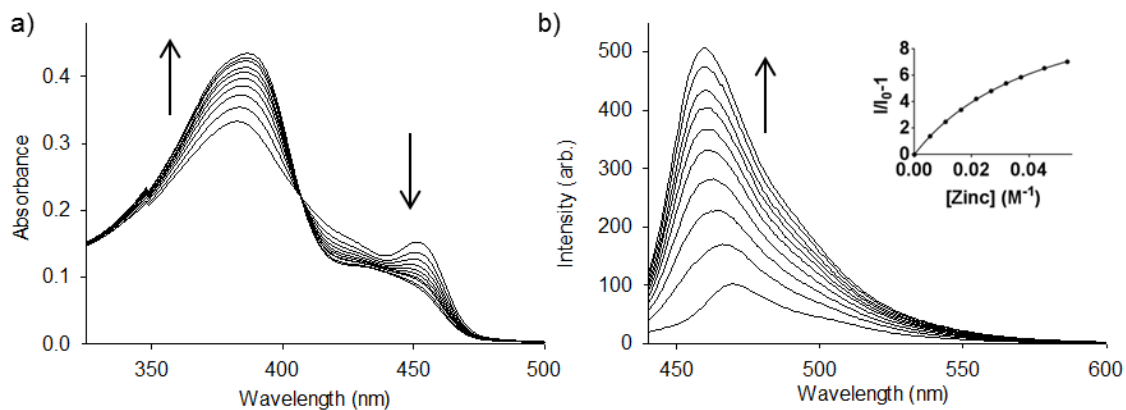


**Figure 4-7.** a) UV/vis (20  $\mu$ M) and b) fluorescence (1  $\mu$ M) titration of ES470 (**56c**) with 300 mM glutamate in buffer (50 mM bis-tris propane, 120 mM NaCl, 1% DMSO, pH 5.0) adding 5-8  $\mu$ L aliquots of 1.1 M zinc acetate.  $\lambda_{ex}$  = 393 nm. Inset is the fit to a one-site binding isotherm.

Table 4-1 details the results from pH and binding titrations with sensors **56a-d**. Excitation and emission wavelengths increase  $\sim$ 10 nm with each additional methyl group, demonstrating an effective technique to tune chemosensors for specific excitation wavelengths used in conventional microscopy setups. The  $pK_a$  values of the three-input sensors were all approximately 6 which suits neuronal studies, as they will be protonated in the secretory vesicle (pH 5) and deprotonated in the synaptic cleft (pH 7.4). Glutamate binding constants were all single-digit values which agrees with previously-obtained binding constants of coumarin aldehydes with glutamate.<sup>46, 48</sup> The binding of zinc to the sensor-glutamate complex was comparable for all sensors and ranged from 24-32  $M^{-1}$ . While these binding constants appear low, they are actually preferred for reversible analyte detection because glutamate and zinc are found in hundreds of millimolar and

low millimolar concentrations, respectively, within glutamatergic secretory vesicles.<sup>51-52,</sup>

122-123,127

**Table 4-1.** Spectroscopic and Binding Properties of Sensors **56a-d**

Sensor	$\lambda_{\text{ex}}, \lambda_{\text{em}}$ (nm) <sup>a</sup>	pK <sub>a</sub>	K <sub>a</sub> (Glu) (M <sup>-1</sup> ) <sup>b</sup>	K <sub>app</sub> (Zn <sup>2+</sup> ) (M <sup>-1</sup> ) <sup>c</sup>	I <sub>pH 7.4</sub> / I <sub>pH 5.0</sub> <sup>d</sup>
<b>56a</b>	436,462	6.0	2.1	24	6.7
<b>56b</b>	444,472	6.1	2.6	27	9.3
<b>56c</b> (ES470)	451,470	6.1	2.8	30	11
<b>56d</b>	462,480	5.7	2.7	32	5.8

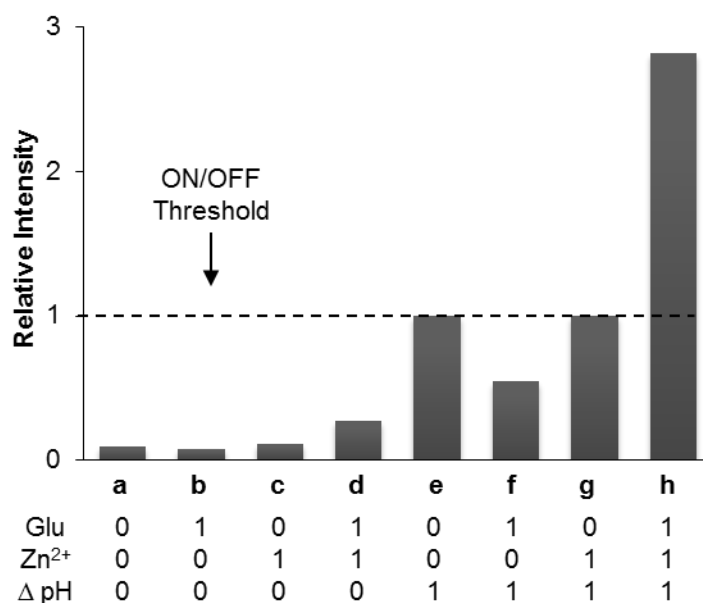
<sup>a</sup>Fluorescence excitation and emission maxima of sensors **1a-d** (1  $\mu\text{M}$ ) in buffer (50 mM bis-tris propane, 120 mM NaCl, 1% DMSO, pH 7.4).  $\lambda_{\text{ex}} = 440 \text{ nm}$ ; <sup>b</sup>Binding of sensors **1a-d** (1  $\mu\text{M}$ ) to glutamate (Glu) in buffer (50 mM bis-tris propane, 120 mM NaCl, 1% DMSO, pH 7.4);

<sup>c</sup>Apparent binding of sensors **1a-d** (1  $\mu\text{M}$ ) and glutamate (300 mM) to zinc acetate in buffer (50 mM bis-tris propane, 120 mM NaCl, 1% DMSO, pH 5.0); <sup>d</sup>Fluorescence intensity of a mixture of sensors **1a-d** (1  $\mu\text{M}$ ), glutamate (500 mM) and zinc acetate (40 mM) monitored at pH 5.0 and 7.4.  $\lambda_{\text{ex}} = 440 \text{ nm}$ .

The key parameter to note is the change in fluorescence intensity ( $I_{\text{pH } 7.4}/I_{\text{pH } 5.0}$ ) of the sensor-glutamate-zinc complex over the pH range associated with exocytosis of the vesicle. This value indicates the factor by which the fluorescence should increase upon exocytosis of the fully bound complex. The greatest fluorescence enhancement was observed with ES470 at 11-fold.

The potential fluorescence outputs of ES470 are shown in Figure 4-8. Bars **a-d** represent the fluorescence intensity of ES470 in various states *before* exocytosis (pH 5.0) and bars **e-h** represent the fluorescence intensity *after* exocytosis (pH 7.4). Bar **h** shows the only combination of inputs that gives a fluorescence turn-on response above the ON/OFF threshold using exocytotic pH conditions. Bar **e** depicts the next highest

fluorescence response; however, the unbound sensor is chargeless and would not accumulate within acidic secretory vesicles, but would instead be washed away during pre-imaging cell preparations.<sup>46</sup> The sensor-zinc complex (bar **g**) would also not be present given the high concentration of glutamate within glutamatergic vesicles (hundreds of millimolar).<sup>51-52, 56, 122-123</sup> Therefore states **e** and **g** are not even relevant to imaging applications.

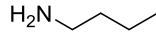
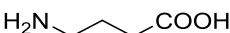
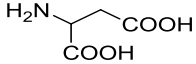
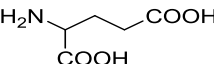
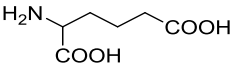


**Figure 4-8.** Relative fluorescence intensities and truth table for **1c**, a three-input AND gate. Samples contained ES470 (1  $\mu$ M) in buffer (50 mM HEPES, 120 mM NaCl, 1% DMSO) in the presence or absence of glutamate (Glu, 500 mM) and zinc acetate (Zn<sup>2+</sup>, 40 mM).  $\Delta$  pH = increase in pH from 5.0 to 7.4 to mimic exocytosis from the acidic vesicle to the synaptic cleft.

To further probe the binding interaction between the sensor, the amine, and zinc, titrations were repeated with other primary amine analytes (Table 4-2). When added to ES470, all of the amines decreased the fluorescence intensity by ~65-70%, as seen with glutamate. Furthermore, there was indication that the amines containing an  $\alpha$ -carboxylate

bound better to the added zinc than did amines lacking an  $\alpha$ -carboxylate functional group. Glutamate was still shown to have the highest fluorescence enhancement ( $I_{\text{pH } 7.4}/I_{\text{pH } 5.0}$ ) under conditions mimicking exocytosis compared to the other analytes. We also evaluated the effect of zinc binding on the sensor-amine complex ( $I_{\text{Glu-Zn}^{2+}}/I_{\text{Glu}}$ ). For amines containing an  $\alpha$ -carboxylate, zinc addition increased fluorescence, but for amines lacking the  $\alpha$ -carboxylate, zinc addition decreased fluorescence. This result also indicates that the  $\alpha$ -carboxylate plays an important role in enabling proper zinc coordination to occur.

**Table 4-2.** Spectroscopic and Binding Properties of ES470 (**56c**) with Various Amine Analytes

Amine	$K_a$ (amine) ( $\text{M}^{-1}$ ) <sup>a</sup>	$K_{\text{app}}$ ( $\text{Zn}^{2+}$ ) ( $\text{M}^{-1}$ ) <sup>b</sup>	$I_{\text{pH } 7.4} / I_{\text{pH } 5.0}$ <sup>c</sup>	$I_{\text{Glu-Zn}^{2+}} / I_{\text{Glu}}$ <sup>d</sup>
 N-butylamine	0.8	-	6	0.36
 GABA	1.6	-	8	0.37
 aspartic acid	1.9	24	11	1.09
 glutamic acid	2.8	30	11	2.82
 2-aminoadipic acid	2.2	26	9	2.16

<sup>a</sup>Binding constant of sensor ES470 (1  $\mu\text{M}$ ) to various amine guests in buffer (50 mM bis-tris propane, 120 mM NaCl, 1% DMSO, pH 7.4); <sup>b</sup>Apparent binding of ES470 (1  $\mu\text{M}$ ) and amine guest (300  $\mu\text{M}$ ) adding aliquots of 1.1 M zinc acetate in buffer (50 mM bis-tris propane, 120 mM NaCl, 1% DMSO, pH 5.0); <sup>c</sup>Fluorescence intensity of ES470 (1  $\mu\text{M}$ ), glutamate (500  $\mu\text{M}$ ), and zinc acetate (40  $\mu\text{M}$ ) monitored at pH 5.0 and 7.4.  $\lambda_{\text{ex}} = 440$  nm. The enhancement represents the fluorescence increase upon exocytosis; <sup>d</sup>Ratio of the fluorescence intensity of the ES470-amine complex with and without  $\text{Zn}^{2+}$ .  $\lambda_{\text{ex}} = 440$  nm.

In conclusion, sensors **56a-d** were designed and synthesized as water-soluble three-input AND molecular logic gates for the purpose of neuronal imaging. The sensors are easily modified to incorporate multiple functionalities that are integrated into the fluorophore  $\pi$ -system which directly modulate the optical properties upon interaction with analyte. The unique sensing mechanism capitalizes on the large quantities of glutamate already packaged in zinc-containing secretory vesicles to create a reversible binding pocket for zinc which is only visualized upon release into the synaptic cleft. The molecular logic-based approach is a proof-of-concept that may serve as a useful prototype from which other bioanalyte detection systems can be constructed.



## APPENDIX

### Experimental Procedures and Characterization Data

#### Part I. General Information

All reagents and solvents were purchased from commercial sources and used without further purification unless stated otherwise. Anhydrous dichloromethane, acetonitrile, and triethylamine were obtained by distillation from CaH<sub>2</sub>. Anhydrous THF and toluene were obtained by distillation from sodium metal and benzophenone. All reactions were conducted using oven or flame dried glassware and under N<sub>2</sub> atmosphere unless stated otherwise. Flash column chromatography was carried by using 32-63 μm silica gel.

NMR spectra were obtained by a Bruker ARX-250 MHz, DRX-300 MHz, or DRX-500 MHz in CDCl<sub>3</sub> or DMSO-d<sub>6</sub> using tetramethylsilane (TMS) as a reference. IR spectra were obtained by a Thermo Scientific Auxiliary Equipment Module (AEM) for Nicolet FT-IR spectrometers. High resolution mass spectra (HRMS) were carried by a Bruker Apex-Qe FTMS at the Old Dominion University in Norfolk, VA.

#### Part II. Spectroscopic Studies

UV-Visible spectra were obtained by a Varian Cary-1E UV-Visible spectrometer. Fluorescence spectra were obtained by a Shimadzu RF-5301 PC spectrofluorimeter.

Titration curves were performed by using bis tris propane or HEPES buffer with NaCl or Na<sub>2</sub>S<sub>2</sub>O<sub>3</sub> added unless otherwise stated. Absorbance and fluorescence spectra were processed using SigmaPlot™ 12.3 and best-fit lines fit using GraphPad Prism 6.01.

## Analyte Titrations

### Analyte Titrations for 3-Formyl-7-hydroxy-4-phenylcoumarin (**41**)

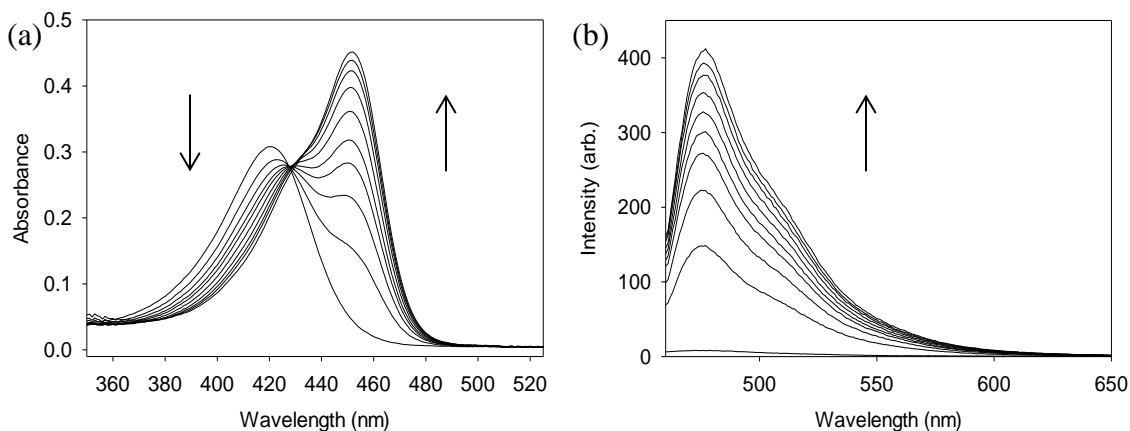


**Figure A-1.** (a) UV/vis and (b) fluorescence titration of compound **41** (10 μM) in buffer (50 mM bis tris propane, 50 mM Na<sub>2</sub>S<sub>2</sub>O<sub>3</sub>, 1% DMSO, pH 7.4) adding 20-220 μL aliquots of 1.5 M glutamate.  $\lambda_{\text{ex}} = 450$  nm.

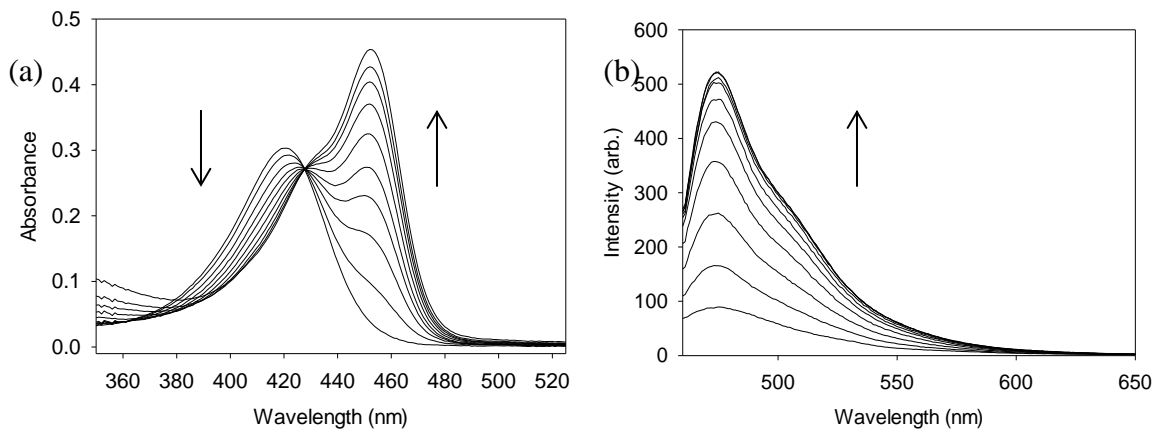


**Figure A-2.** (a) UV/vis and (b) fluorescence titration of compound **41** (10 μM) in buffer (50 mM bis tris propane, 50 mM Na<sub>2</sub>S<sub>2</sub>O<sub>3</sub>, 1% DMSO, pH 7.4) adding 20-220 μL aliquots of 100 mM norepinephrine.  $\lambda_{\text{ex}} = 450$  nm.

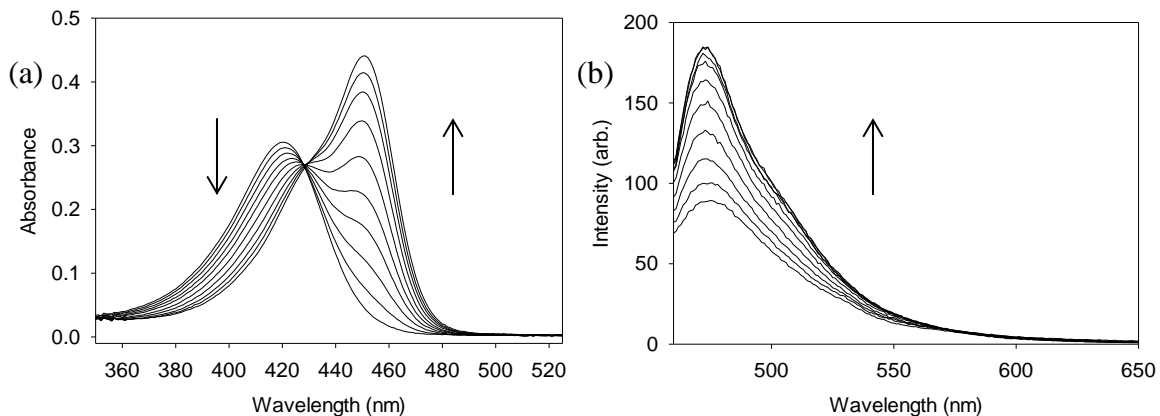


**Figure A-3.** (a) UV/vis and (b) fluorescence titration of compound **41** (10  $\mu$ M) in buffer (50 mM bis tris propane, 50 mM  $\text{Na}_2\text{S}_2\text{O}_3$ , 1% DMSO, pH 7.4) adding 20-220  $\mu$ L aliquots of 100 mM dopamine.  $\lambda_{\text{ex}} = 450$  nm.

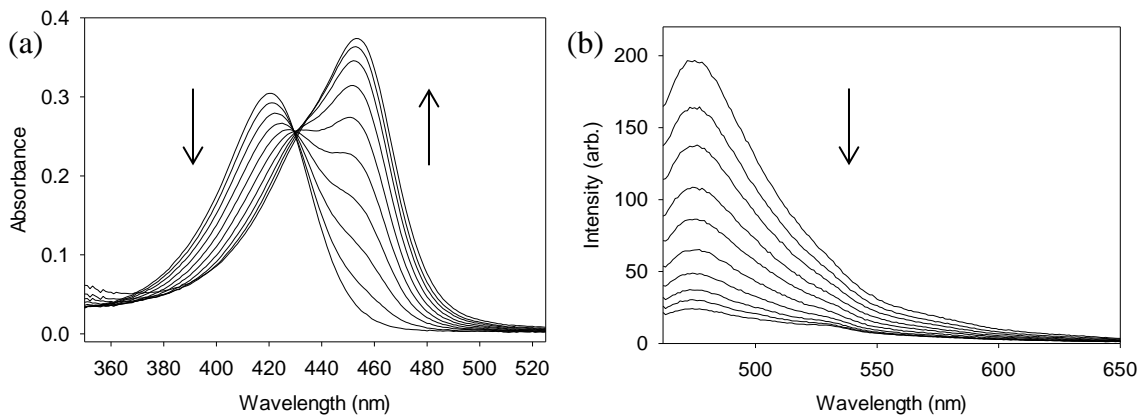


**Figure A-4.** (a) UV/vis and (b) fluorescence titration of compound **41** (10  $\mu$ M) in buffer (50 mM bis tris propane, 50 mM  $\text{Na}_2\text{S}_2\text{O}_3$ , 1% DMSO, pH 7.4) adding 20-220  $\mu$ L aliquots of 100 mM serotonin.  $\lambda_{\text{ex}} = 450$  nm.

Analyte Titrations for ES517

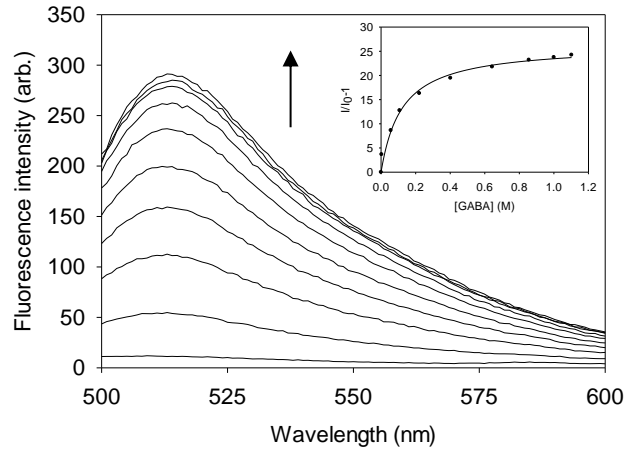


**Figure A-5.** Fluorescence titration of ES517 (20  $\mu\text{M}$ ) with 20-800  $\mu\text{L}$  of 1.5 M GABA in buffer (50 mM bis tris propane, pH 7.4, 50 mM  $\text{Na}_2\text{S}_2\text{O}_3$ , 1% DMSO).  $\lambda_{\text{ex}} = 488 \text{ nm}$ . Inset is the fit to a binding isotherm.  $\lambda_{\text{em}} = 514 \text{ nm}$ .

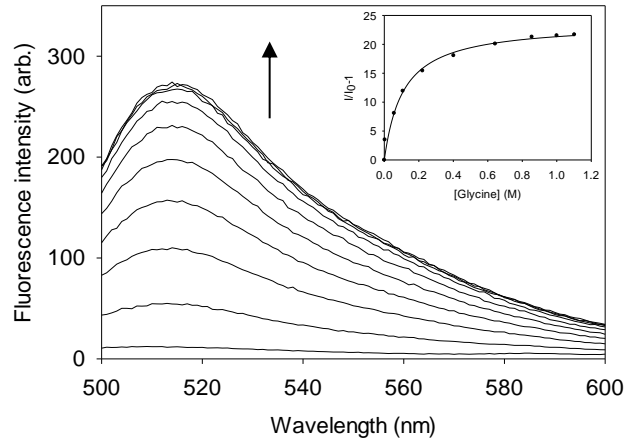


**Figure A-6.** Fluorescence titration of ES517 (20  $\mu\text{M}$ ) with 20-800  $\mu\text{L}$  of 1.5 M glycine in buffer (50 mM bis tris propane, pH 7.4, 50 mM  $\text{Na}_2\text{S}_2\text{O}_3$ , 1% DMSO).  $\lambda_{\text{ex}} = 488 \text{ nm}$ . Inset is the fit to a binding isotherm.  $\lambda_{\text{em}} = 515 \text{ nm}$ .

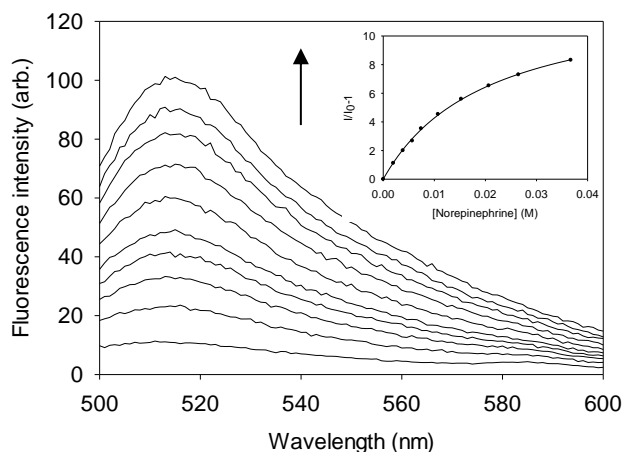


**Figure A-7.** Fluorescence titration of ES517 (20  $\mu$ M) with 20-220  $\mu$ L of 100 mM norepinephrine in buffer (50 mM bis tris propane, pH 7.4, 50 mM  $\text{Na}_2\text{S}_2\text{O}_3$ , 1% DMSO).  $\lambda_{\text{ex}} = 488$  nm. Inset is the fit to a binding isotherm.  $\lambda_{\text{em}} = 515$  nm.

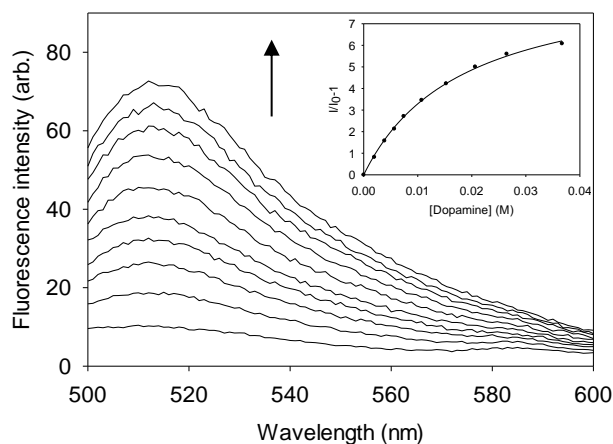


**Figure A-8.** Fluorescence titration of ES517 (20  $\mu$ M) with 20-220  $\mu$ L of 100 mM dopamine in buffer (50 mM bis tris propane, pH 7.4, 50 mM  $\text{Na}_2\text{S}_2\text{O}_3$ , 1% DMSO).  $\lambda_{\text{ex}} = 488$  nm. Inset is the fit to a binding isotherm.  $\lambda_{\text{em}} = 513$  nm.

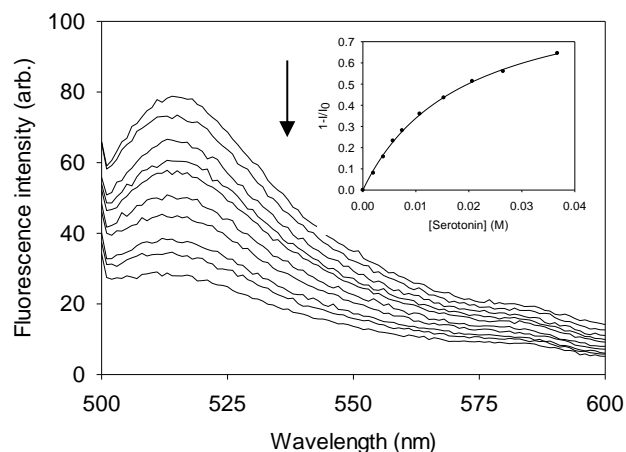


**Figure A-9.** Fluorescence titration of ES517 (20  $\mu\text{M}$ ) with 20-220  $\mu\text{L}$  of 100 mM serotonin in buffer (50 mM bis tris propane, pH 7.4, 50 mM  $\text{Na}_2\text{S}_2\text{O}_3$ , 1% DMSO).  $\lambda_{\text{ex}} = 488 \text{ nm}$ . Inset is the fit to a binding isotherm.  $\lambda_{\text{em}} = 514 \text{ nm}$ .

*Analyte Titrations for 3-Formyl-4-methylsulfonamide-4-phenylcoumarin (28)*

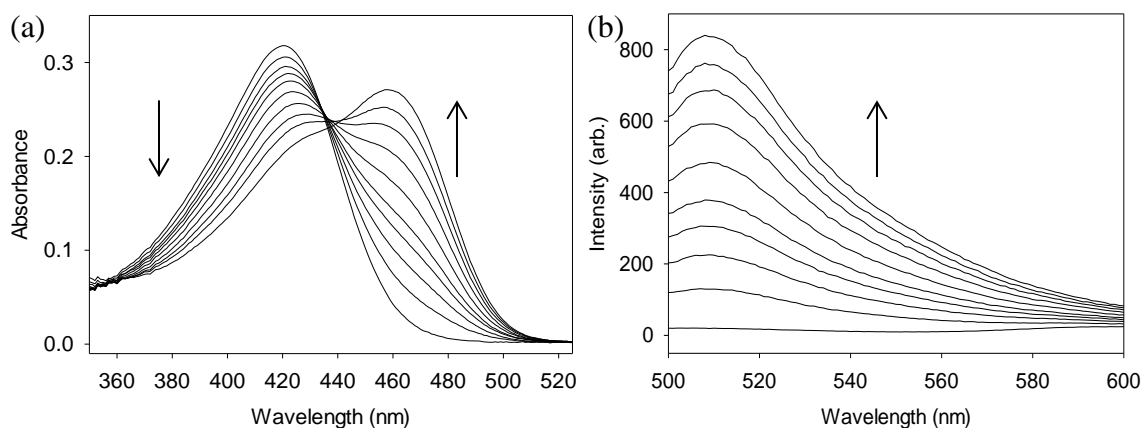


**Figure A-10.** (a) UV/vis and (b) fluorescence titration of compound **28** (10  $\mu\text{M}$ ) in buffer (50 mM bis tris propane, 50 mM  $\text{Na}_2\text{S}_2\text{O}_3$ , 1% DMSO, pH 7.4) adding 20-220  $\mu\text{L}$  aliquots of 1.5 M glutamate.  $\lambda_{\text{ex}} = 488 \text{ nm}$ .

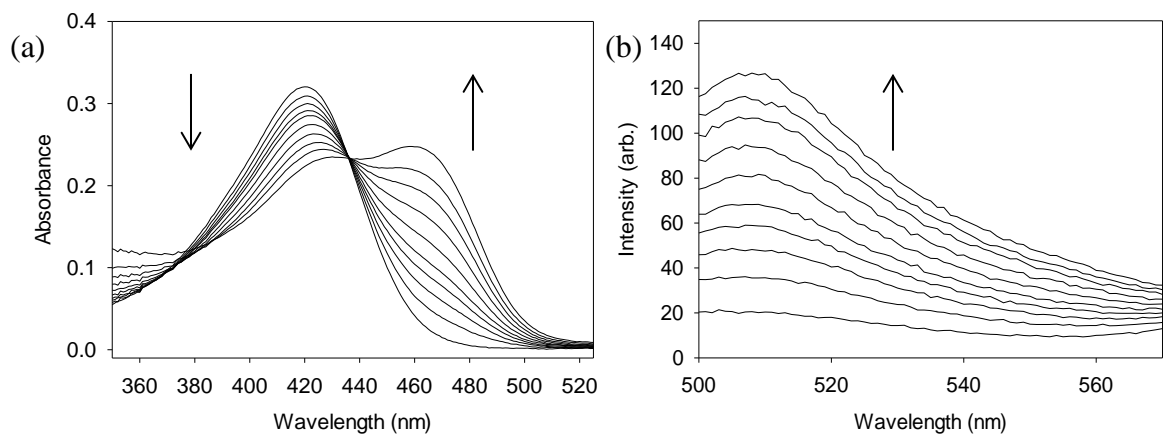


**Figure A-11.** (a) UV/vis and (b) fluorescence titration of compound **28** (10  $\mu\text{M}$ ) in buffer (50 mM bis tris propane, 50 mM  $\text{Na}_2\text{S}_2\text{O}_3$ , 1% DMSO, pH 7.4) adding 20-220  $\mu\text{L}$  aliquots of 100 mM norepinephrine.  $\lambda_{\text{ex}} = 488 \text{ nm}$ .

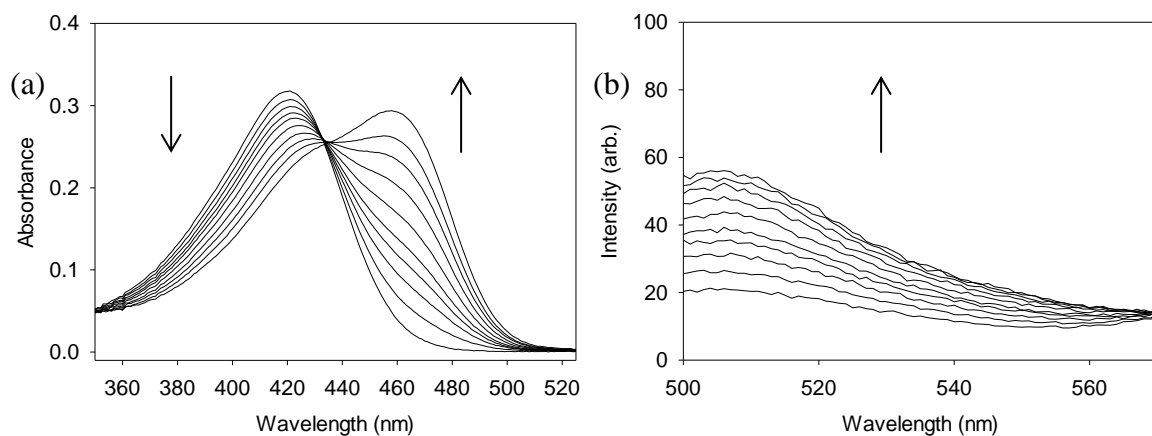


**Figure A-12.** (a) UV/vis and (b) fluorescence titration of compound **28** (10  $\mu\text{M}$ ) in buffer (50 mM bis tris propane, 50 mM  $\text{Na}_2\text{S}_2\text{O}_3$ , 1% DMSO, pH 7.4) adding 20-220  $\mu\text{L}$  aliquots of 100 mM dopamine.  $\lambda_{\text{ex}} = 488 \text{ nm}$ .

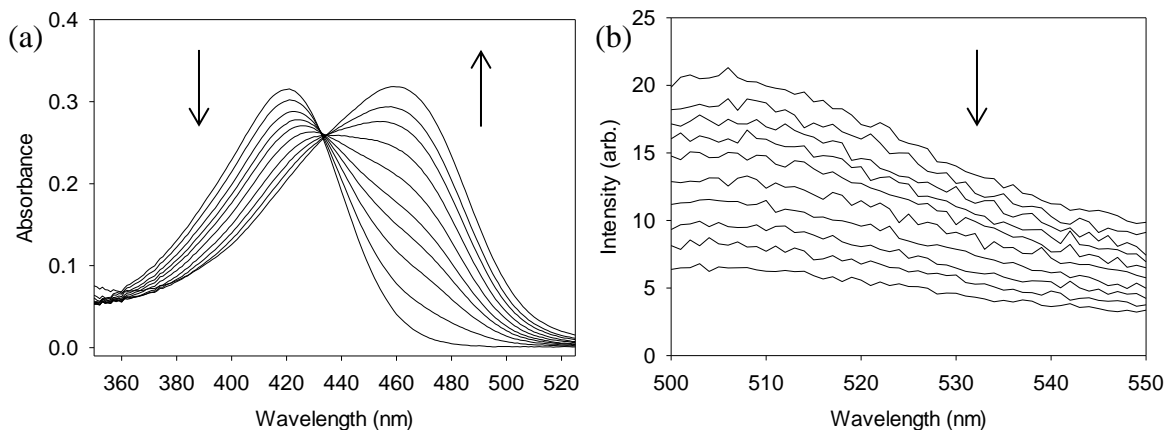


**Figure A-13.** (a) UV/vis and (b) fluorescence titration of compound **28** (10  $\mu\text{M}$ ) in buffer (50 mM bis tris propane, 50 mM  $\text{Na}_2\text{S}_2\text{O}_3$ , 1% DMSO, pH 7.4) adding 20-220  $\mu\text{L}$  aliquots of 100 mM serotonin.  $\lambda_{\text{ex}} = 488 \text{ nm}$ .

*Analyte Titrations for 3-Formyl-4-phenyl-7-phenylsulfonamidocoumarin (43)*

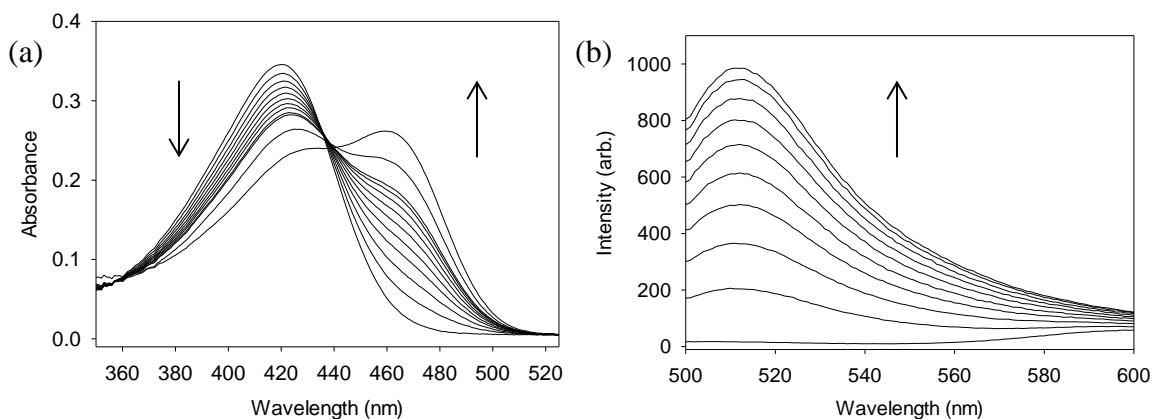


**Figure A-14.** (a) UV/vis and (b) fluorescence titration of compound **43** (10  $\mu\text{M}$ ) in buffer (50 mM bis tris propane, 50 mM  $\text{Na}_2\text{S}_2\text{O}_3$ , 1% DMSO, pH 7.4) adding 20-220  $\mu\text{L}$  aliquots of 1.5 M glutamate.  $\lambda_{\text{ex}} = 488 \text{ nm}$ .



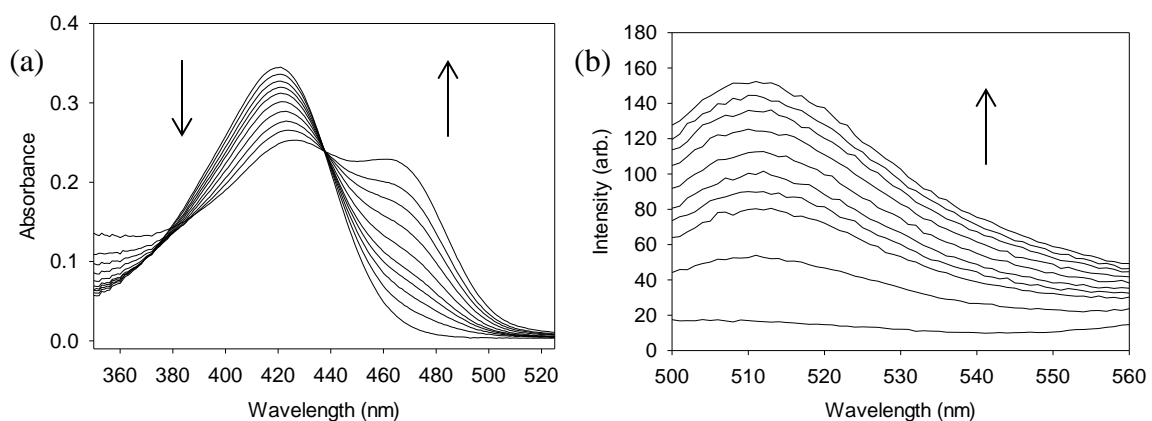


**Figure A-15.** (a) UV/vis and (b) fluorescence titration of compound **43** (10  $\mu\text{M}$ ) in buffer (50 mM bis tris propane, 50 mM  $\text{Na}_2\text{S}_2\text{O}_3$ , 1% DMSO, pH 7.4) adding 20-220  $\mu\text{L}$  aliquots of 100 mM norepinephrine.  $\lambda_{\text{ex}} = 488 \text{ nm}$ .

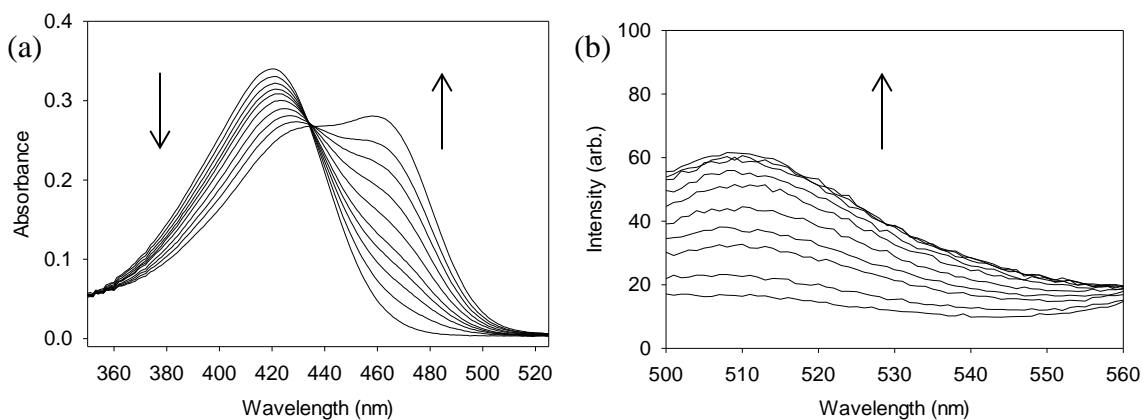


**Figure A-16.** (a) UV/vis and (b) fluorescence titration of compound **43** (10  $\mu\text{M}$ ) in buffer (50 mM bis tris propane, 50 mM  $\text{Na}_2\text{S}_2\text{O}_3$ , 1% DMSO, pH 7.4) adding 20-220  $\mu\text{L}$  aliquots of 100 mM dopamine.  $\lambda_{\text{ex}} = 488 \text{ nm}$ .

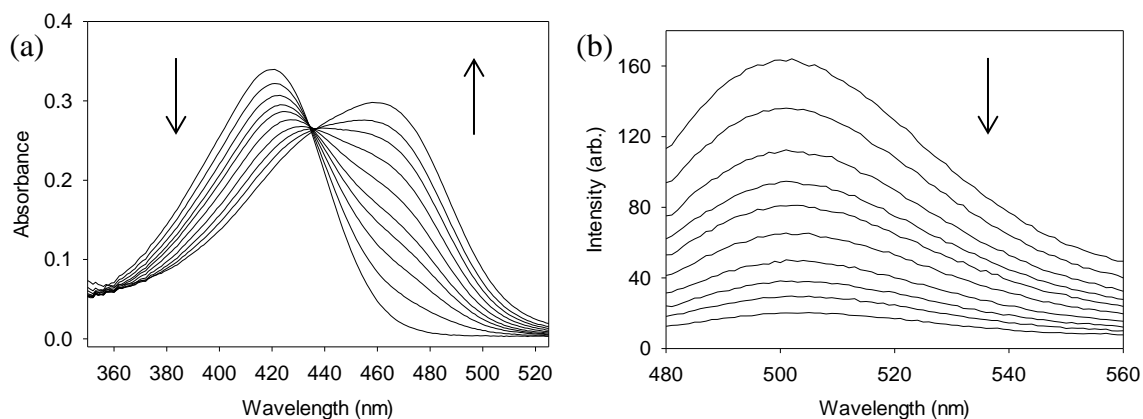


**Figure A-17.** (a) UV/vis and (b) fluorescence titration of compound **43** (10  $\mu\text{M}$ ) in buffer (50 mM bis tris propane, 50 mM  $\text{Na}_2\text{S}_2\text{O}_3$ , 1% DMSO, pH 7.4) adding 20-220  $\mu\text{L}$  aliquots of 100 mM serotonin.  $\lambda_{\text{ex}} = 470 \text{ nm}$ .

*Analyte Titrations for 3-Formyl-4-phenyl-7-thiophenesulfonamidecoumarin (**44**)*

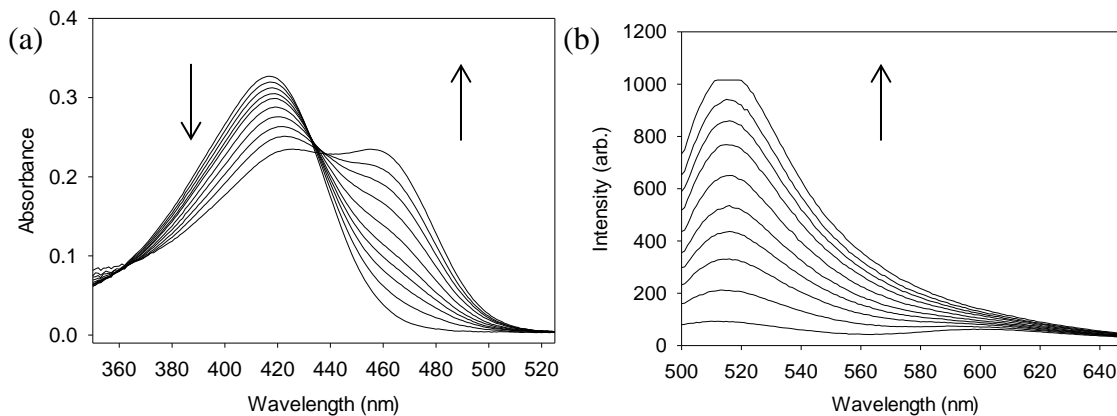


**Figure A-18.** (a) UV/vis and (b) fluorescence titration of compound **44** (10  $\mu\text{M}$ ) in buffer (50 mM bis tris propane, 50 mM  $\text{Na}_2\text{S}_2\text{O}_3$ , 1% DMSO, pH 7.4) adding 20-220  $\mu\text{L}$  aliquots of 1.5 M glutamate.  $\lambda_{\text{ex}} = 488 \text{ nm}$ .

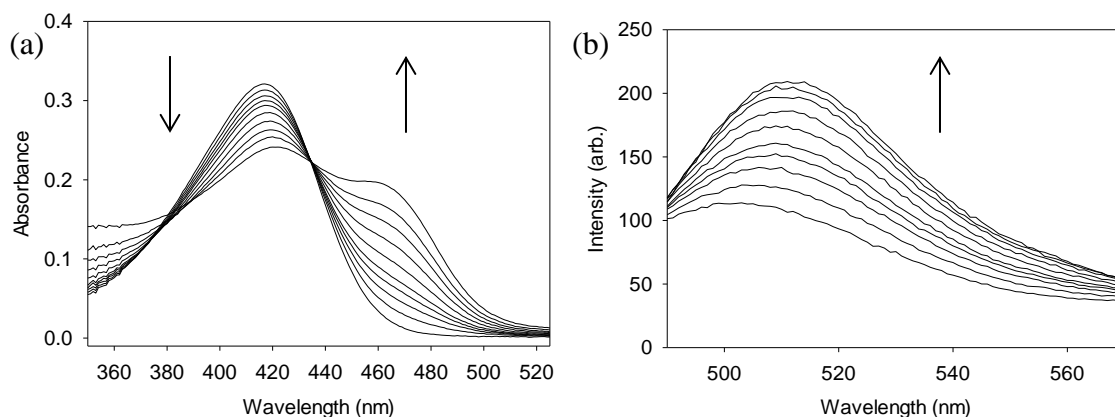


**Figure A-19.** (a) UV/vis and (b) fluorescence titration of compound **44** (10  $\mu\text{M}$ ) in buffer (50 mM bis tris propane, 50 mM  $\text{Na}_2\text{S}_2\text{O}_3$ , 1% DMSO, pH 7.4) adding 20-220  $\mu\text{L}$  aliquots of 100 mM norepinephrine.  $\lambda_{\text{ex}} = 470 \text{ nm}$ .

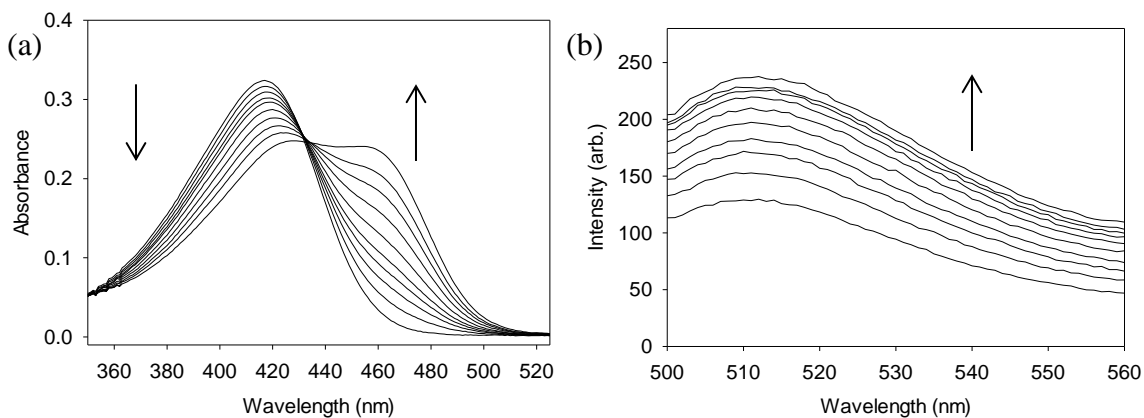


**Figure A-20.** (a) UV/vis and (b) fluorescence titration of compound **44** (10  $\mu\text{M}$ ) in buffer (50 mM bis tris propane, 50 mM  $\text{Na}_2\text{S}_2\text{O}_3$ , 1% DMSO, pH 7.4) adding 20-220  $\mu\text{L}$  aliquots of 100 mM dopamine.  $\lambda_{\text{ex}} = 488 \text{ nm}$ .

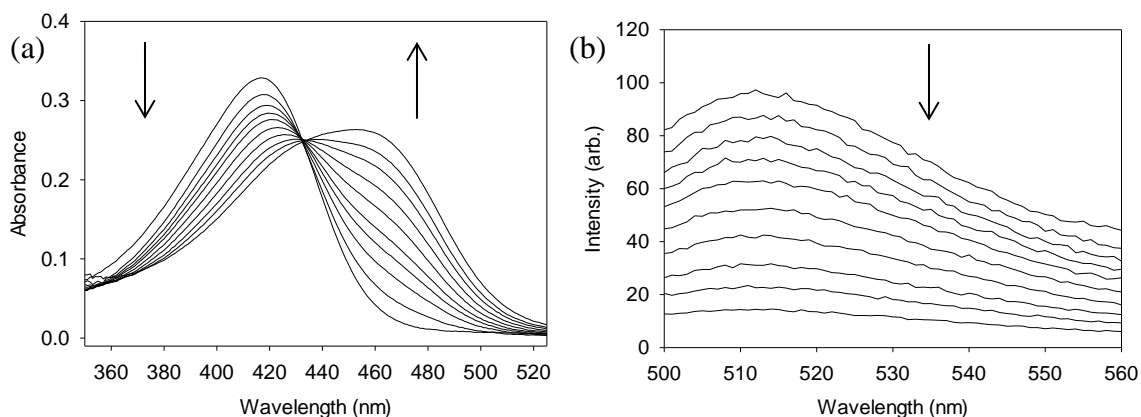


**Figure A-21.** (a) UV/vis and (b) fluorescence titration of compound **44** (10  $\mu\text{M}$ ) in buffer (50 mM bis tris propane, 50 mM  $\text{Na}_2\text{S}_2\text{O}_3$ , 1% DMSO, pH 7.4) adding 20-220  $\mu\text{L}$  aliquots of 100 mM serotonin.  $\lambda_{\text{ex}} = 488 \text{ nm}$ .

*Analyte Titrations for Compounds **56a,b,d** with Glutamate*

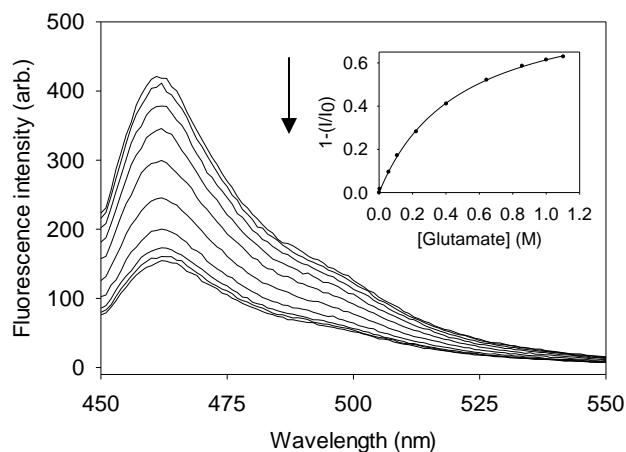


**Figure A-22.** Fluorescence titration of **56a** (1  $\mu\text{M}$ ) adding 20-800  $\mu\text{L}$  aliquots of 1.5 M glutamate in buffer (50 mM bis-tris propane, 120 mM NaCl, 1% DMSO, pH 7.4).  $\lambda_{\text{ex}} = 440 \text{ nm}$ . Inset is the fit to a one-site binding isotherm.

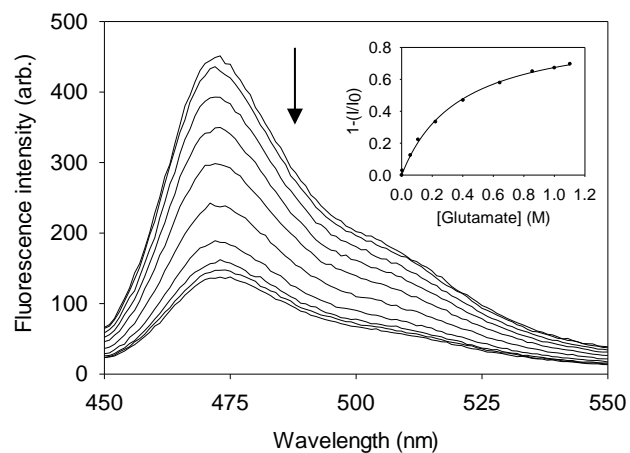


**Figure A-23.** Fluorescence titration of **56b** (1  $\mu\text{M}$ ) adding 20-800  $\mu\text{L}$  aliquots of 1.5 M glutamate in buffer (50 mM bis-tris propane, 120 mM NaCl, 1% DMSO, pH 7.4).  $\lambda_{\text{ex}} = 440$  nm. Inset is the fit to a one-site binding isotherm.

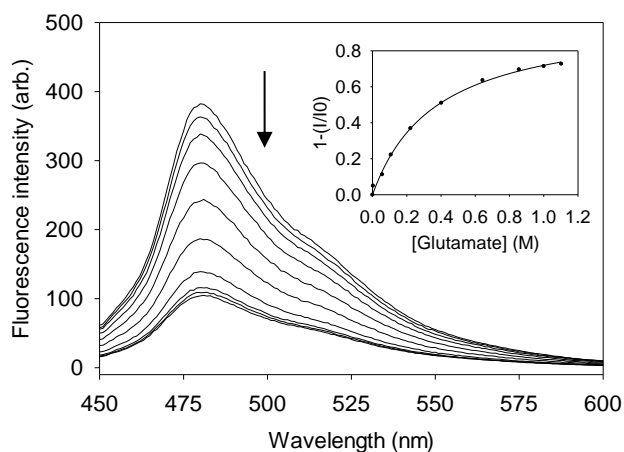


**Figure A-24.** Fluorescence titration of **56d** (1  $\mu\text{M}$ ) adding 20-800  $\mu\text{L}$  aliquots of 1.5 M glutamate in buffer (50 mM bis-tris propane, 120 mM NaCl, 1% DMSO, pH 7.4).  $\lambda_{\text{ex}} = 440$  nm. Inset is the fit to a one-site binding isotherm.

Analyte Titrations for Amine-Bound Compounds **56a-d** Upon Adding Zinc

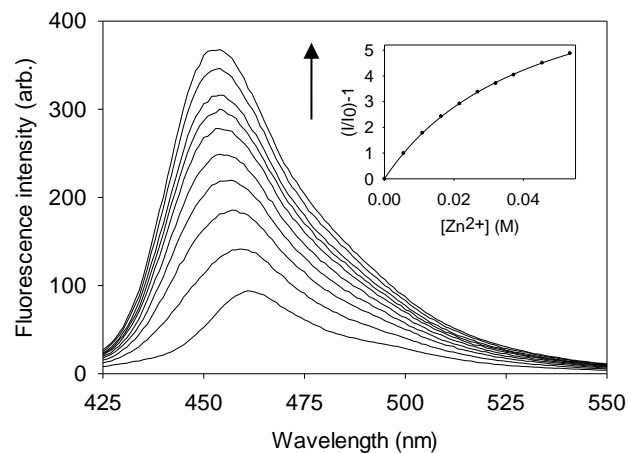


**Figure A-25.** Fluorescence titration of **56a** (1  $\mu$ M) and 300 mM glutamate adding 5-8  $\mu$ L aliquots of 1.1 M zinc acetate in buffer (50 mM bis-tris propane, 120 mM NaCl, 1% DMSO, pH 5.0).  $\lambda_{ex}$  = 380 nm. Inset is the fit to a one-site binding isotherm.

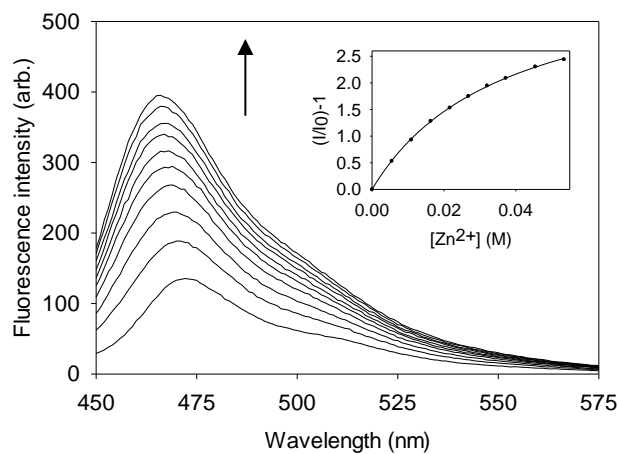


**Figure A-26.** Fluorescence titration of **56b** (1  $\mu$ M) and 300 mM glutamate adding 5-8  $\mu$ L aliquots of 1.1 M zinc acetate in buffer (50 mM bis-tris propane, 120 mM NaCl, 1% DMSO, pH 5.0).  $\lambda_{ex}$  = 380 nm. Inset is the fit to a one-site binding isotherm.

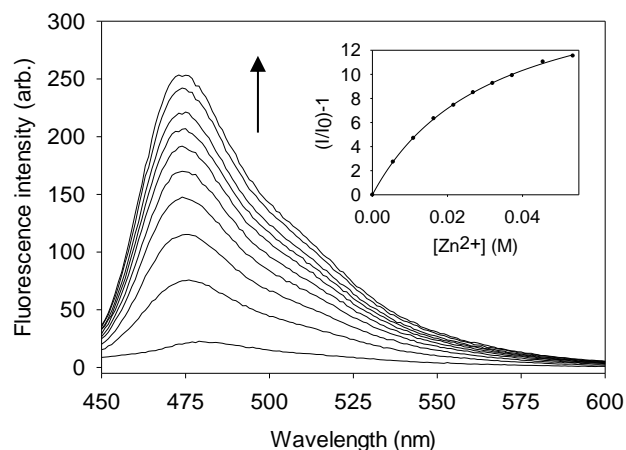


**Figure A-27.** Fluorescence titration of **56d** (1  $\mu\text{M}$ ) and 300 mM glutamate adding 5-8  $\mu\text{L}$  aliquots of 1.1 M zinc acetate in buffer (50 mM bis-tris propane, 120 mM NaCl, 1% DMSO, pH 5.0).  $\lambda_{\text{ex}} = 390$  nm. Inset is the fit to a one-site binding isotherm.

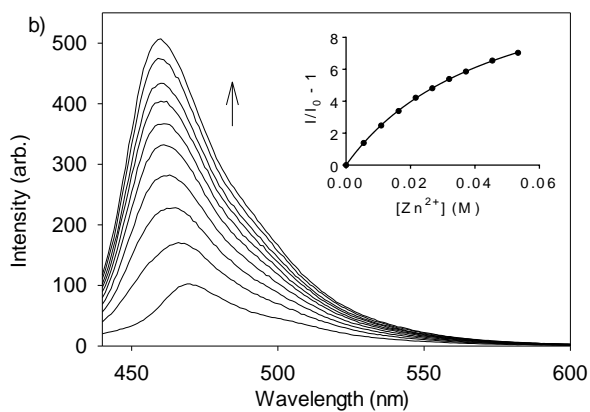


**Figure A-28.** Fluorescence titration (1  $\mu\text{M}$ ) of ES470 (**56c**) with 300 mM glutamate in buffer (50 mM bis-tris propane, 120 mM NaCl, 1% DMSO, pH 5.0) adding 5-8  $\mu\text{L}$  aliquots of 1.1 M zinc acetate.  $\lambda_{\text{ex}} = 393$  nm. Inset is the fit to a one-site binding isotherm.

Analyte Titrations for ES470 (56c) with Various Amine Analytes

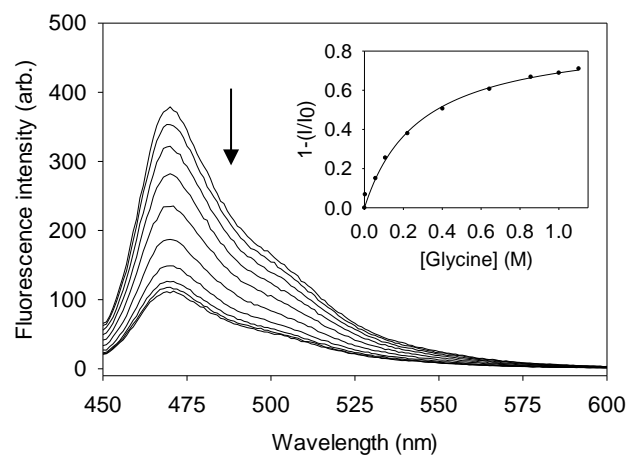


**Figure A-29.** Fluorescence titration of ES470 (1 μM) adding 20-800 μL aliquots of 1.5 M glycine in buffer (50 mM bis-tris propane, 120 mM NaCl, 1% DMSO, pH 7.4).  $\lambda_{\text{ex}} = 440$  nm. Inset is the fit to a one-site binding isotherm.

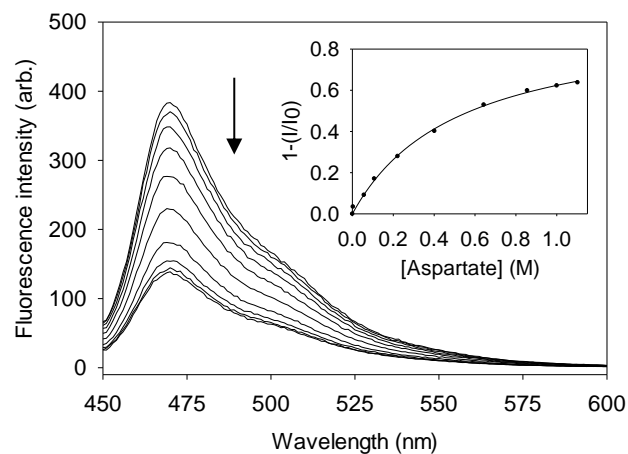


**Figure A-30.** Fluorescence titration of ES470 (1 μM) adding 20-800 μL aliquots of 1.5 M aspartate in buffer (50 mM bis-tris propane, 120 mM NaCl, 1% DMSO, pH 7.4).  $\lambda_{\text{ex}} = 440$  nm. Inset is the fit to a one-site binding isotherm.



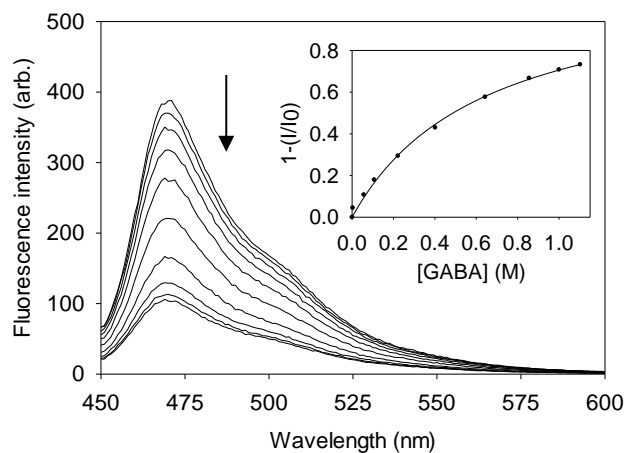


**Figure A-31.** Fluorescence titration of ES470 (1  $\mu$ M) adding 20-800  $\mu$ L aliquots of 1.5 M GABA in buffer (50 mM bis-tris propane, 120 mM NaCl, 1% DMSO, pH 7.4).  $\lambda_{\text{ex}} = 440$  nm. Inset is the fit to a one-site binding isotherm.

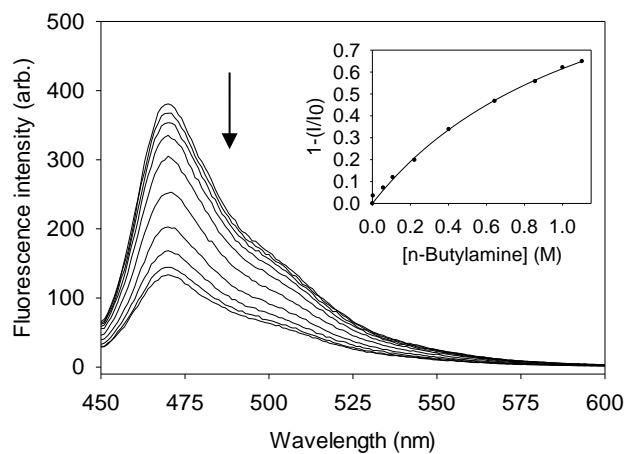


**Figure A-32.** Fluorescence titration of ES470 (1  $\mu$ M) adding 20-800  $\mu$ L aliquots of 1.5 M N-butylamine in buffer (50 mM bis-tris propane, 120 mM NaCl, 1% DMSO, pH 7.4).  $\lambda_{\text{ex}} = 440$  nm. Inset is the fit to a one-site binding isotherm.

## pH Titrations

### *pH Titration of 3-Formyl-7-methylsulfonamide-4-phenylcoumarin (28)*

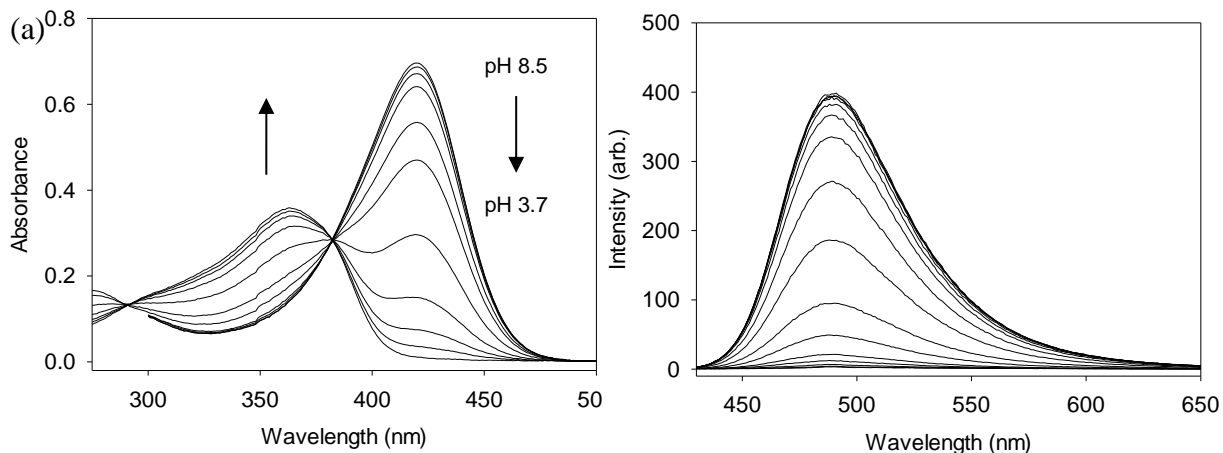


**Figure A-33.** (a) UV/vis and (b) fluorescence pH titration of compound **28** (20  $\mu$ M) in buffer (50 mM bis tris propane, 120 mM NaCl, 1% DMSO) adding aliquots of 1-12 M HCl from pH 8.5 to 3.7.  $\lambda_{\text{ex}} = 420$  nm.

### *pH Titration of 3-Formyl-4-phenyl-7-phenylsulfonamidocoumarin (43)*

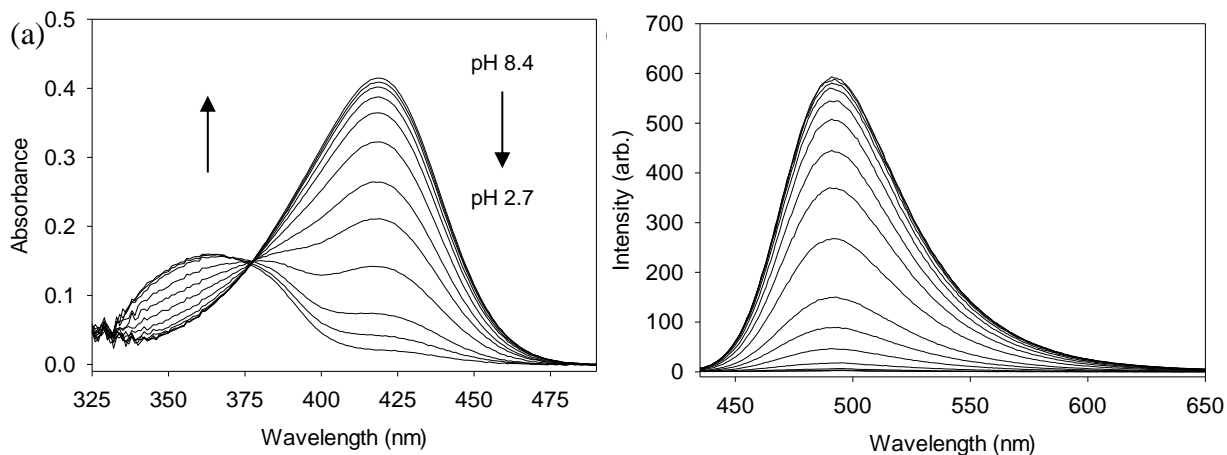


**Figure A-34.** (a) UV/vis and (b) fluorescence pH titration of compound **43** (20  $\mu$ M) in buffer (50 mM bis-tris propane, 120 mM NaCl, 1% DMSO) adding aliquots of 1-12 M HCl from pH 8.4 to 2.7.  $\lambda_{\text{ex}} = 425$  nm.

*pH Titration of 3-Formyl-4-phenyl-7-thiophenesulfonamidocoumarin (44)*

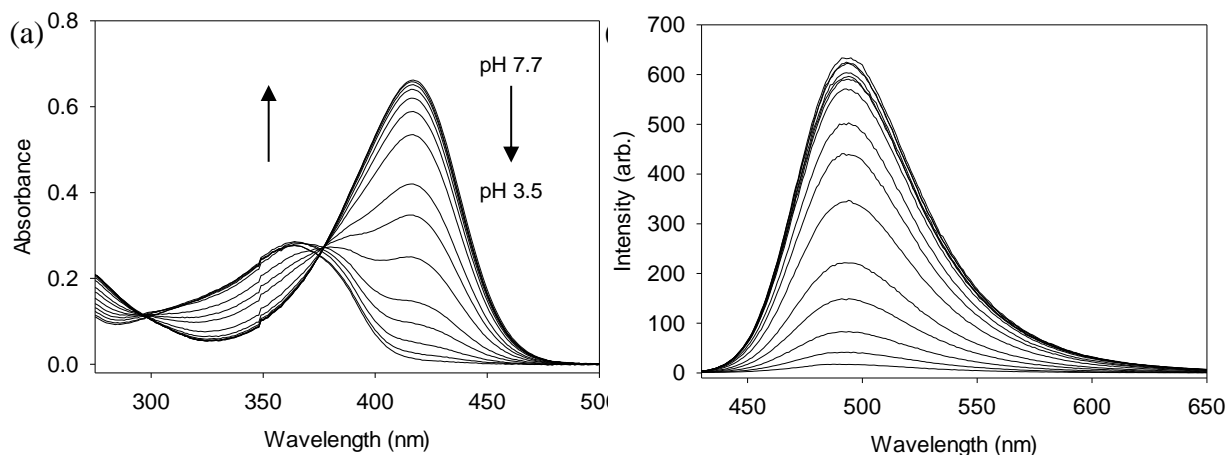


**Figure A-35.** (a) UV/vis and (b) fluorescence pH titration of compound **44** (20  $\mu\text{M}$ ) in buffer (50 mM bis-tris propane, 120 mM NaCl, 1% DMSO) adding aliquots of 1-12 M HCl from pH 7.7 to 3.5.  $\lambda_{\text{ex}} = 416$  nm.

*pH Titration of 3-Formyl-7-hydroxy-4-phenylcoumarin (41)*

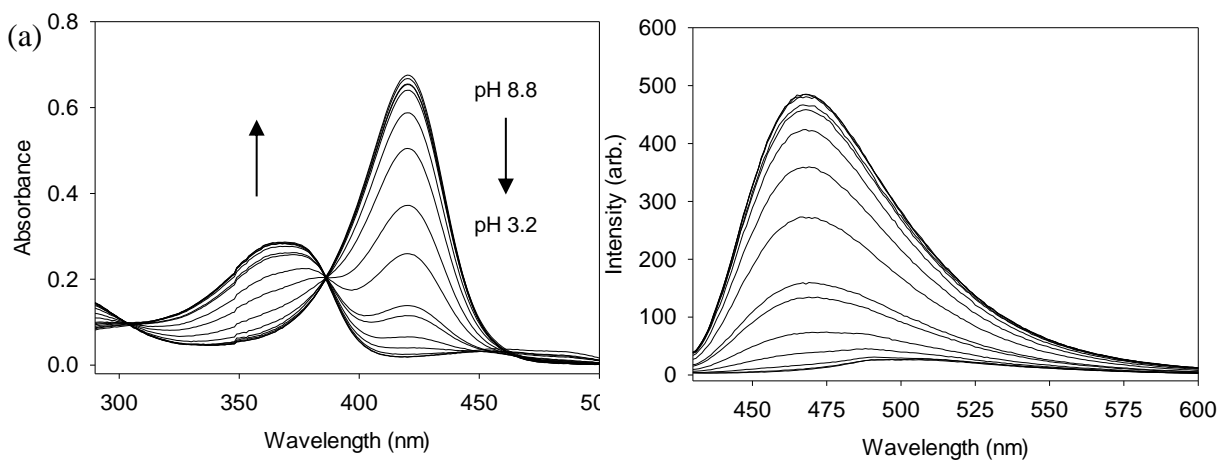


**Figure A-36.** (a) UV/vis and (b) fluorescence pH titration of compound **41** (20  $\mu\text{M}$ ) in buffer (50 mM bis-tris propane, 120 mM NaCl, 1% DMSO) adding aliquots of 1-12 M HCl from pH 8.8 to 3.2.  $\lambda_{\text{ex}} = 420$  nm.

*pH Titration of 3-formyl-7-hydroxycoumarin (56a)*

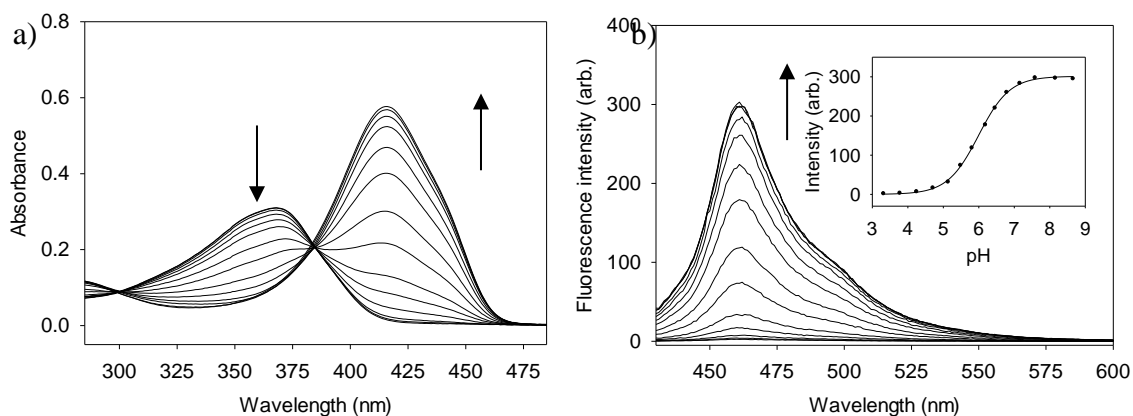


**Figure A-37.** a) UV/vis (20 μM) and b) fluorescence titration (1 μM) of **56a** in buffer (50 mM bis-tris propane, 120 mM NaCl, 1% DMSO) adding 1 μL aliquots of aq. NaOH.  $\lambda_{\text{ex}} = 416$  nm. Inset is the fit to a sigmoidal regression curve.

*pH Titration of 3-formyl-7-hydroxy-8-methylcoumarin (56b)*

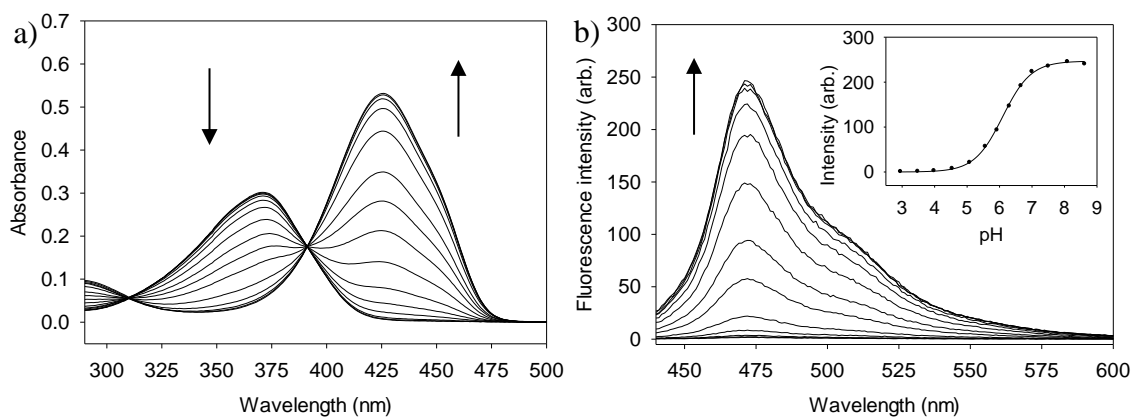


**Figure A-38.** a) UV/vis (20 μM) and b) fluorescence (1 μM) titration of **56b** in buffer (50 mM bis-tris propane, 120 mM NaCl, 1% DMSO) adding 1 μL aliquots of aq. NaOH.  $\lambda_{\text{ex}} = 426$  nm. Inset is the fit to a sigmoidal regression curve.

*pH Titration of 3-formyl-7-hydroxy-5,6-dimethylcoumain (ES470, 56c)*

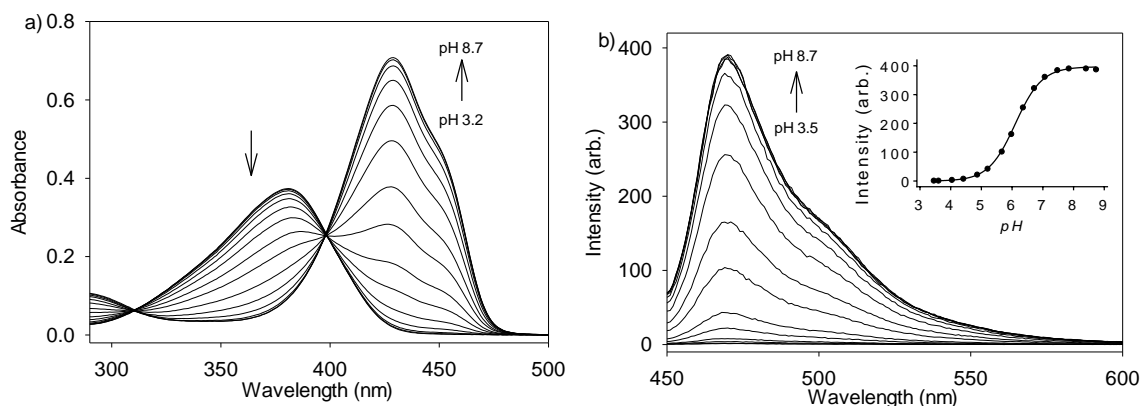


**Figure A-39.** a) UV/vis (20  $\mu\text{M}$ ) and b) fluorescence (1  $\mu\text{M}$ ) pH titration of ES470 in buffer (50 mM bis-tris propane, 120 mM NaCl, 1% DMSO) adding 1  $\mu\text{L}$  aliquots of aq. NaOH.  $\lambda_{\text{ex}} = 440 \text{ nm}$ . Inset is the fit to a sigmoidal regression curve.

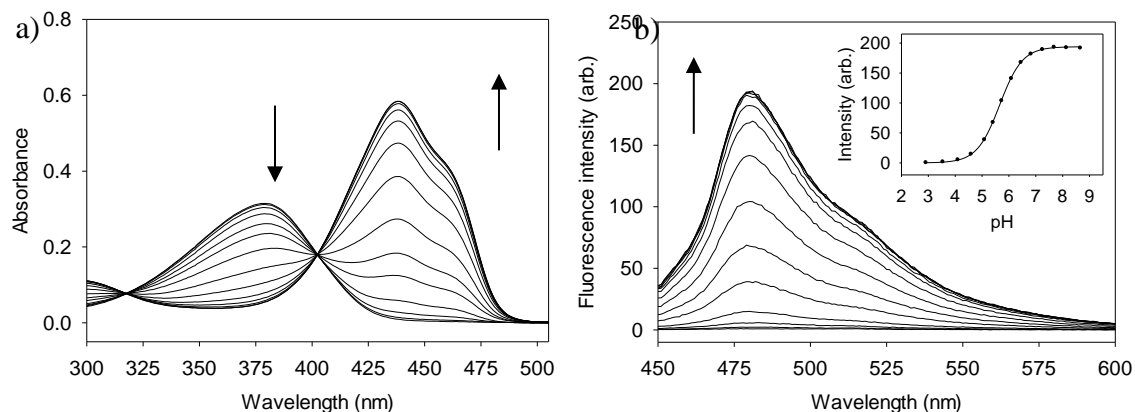


**Figure A-40.** a) UV/vis (20  $\mu\text{M}$ ) and b) fluorescence (1  $\mu\text{M}$ ) titration of **56d** in buffer (50 mM bis-tris propane, 120 mM NaCl, 1% DMSO) adding 1  $\mu\text{L}$  aliquots of aq. NaOH.  $\lambda_{\text{ex}} = 438 \text{ nm}$ . Inset is the fit to a sigmoidal regression curve.

*pH Titration of the Glutamate-Bound 3-Formyl-7-methoxy-4-phenylcoumarin (40)  
(to determine the  $pK_a$  of the iminium ion)*

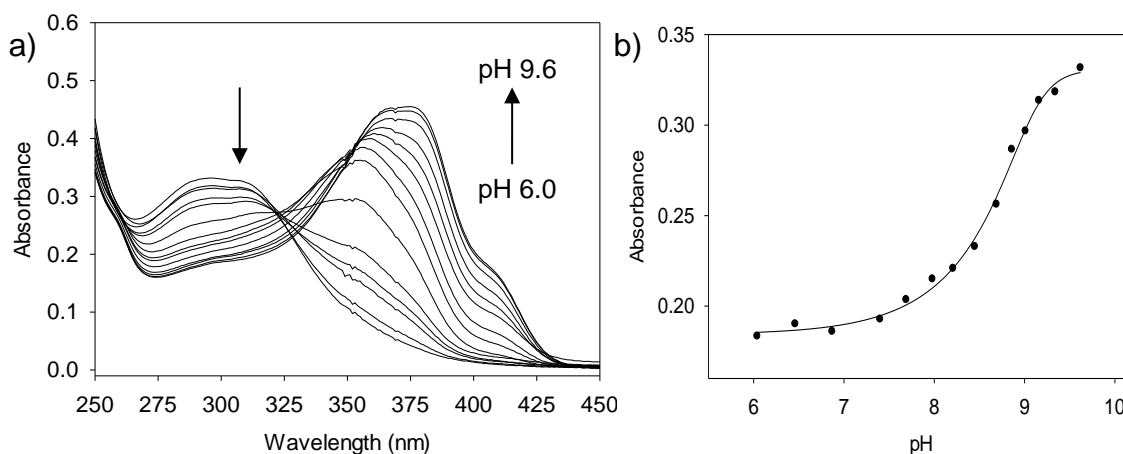
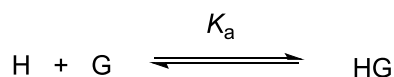


**Figure A-41.** (a) UV/vis titration and (b) fit to a sigmoidal regression curve for compound **40** (20  $\mu$ M) and 0.5 M glutamate adding aliquots of 1-8 M NaOH in buffer (50 mM bis tris propane, 120 mM NaCl).  $pK_a = 9.1$

### Part III. Binding Constant Determination



For host (H) – guest (G) binding studies, the data was fit to a 1:1 binding isotherm. Equation 1 shows the relationship between concentrations of bound and unbound host and guest species and the association constant ( $K_a$ ).

$$K_a = \frac{[HG]}{[H][G]} \quad (\text{Eq. 1})$$

For our experiments,  $[G]$  is much larger than the  $K_a$  meaning that G is virtually free at all concentrations used in the experiment. Therefore,  $G_{\text{free}} = G_{\text{total}}$ , and the plot of

$G_{\text{total}}$  vs. the fluorescence ( $I/I_0$ ) provides a hyperbolic curve where the  $K_d$  is equal to the concentration of G at half-saturation (Figure A-42). The guest concentration at which the sensor is half bound is equal to the dissociation constant ( $K_d$ ). The dissociation constant is inversely related to the association constant as described in Equation 2. Therefore, in the example below, the  $K_a$  would be  $1/0.006$  or  $167 \text{ M}^{-1}$ .

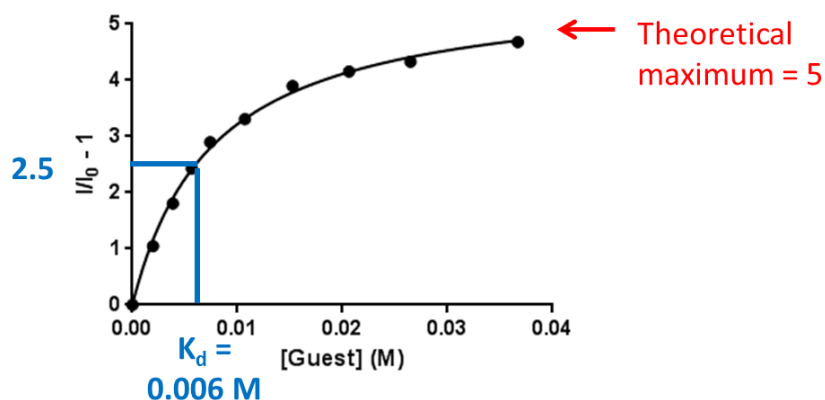


**Figure A-42.** Sample binding isotherm from a host-guest fluorescence titration

$$K_a = \frac{1}{K_d} \quad (\text{Eq. 2})$$

Equation 3 is used to solve for the dissociation constant.  $B_{\text{max}}$  is the theoretical maximum of the Y-axis if the parabolic were to go on to infinity.  $F_0$  is the initial fluorescence output with no guest present, and  $F$  is the fluorescence output at a given concentration of guest.

$$\left| \frac{F}{F_0} - 1 \right| = \frac{B_{\max} * G_{\text{total}}}{K_d + G_{\text{total}}} \quad (\text{Eq. 3})$$

#### Part IV. $pK_a$ Determination

The  $pK_a$  values were determined from either the UV/vis or fluorescence spectra. The pH was measured after addition of each aliquot of acid or base and the absorbance or fluorescence intensity was observed. Plotting the pH versus the absorbance or fluorescence intensity yields a sigmoidal shape (Figure A-43) to which a best-fit regression curve is assigned. The theoretical maximum and minimum of the best fit line are determined and the pH that corresponds with the inflection point represents the  $pK_a$  value for the given compound.

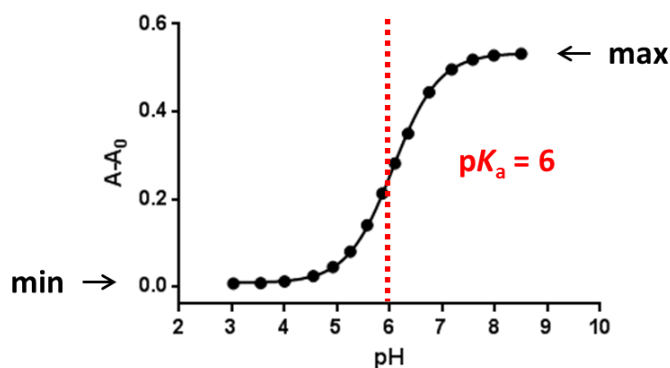


**Figure A-43.** Sigmoidal regression from a sample pH titration.

The regression curve used to determine the  $pK_a$  is shown in Equation 4. X is the logarithm of the pH value and Y is the response (i.e. absorbance or fluorescence intensity). The LogEC50 is the logarithm of the effective concentration (or the pH) at



which the response is half way (50%) between the maximum and minimum Y values. The standard slope used means that the response goes from 10-90% of max for every two log units.

$$Y = \text{Min} + \frac{(\text{Max} - \text{Min})}{1 + 10^{\text{LogEC50} - X}} \quad \text{Eq. 4}$$

### **Part V. Cellular Analyses**

Cellular analyses were performed using bovine adrenal chromaffin cells from a local slaughterhouse. Chromaffin cells are a standard model for studying exocytosis as the adrenal gland secretes hormones, i.e., epinephrine (EP) & norepinephrine (NE), that are packaged at high concentrations similar to neurotransmitters in neuronal vesicles.<sup>51-52,53, 128</sup>

The chromaffin cells were isolated from the adrenal glands using the following procedure:<sup>129</sup>

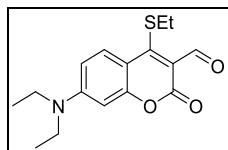
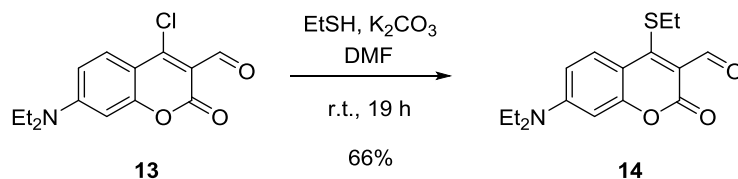
1. Inject a buffered solution of collagenase type P (1 mg/mL, Roche Diagnostics) into the portal vein. Shake glands at 37 °C for 20 min.
2. Cut around the cortex to open glands and peel away the medulla. Mince the medullae with a scalpel.
3. Filter the medullae suspension through a nylon mesh and centrifuge the liquid at 1000 rpm for 10 min. Discard supernatant. Resuspend pellet in isolation buffer.
4. Make a mixture of buffer and percoll in a 1:9 ratio, add to the cell solution, and centrifuge at 18 °C at 13,000 rpm for 45 min.

5. The cells can now be separated using a pipette into fractions that are EP-secreting (dense band) and NE-secreting (light band).<sup>130</sup>

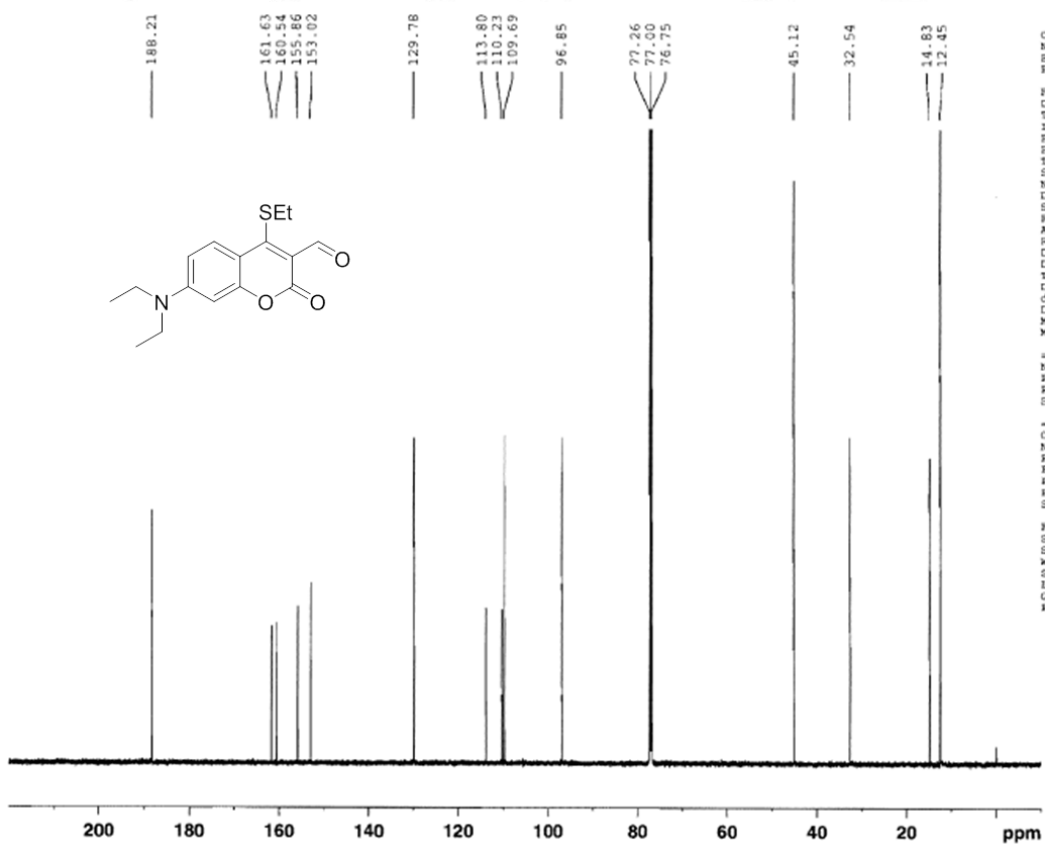
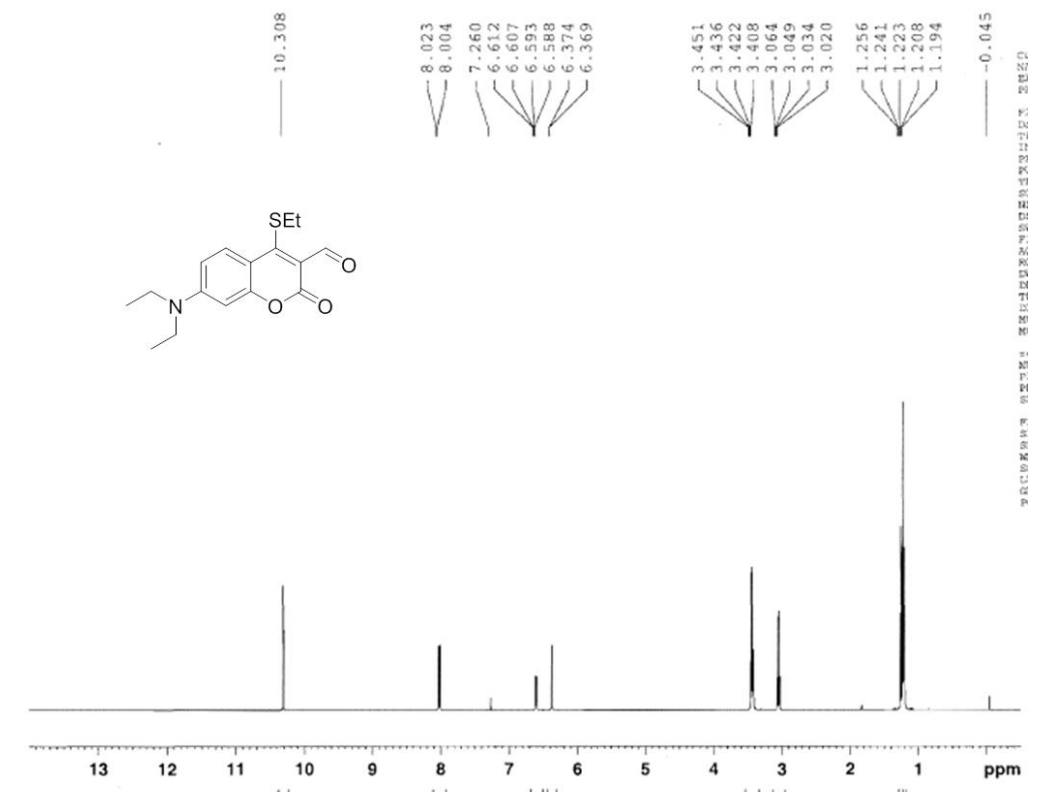
Most of the cells in the dense fraction (~90%) are EP-secreting whereas only ~67% of cells in the light band are NE-secreting.<sup>131</sup> The cells were cultured in Hibernate A media with calcium (Brain Bits, Springfield, IL), refrigerated, and used within 6 days of preparation.

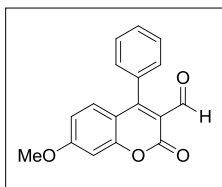
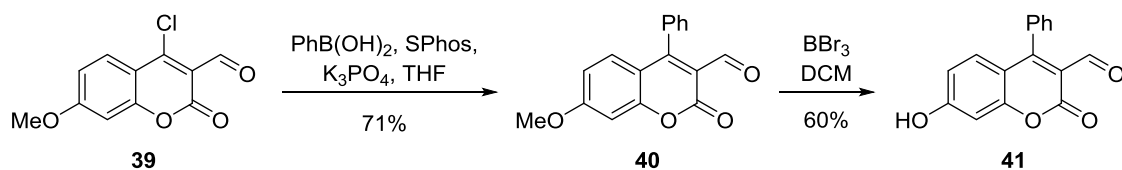
For the live cell imaging, approximately 5 mL of culture media containing either suspended NE or EP cells was centrifuged at 1000 rpm for 5 min and the supernatant discarded. Dulbecco's modified Eagle's medium (DMEM, 1 mL) was added, and the cells incubated on a Petri dish with sensor (0.1-10  $\mu$ L) at physiological temperature for 30 min. The cells were then transferred to a centrifuge tube, spun, washed twice with prewarmed PBS (Gibco, Grand Island, NY), then taken up in prewarmed chromaffin cell regular medium (DMEM with 10% (v/v) fetal bovine serum and 1% penicillin/streptomycin). To help the cells stick, they were plated onto coverslips coated with poly-lysine and incubated at 37 °C for 10 min. The coverslips were imaged using an Olympus Optical FluoView FV1000 confocal laser scanning biological microscope. A standard cell bath solution was added (150 mM NaCl, 5 mM KCl, 2 mM CaCl<sub>2</sub>, 1.2 mM MgCl<sub>2</sub>, 10 mM HEPES, and 11 mM glucose, pH 7.2), and the images were acquired using a laser with a wavelength of either 488 or 440 nm.

## Part VI. Synthetic Procedures and Characterization Data

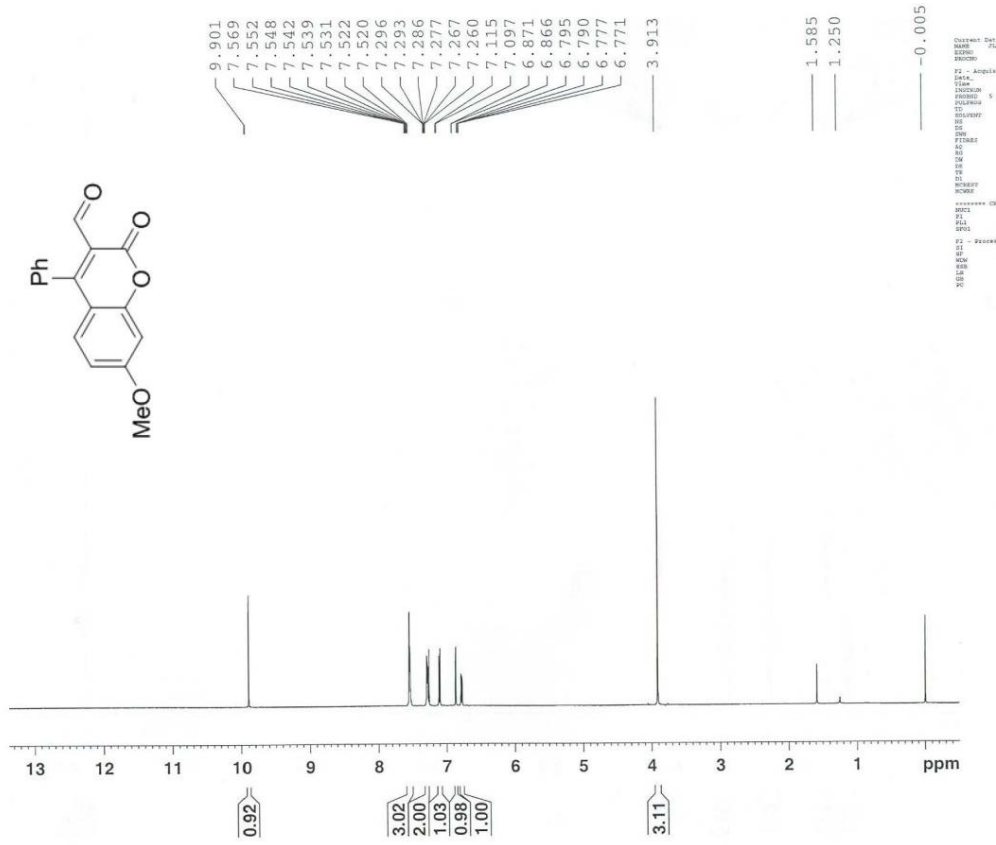


**Sensor 14.** Compound **13**<sup>132</sup> (200 mg, 0.715 mmol) and K<sub>2</sub>CO<sub>3</sub> (395 mg, 2.860 mmol) were measured into a flame-dried round bottom flask. To the starting material was added a 0.1 M solution of ethanethiol in DMF (6.9 mL). The solution stirred at room temperature for 19 h. The DMF was removed in vacuo and the remaining crude material was purified by chromatography (95:5 CH<sub>2</sub>Cl<sub>2</sub>/ EtOAc) to yield sensor **14** as a yellow oil (145 mg, 66%): <sup>1</sup>H NMR (500 MHz, CDCl<sub>3</sub>) δ 10.31 (s, 1H), 8.01 (d, 1H, *J* = 9.5 Hz), 6.60 (dd, 1H, *J* = 9.5, 2.5 Hz), 6.37 (d, 1H, *J* = 2.5 Hz), 3.43 (q, 4H, *J* = 7.5), 3.04 (q, 2H, *J* = 7.5 Hz), 1.24 (t, 3H, *J* = 7.5 Hz), 1.21 (t, 6H, *J* = 7.5 Hz); <sup>13</sup>C NMR (125 MHz, CDCl<sub>3</sub>) δ 188.2, 161.6, 160.5, 155.9, 153.0, 129.8, 113.8, 110.2, 109.7, 96.9, 45.1, 32.5, 14.8, 12.5; IR (neat, cm<sup>-1</sup>) 2970, 2925, 2868, 1712, 1610, 1487, 1409, 1352, 1136; HRMS calculated for C<sub>16</sub>H<sub>19</sub>NNaO<sub>3</sub>S (M + Na<sup>+</sup>): 328.0983. Found: 328.0974.

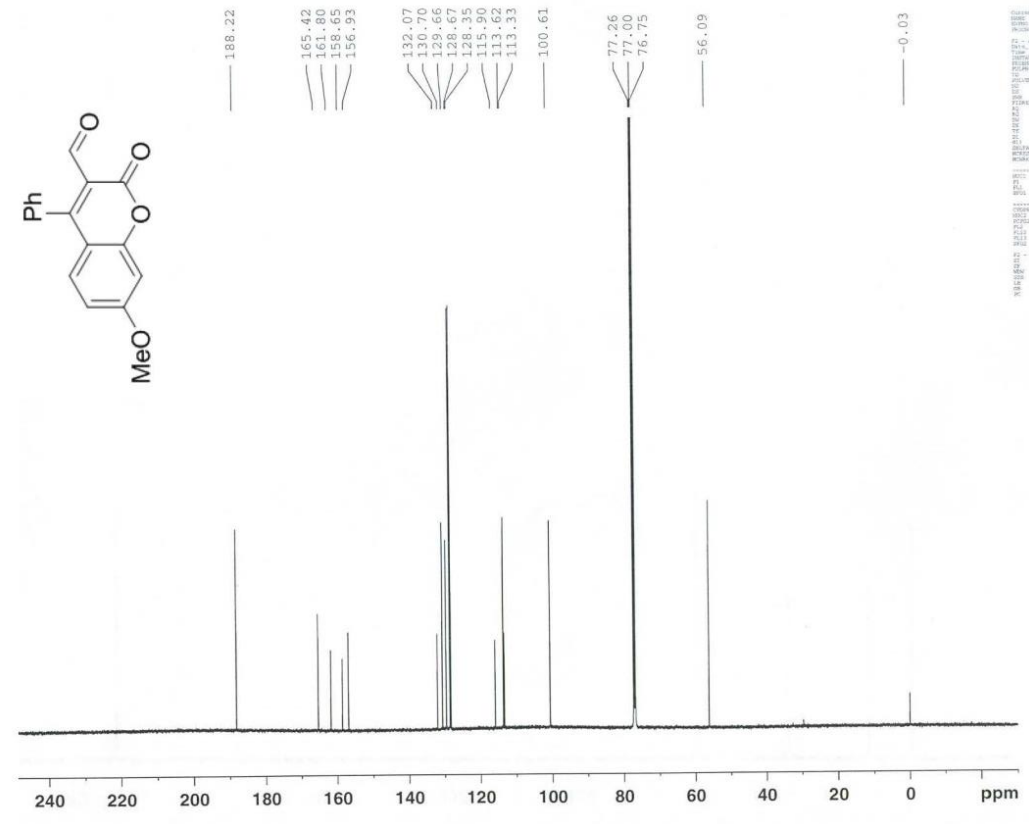




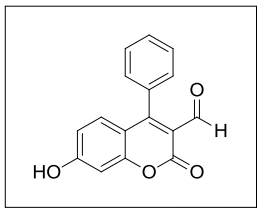
**Compound 40.** A mixture of compound **39** (129 mg, 0.541 mmol),  $\text{PhB(OH)}_2$  (79.1 mg, 0.649 mmol),  $\text{Pd}_2\text{dba}_3$  (24.7 mg, 0.027 mmol), SPhos (33.0 mg, 0.081 mmol),  $\text{K}_3\text{PO}_4$  (230 mg, 1.082 mmol) degassed for 15 minutes. Dry, degassed THF (3.2 mL) was added and the solution stirred at 60 °C for 12 h. The solution was filtered and the solvent removed *in vacuo*. The remaining residue was purified by chromatography (95:5  $\text{CH}_2\text{Cl}_2/\text{EtOAc}$ ) to yield compound **40** (107 mg, 71%) as a yellow solid (mp 164 °C):  $^1\text{H}$  NMR (500 MHz,  $\text{CDCl}_3$ )  $\delta$  9.90 (s, 1H), 7.51-7.58 (m, 3H), 7.26-7.31 (m, 2H), 7.11 (d, 1H,  $J = 9.0$  Hz), 6.87 (d, 1H,  $J = 2.5$  Hz), 6.78 (dd, 1H,  $J = 9.2, 2.5$  Hz), 3.91 (s, 3H);  $^{13}\text{C}$  NMR (125 MHz,  $\text{CDCl}_3$ )  $\delta$  188.2, 165.4, 161.8, 158.7, 156.9, 132.0, 130.7, 129.7, 128.7, 128.4, 115.9, 113.6, 113.3, 100.6, 56.1; IR (neat,  $\text{cm}^{-1}$ ) 2846, 1756, 1720, 1614, 1581, 1532, 1374, 1296; HRMS calculated for  $\text{C}_{17}\text{H}_{12}\text{O}_4\text{Na}$  ( $\text{M} + \text{Na}^+$ ): 303.0628. Found: 303.0628.



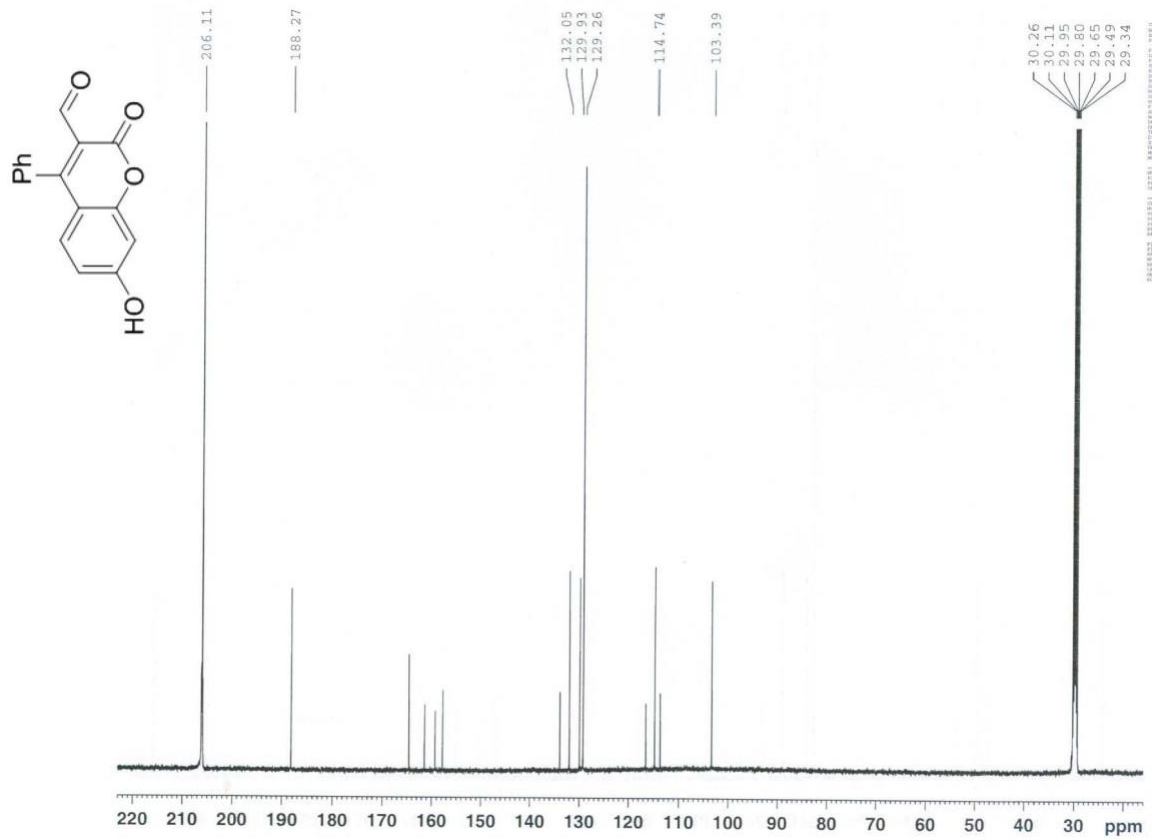
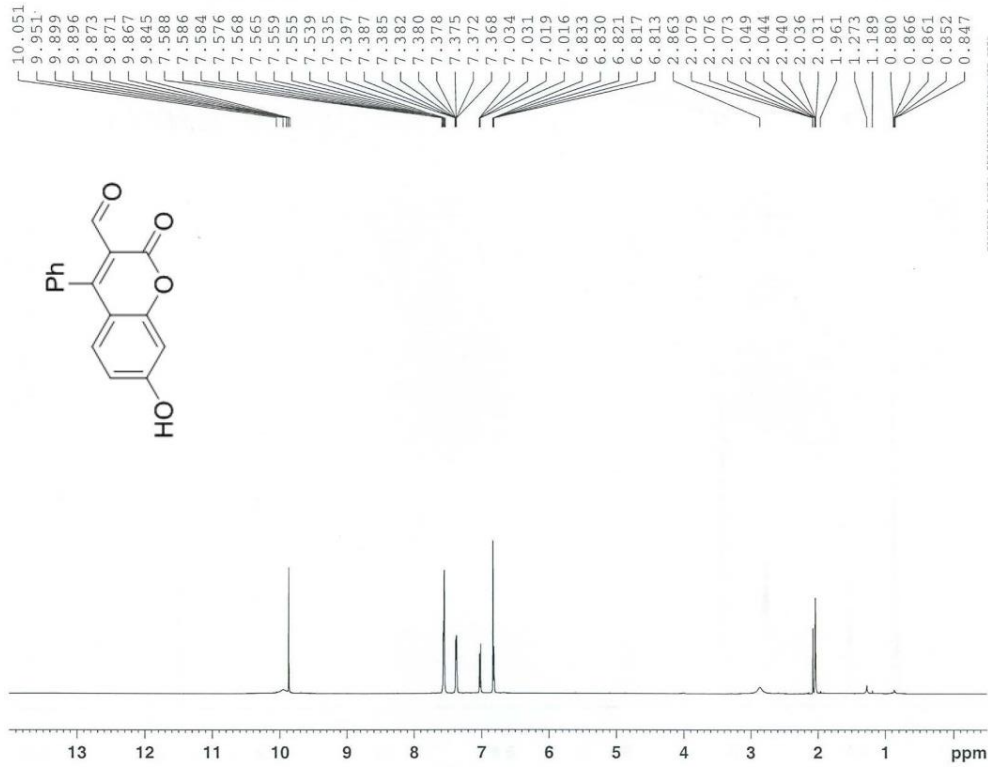
Channel 1  
 Name  
 F2 - Acquis  
 Date  
 Time  
 Instrument  
 Program  
 Operator  
 Sample  
 Solvent  
 P1  
 P2  
 P3  
 P4  
 P5  
 P6  
 P7  
 P8  
 P9  
 P10  
 P11  
 P12  
 P13  
 P14  
 P15  
 P16  
 P17  
 P18  
 P19  
 P20  
 P21  
 P22  
 P23  
 P24  
 P25  
 P26  
 P27  
 P28  
 P29  
 P30  
 P31  
 P32  
 P33  
 P34  
 P35  
 P36  
 P37  
 P38  
 P39  
 P40  
 P41  
 P42  
 P43  
 P44  
 P45  
 P46  
 P47  
 P48  
 P49  
 P50  
 P51  
 P52  
 P53  
 P54  
 P55  
 P56  
 P57  
 P58  
 P59  
 P60  
 P61  
 P62  
 P63  
 P64  
 P65  
 P66  
 P67  
 P68  
 P69  
 P70  
 P71  
 P72  
 P73  
 P74  
 P75  
 P76  
 P77  
 P78  
 P79  
 P80  
 P81  
 P82  
 P83  
 P84  
 P85  
 P86  
 P87  
 P88  
 P89  
 P90  
 P91  
 P92  
 P93  
 P94  
 P95  
 P96  
 P97  
 P98  
 P99  
 P100



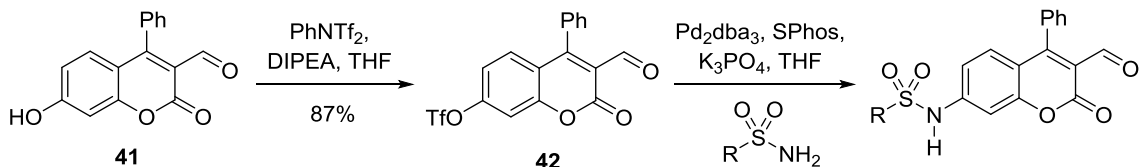
Name  
 F2 - Acquis  
 Date  
 Time  
 Instrument  
 Program  
 Operator  
 Sample  
 Solvent  
 P1  
 P2  
 P3  
 P4  
 P5  
 P6  
 P7  
 P8  
 P9  
 P10  
 P11  
 P12  
 P13  
 P14  
 P15  
 P16  
 P17  
 P18  
 P19  
 P20  
 P21  
 P22  
 P23  
 P24  
 P25  
 P26  
 P27  
 P28  
 P29  
 P30  
 P31  
 P32  
 P33  
 P34  
 P35  
 P36  
 P37  
 P38  
 P39  
 P40  
 P41  
 P42  
 P43  
 P44  
 P45  
 P46  
 P47  
 P48  
 P49  
 P50  
 P51  
 P52  
 P53  
 P54  
 P55  
 P56  
 P57  
 P58  
 P59  
 P60  
 P61  
 P62  
 P63  
 P64  
 P65  
 P66  
 P67  
 P68  
 P69  
 P70  
 P71  
 P72  
 P73  
 P74  
 P75  
 P76  
 P77  
 P78  
 P79  
 P80  
 P81  
 P82  
 P83  
 P84  
 P85  
 P86  
 P87  
 P88  
 P89  
 P90  
 P91  
 P92  
 P93  
 P94  
 P95  
 P96  
 P97  
 P98  
 P99  
 P100



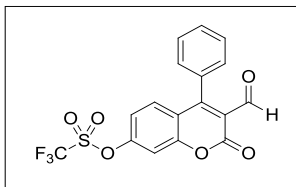
**Compound 41.** A solution of compound **40** (38 mg, 0.136 mmol) in CH<sub>2</sub>Cl<sub>2</sub> (2 mL) was added to a flame-dried round bottom and cooled to -78 °C. BBr<sub>3</sub> (0.68 mL of a 1.0 M solution in CH<sub>2</sub>Cl<sub>2</sub>, 0.678 mmol) was added dropwise. The reaction was warmed to room temperature over 12 h. After being quenched with cold deionized water (3 mL), the mixture was extracted with CH<sub>2</sub>Cl<sub>2</sub> (10 mL x 5). The combined organic layers were dried over Na<sub>2</sub>SO<sub>4</sub>, and the solvent was removed *in vacuo*. The residue was purified by chromatography (7:3 hexanes/EtOAc) to yield compound **41** (21.7 mg, 60%) as a yellow solid (mp 165 °C): <sup>1</sup>H NMR (500 MHz, d-acetone) δ 9.95 (s, 1H), 9.87 (s, 1H), 7.53-7.59 (m, 3H), 7.35-7.41 (m, 2H), 7.03 (d, 1H, *J* = 7.5 Hz), 6.80-6.85 (m, 2H); <sup>13</sup>C NMR (125 MHz, d-acetone) δ 188.3, 164.7, 161.3, 159.3, 157.8, 133.9, 132.1, 129.9, 129.3, 116.5, 114.7, 113.8, 103.4; IR (neat, cm<sup>-1</sup>) 3273, 1734, 1614, 1535, 1385, 1120; HRMS calculated for C<sub>16</sub>H<sub>10</sub>O<sub>4</sub>Na (M + Na<sup>+</sup>): 289.0471. Found: 289.0471.



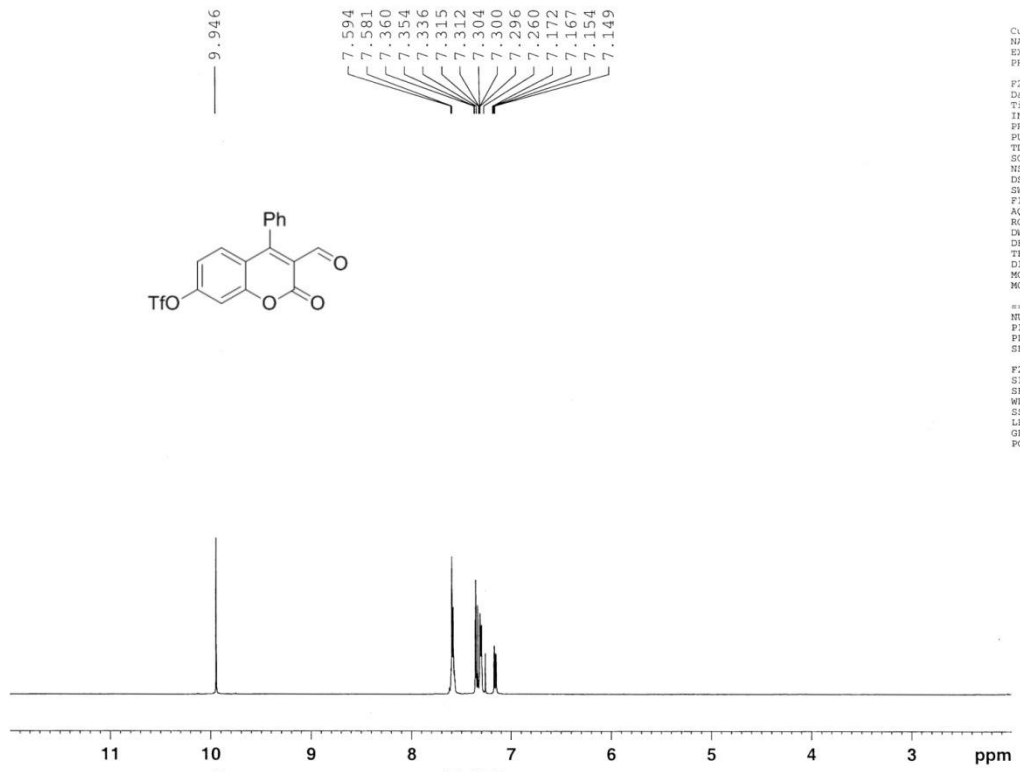




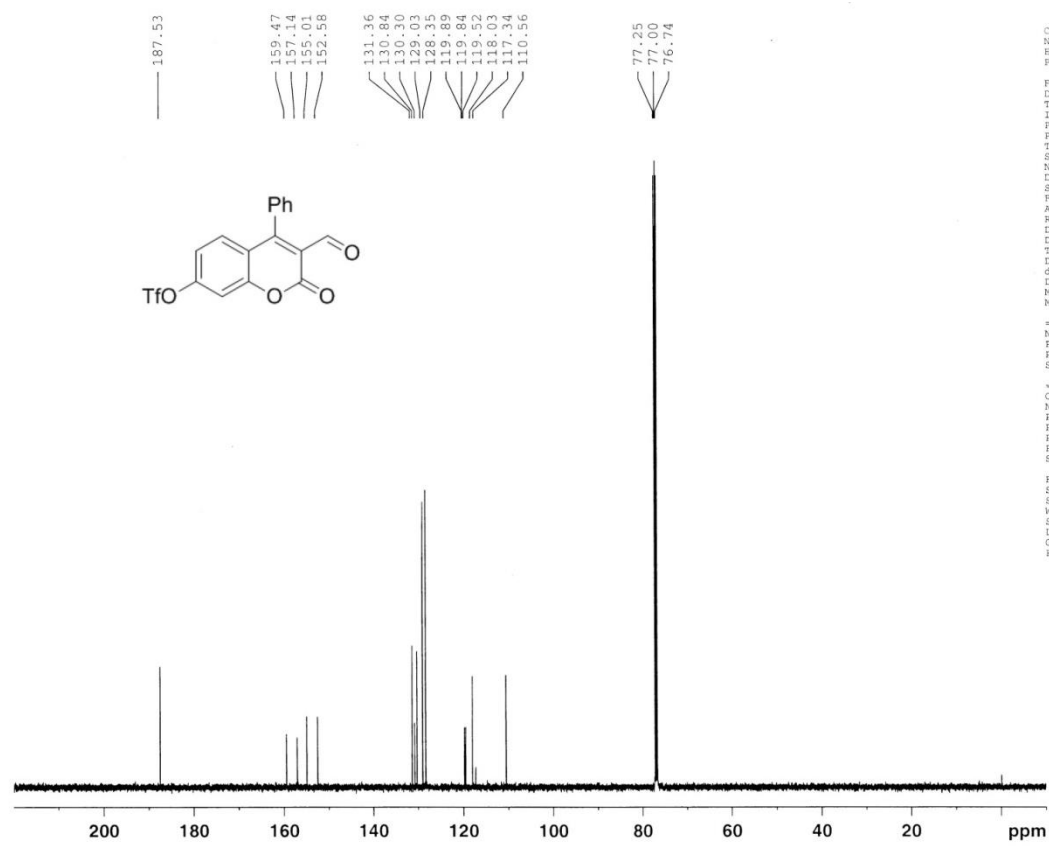
**ES517**, R = Me<sub>2</sub>N, 47%; **28**, R = Me, 33%; **43**, R = Ph, 50%; **44**, R = thiophene, 49%



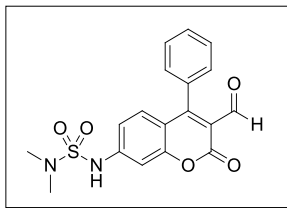
**Compound 42.** Compound **41** (465 mg, 1.746 mmol) and N-phenyltriflimide (686 mg, 1.921 mmol) were combined in a round bottom flask. THF (24 mL) was added and then DIPEA was added dropwise (0.38 mL, 2.270 mmol). The mixture stirred at ambient temperature for 3 h followed by removal of the solvent *in vacuo*. The residue was purified by chromatography (95:5 CH<sub>2</sub>Cl<sub>2</sub>/EtOAc) to yield compound **42** (607.2 mg, 87%) as a golden oil: <sup>1</sup>H NMR (500 MHz, CDCl<sub>3</sub>) δ 9.95 (s, 1H), 7.56-7.62 (m, 3H), 7.33-7.37 (m, 2H), 7.29-7.32 (m, 2H), 7.16 (dd, 1H, *J* = 9.0, 2.5 Hz); <sup>13</sup>C NMR (125 MHz, CDCl<sub>3</sub>) δ 187.5, 159.5, 157.1, 155.0, 152.6, 131.4, 130.8, 130.3, 129.0, 128.4, 119.9, 119.7 (q, C-F, *J* = 40 Hz), 118.0, 117.3, 110.6; IR (neat, cm<sup>-1</sup>) 1765, 1605, 1552, 1422, 1364, 1217, 1136, 1107, 980; HRMS calculated for C<sub>17</sub>H<sub>9</sub>F<sub>3</sub>O<sub>6</sub>SNa (M + Na<sup>+</sup>): 420.9964. Found: 420.9961.



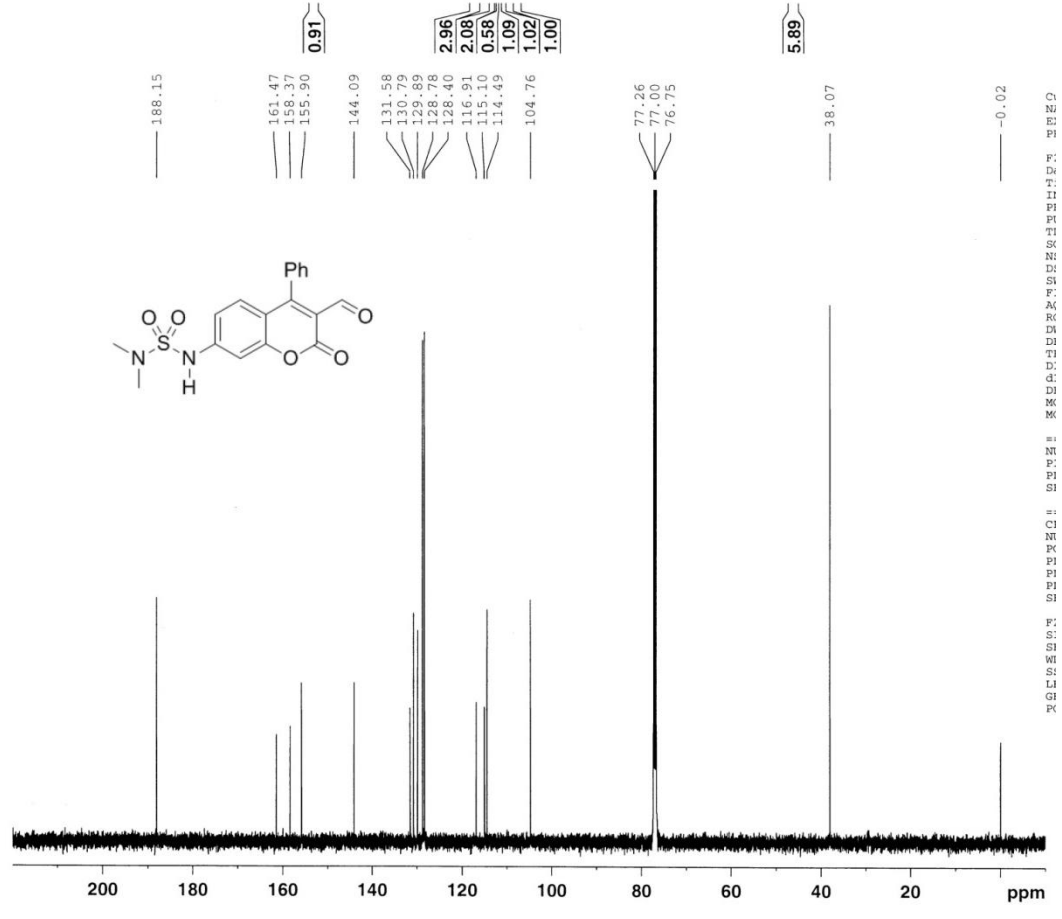
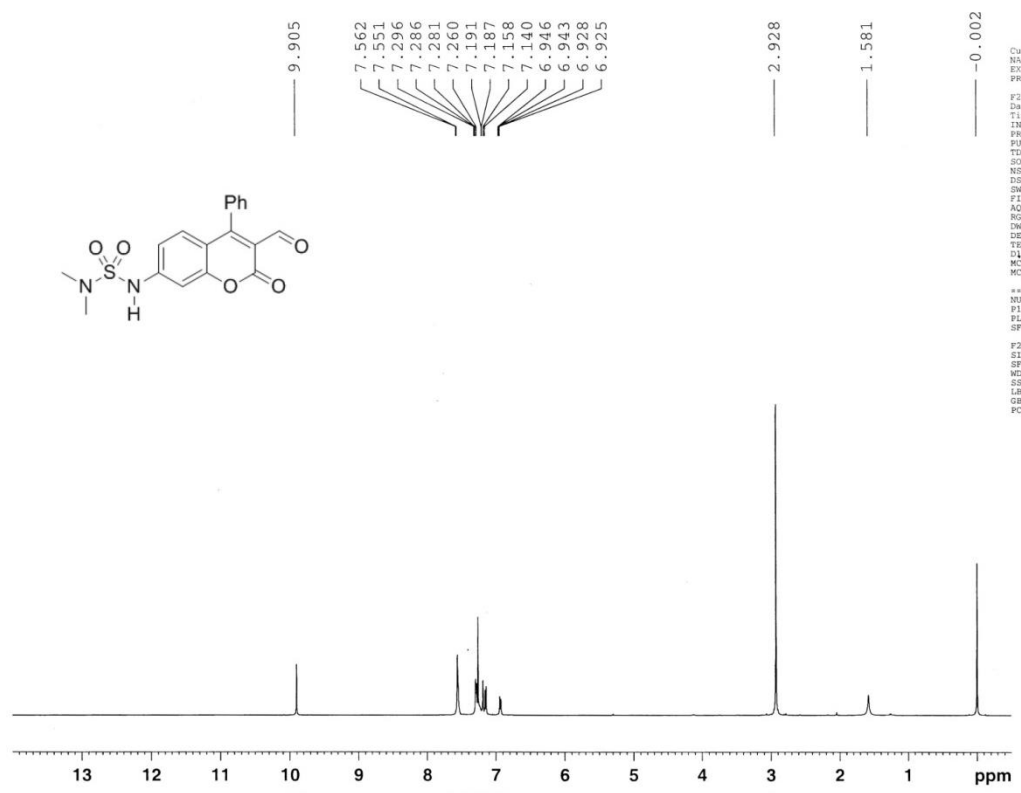
CU  
NA  
EX  
PR  
  
F2  
Da  
TL  
IN  
FR  
FU  
TD  
SO  
NS  
DS  
SW  
FI  
AQ  
RG  
SW  
DE  
TE  
DI  
MC  
MC  
  
==  
NU  
F1  
PL  
SF  
  
F2  
SI  
SF  
WD  
SS  
LS  
OB  
PC



F  
D  
T  
I  
P  
P  
T  
S  
N  
N  
S  
T  
A  
R  
I  
D  
D  
T  
E  
d  
d  
I  
M  
M  
  
= N  
T  
P  
S  
I  
  
\* C  
M  
P  
P  
P  
P  
P  
P  
S  
  
F  
S  
S  
M  
S  
S  
L  
L  
G  
P



**ES517.** Compound **42** (123 mg, 0.309 mmol) was combined with N,N-dimethylsulfamide (42 mg, 0.340 mmol), Pd<sub>2</sub>dba<sub>3</sub> (14 mg, 0.015 mmol), SPhos (18 mg, 0.046 mmol), and K<sub>3</sub>PO<sub>4</sub> (132 mg, 0.618 mmol) in a round bottom flask and degassed for 20 min. Dry degassed THF was added and the mixture was purged with N<sub>2</sub> for 30 min followed by heating at 55 °C for 24 h. The solvent was evaporated with a stream of N<sub>2</sub>, the crude product taken up in water (pH 5), and extracted with EtOAc (15 mL x 3). Purification by chromatography (95:5 CH<sub>2</sub>Cl<sub>2</sub>/EtOAc) gave **ES517** (54 mg, 47%) as a yellow solid (mp 195 C): <sup>1</sup>H NMR (500 MHz, CDCl<sub>3</sub>) δ 9.91 (s, 1H), 7.52-7.58 (m, 3H), 7.27-7.31 (m, 2H), 7.19 (d, 1H, *J* = 2.0 Hz), 7.15 (d, 1H, *J* = 9.0 Hz), 6.93 (dd, 1H, *J* = 9.0, 2.0 Hz), 2.93 (s, 6H); <sup>13</sup>C NMR (125 MHz, CDCl<sub>3</sub>) δ 188.2, 161.5, 158.4, 155.9, 144.1, 131.6, 130.8, 129.9, 128.8, 128.4, 116.9, 115.1, 114.5, 104.8, 38.1; IR (KBr, cm<sup>-1</sup>) 3260, 1732, 1610, 1528, 1377, 1140; HRMS calculated for C<sub>18</sub>H<sub>16</sub>N<sub>2</sub>O<sub>5</sub>SNa (M + Na<sup>+</sup>): 395.0672. Found: 395.0670.



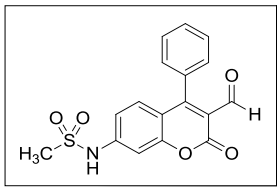
Cu  
NA  
EX  
PR  
F2  
D3  
TI  
IN  
PR  
PU  
TD  
SO  
NS  
DS  
SM  
FI  
AO  
RG  
DW  
DE  
TE  
CL  
MC  
MC  
\*\*  
NI  
PI  
PL  
SF  
F2  
SI  
SF  
MD  
SS  
LB  
GB  
PC

F:  
D:  
T:  
I:  
PI  
PI  
TI  
TI  
SK  
NI  
D:  
SI  
F:  
AG  
RC  
DN  
DJ  
TI  
D:  
D:  
DJ  
K  
M  
K

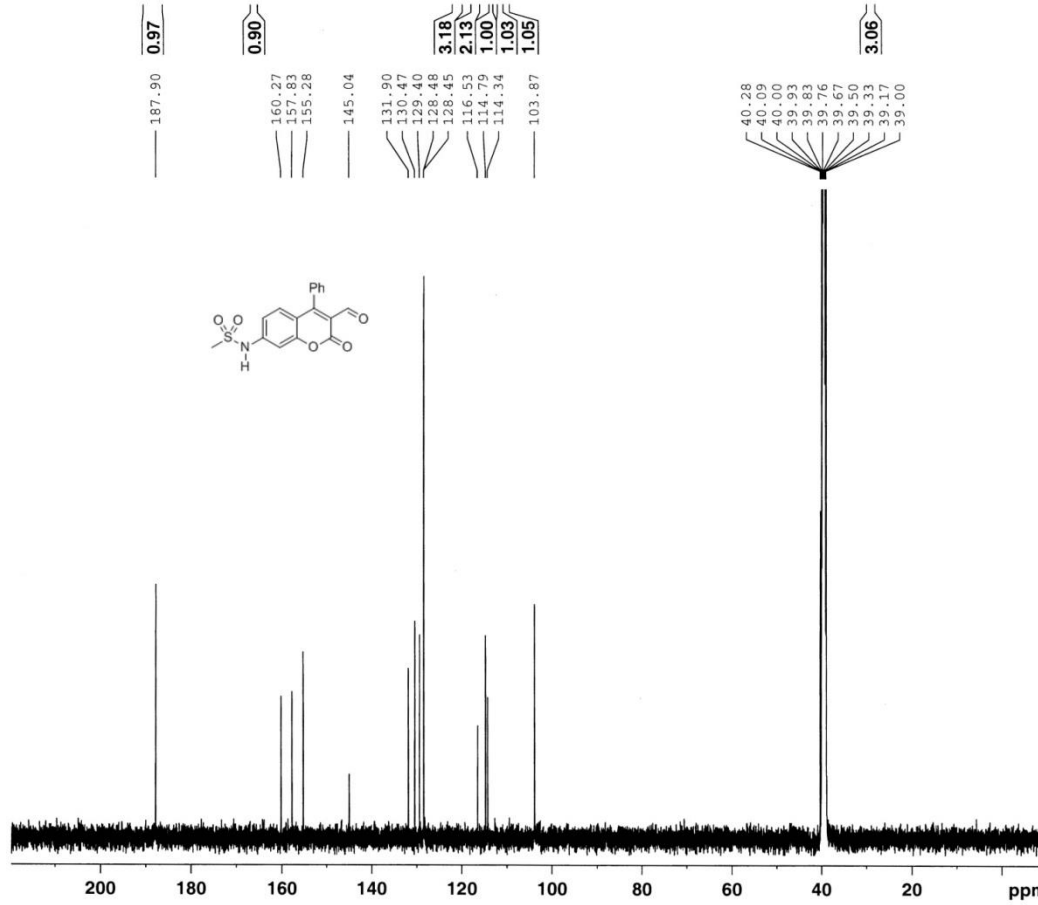
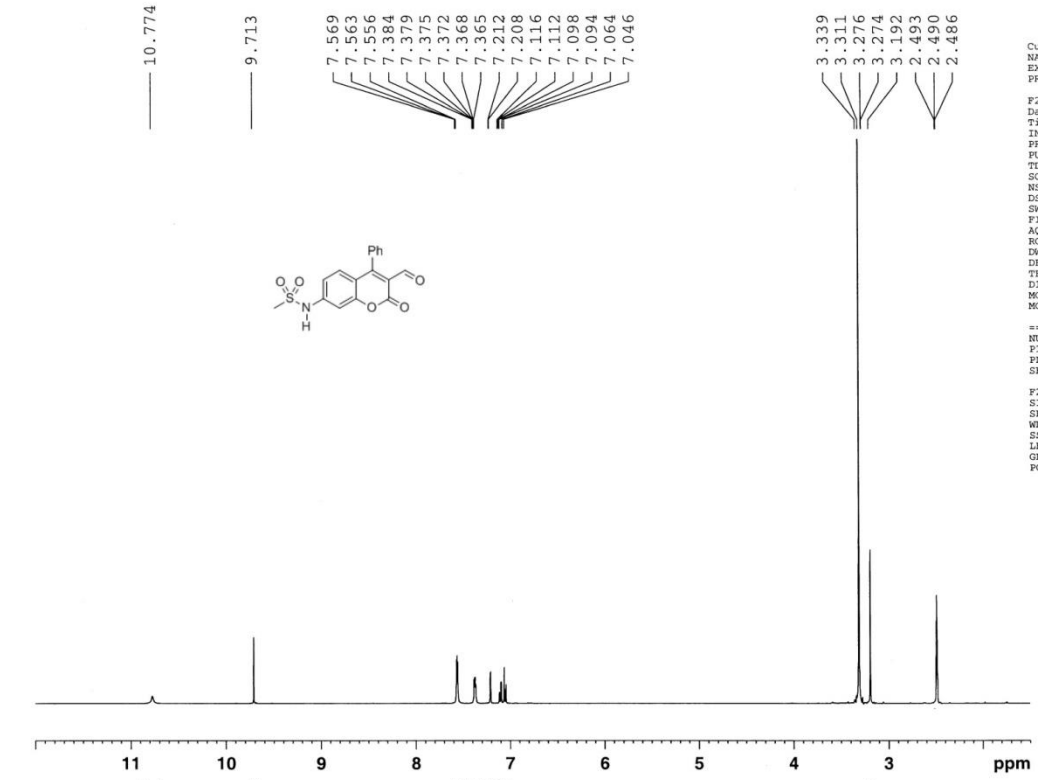
=:  
NI  
P:  
PI  
SI

=:  
CI  
NI  
K  
PI  
PI  
PI  
SI

F:  
S:  
SI  
WE  
SI  
LI  
GH  
K

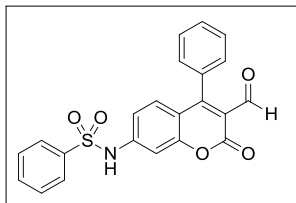


**Compound 28.** Compound **42**<sup>121</sup> (84 mg, 0.211 mmol), methanesulfonamide (22.1 mg, .232 mmol), Pd<sub>2</sub>dba<sub>3</sub> (10.1 mg, .011 mmol), SPhos (13.1 mg, .032 mmol), and K<sub>3</sub>PO<sub>4</sub> (90 mg, .422 mmol) were combined in a round bottom flask and degassed with N<sub>2</sub> for 20 min. Dry degassed THF (1.5 mL) was added and the mixture stirred at 60 C for 18 h. The solvent was removed *in vacuo*. The remaining residue was taken up in EtOAc, washed with a brine solution at pH 4 (10 mL), dried over MgSO<sub>4</sub>, and the solvent removed *in vacuo*. Purification by chromatography (9:1 CH<sub>2</sub>Cl<sub>2</sub>/EtOAc) gave compound **28** (24 mg, 33%) as a beige solid (decomp 238 C): <sup>1</sup>H NMR (500 MHz, DMSO) δ 10.77 (s, 1H), 9.71 (s, 1H), 7.54-7.58 (m, 3H), 7.35-7.39 (m, 2H), 7.21 (d, 1H, *J* = 2.0 Hz), 7.11 (dd, 1H, *J* = 9.0, 2.0 Hz), 7.06 (d, 1H, *J* = 9.0 Hz), 3.19 (s, 3H); <sup>13</sup>C NMR (125 MHz, DMSO) δ 187.9, 160.3, 157.8, 155.3, 145.0, 131.9, 130.5, 129.4, 128.5, 128.5, 116.5, 114.8, 114.3, 103.9, 40.3; IR (KBr, cm<sup>-1</sup>) 3436, 3289, 1753, 1614, 1536, 1373, 1160; HRMS calculated for C<sub>17</sub>H<sub>13</sub>NO<sub>5</sub>S (M + Na<sup>+</sup>): 366.0407. Found: 366.0405.

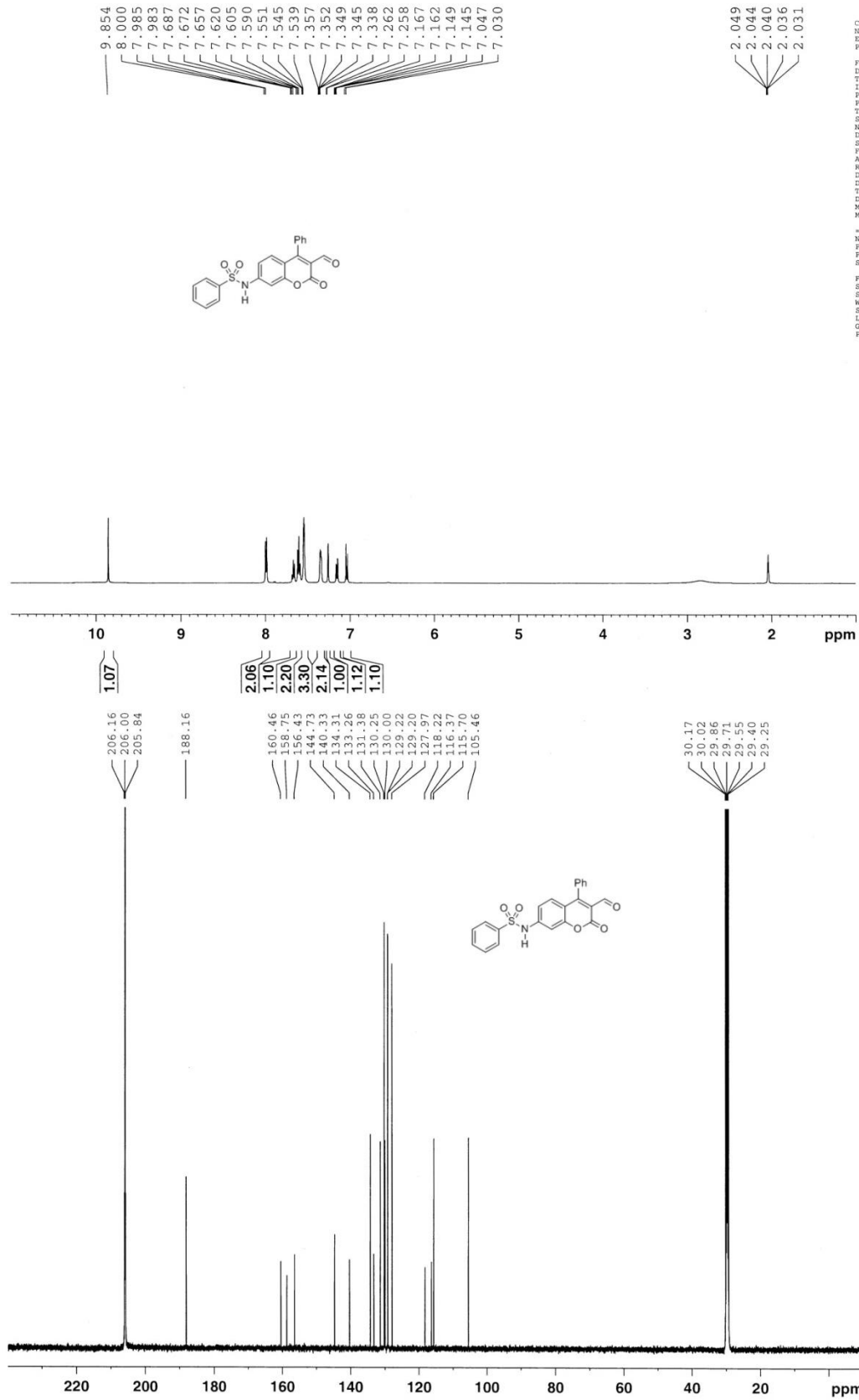


F: D: T: I: P: T: S: K: N: D: S: P: A: R: D: D: T: E: M: K: M: #: M: F: P: I: S: I: F: S: S: S: L: G: R

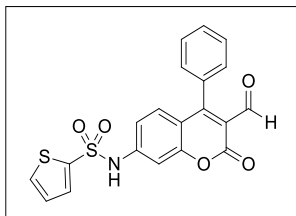
F: D: T: I: P: T: S: K: N: D: S: P: A: R: D: D: T: E: M: K: M: #: M: F: P: I: S: I: F: S: S: S: L: G: R



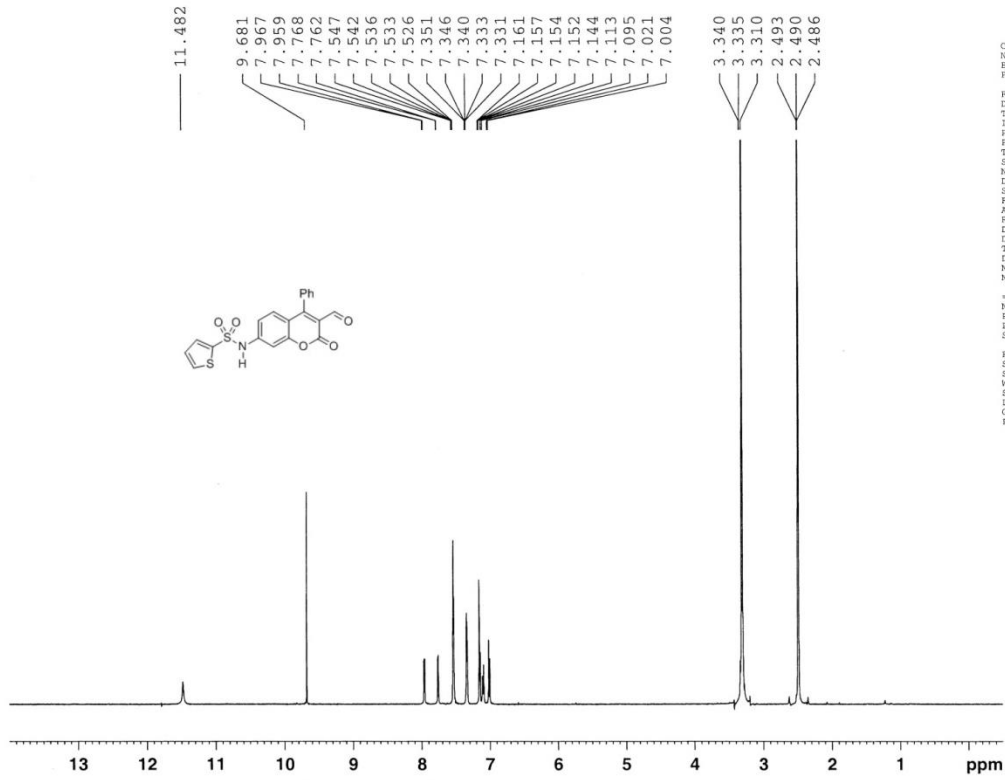
**Compound 43.** Compound **42** (83.3 mg, .209 mmol) was combined with benzenesulfonamide (52.9 mg, .337 mmol), Pd<sub>2</sub>dba<sub>3</sub> (13.7 mg, .015 mmol), SPhos (18.9 mg, .046 mmol), and K<sub>3</sub>PO<sub>4</sub> (130.1 mg, .613 mmol) in a round bottom flask and degassed for 20 min. Dry degassed THF was added and the mixture was purged with N<sub>2</sub> for 10 min followed by heating at 55 C for 22 h. The solvent was evaporated with a stream of N<sub>2</sub>, the crude product taken up in water (pH 4), and extracted with EtOAc (15 mL x 3). Purification by chromatography (95:5 CH<sub>2</sub>Cl<sub>2</sub>/EtOAc) gave compound **43** (61.8 mg, 50%) as a yellow solid (decomp 233 C): <sup>1</sup>H NMR (500 MHz, d-acetone) δ 9.85 (s, 1H), 7.99 (d, 2H, *J* = 7.5 Hz), 7.67 (t, 1H, *J* = 7.5 Hz), 7.61 (t, 2H, *J* = 7.5 Hz), 7.52-7.57 (m, 3H), 7.32-7.37 (m, 2H), 7.26 (d, 1H, *J* = 2.0 Hz), 7.15 (dd, 1H, *J* = 8.5, 2.0 Hz), 7.04 (d, 1H, *J* = 8.5 Hz); <sup>13</sup>C NMR (125 MHz, d-acetone) δ 206.2, 206.0, 188.2, 160.5, 158.8, 156.4, 144.7, 140.3, 134.3, 133.3, 131.4, 130.3, 130.0, 129.2, 129.2, 128.0, 118.2, 116.4, 115.7, 105.5; IR (KBr, cm<sup>-1</sup>) ; HRMS calculated for C<sub>22</sub>H<sub>15</sub>NO<sub>5</sub>S (M + Na<sup>+</sup>): 428.0563. Found: 428.0561.



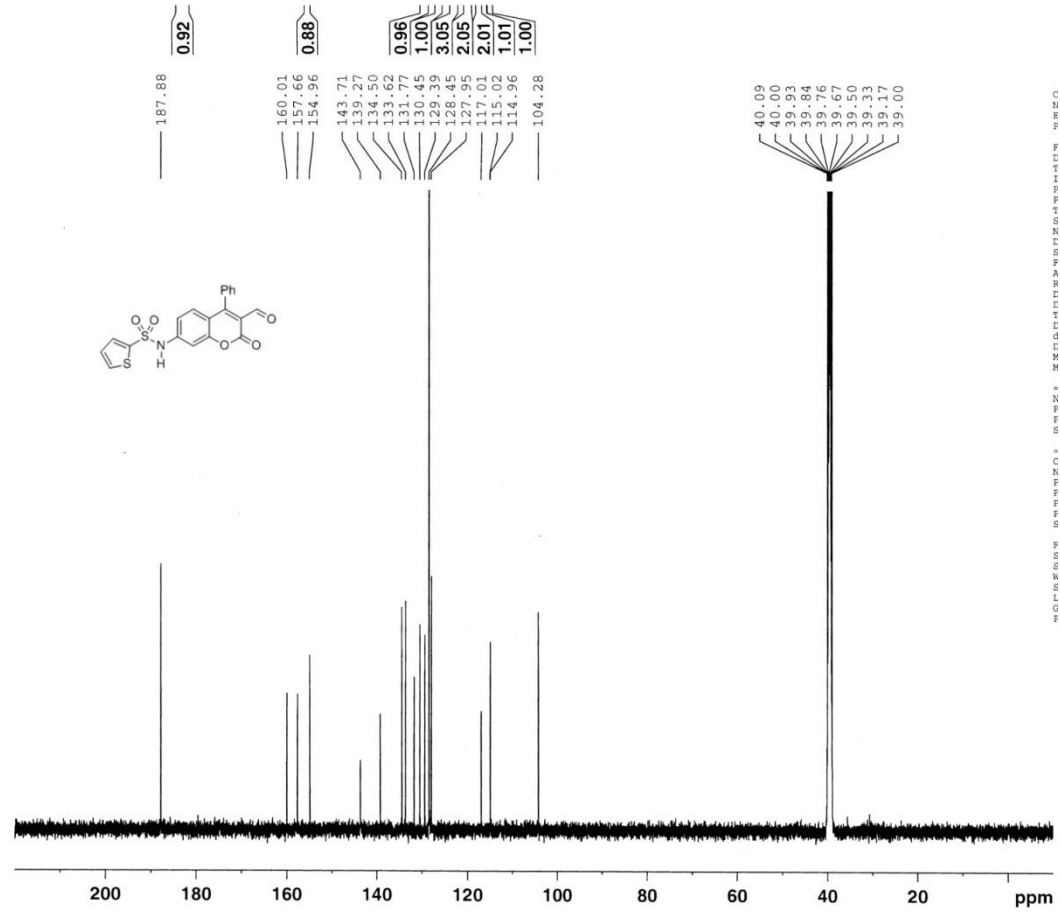




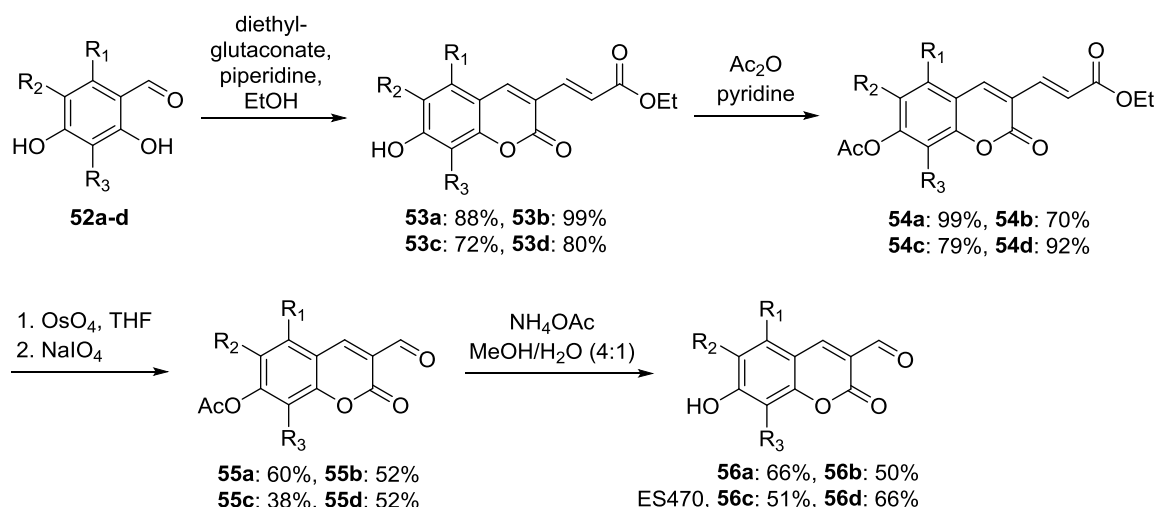
**Compound 44.** Compound **42** (83.3 mg, .209 mmol) was combined with 2-thiophenesulfonamide (37.5 mg, .230 mmol), Pd<sub>2</sub>dba<sub>3</sub> (9.2 mg, .010 mmol), SPhos (12.7 mg, .031 mmol), and K<sub>3</sub>PO<sub>4</sub> (89 mg, .418 mmol) in a round bottom flask and degassed for 20 min. Dry degassed THF was added and the mixture was purged with N<sub>2</sub> for 25 min followed by heating at 55 C for 24 h. The solvent was evaporated with a stream of N<sub>2</sub>, the crude product taken up in water (pH 5), and extracted with EtOAc (10 mL x 3). Purification by chromatography (95:5 CH<sub>2</sub>Cl<sub>2</sub>/EtOAc) gave compound **44** (42 mg, 49%) as a yellow solid (mp 195 C): <sup>1</sup>H NMR (500 MHz, DMSO) δ 11.48 (s, 1H), 9.68 (s, 1H), 7.96 (d, 1H, *J* = 4.0 Hz), 7.77 (d, 1H, *J* = 3.0 Hz), 7.51-7.57 (m, 3H), 7.31-7.37 (m, 2H), 7.13-7.18 (m, 2H), 7.10 (d, 1H, *J* = 9.0 Hz), 7.01 (d, 1H, *J* = 8.5 Hz); <sup>13</sup>C NMR (125 MHz, DMSO) δ 187.9, 160.0, 157.7, 155.0, 143.7, 139.3, 134.5, 133.6, 131.8, 130.4, 129.4, 128.4, 128.0, 117.0, 115.0, 114.9, 104.3; IR (KBr, cm<sup>-1</sup>) 3240, 1740, 1610, 1532, 1377, 1152, 1136; HRMS calculated for C<sub>20</sub>H<sub>13</sub>NO<sub>5</sub>S<sub>2</sub> (M + Na<sup>+</sup>): 434.0127. Found: 434.0125.



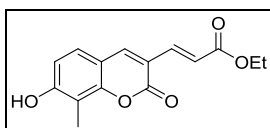
PC123456789101112131415161718192021222324252627282930313233343536373839404142434445464748495051525354555657585960616263646566676869707172737475767778798081828384858687888990919293949596979899100



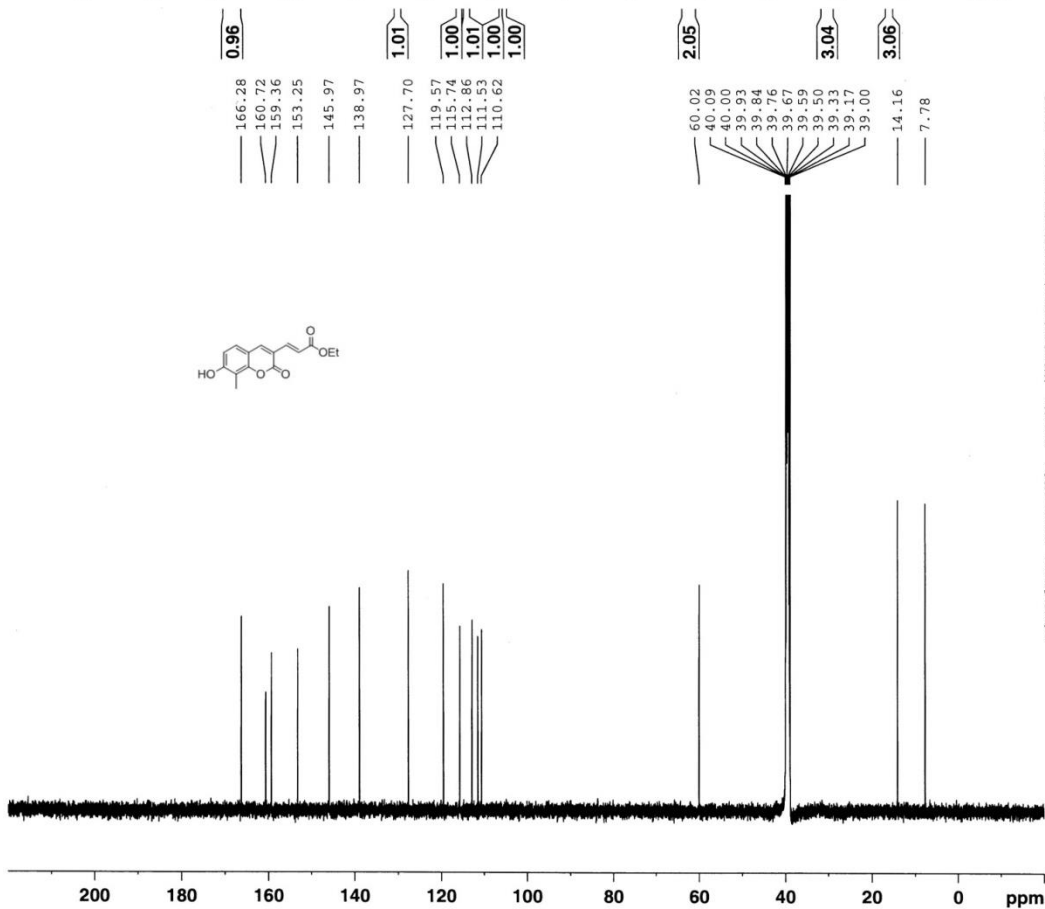
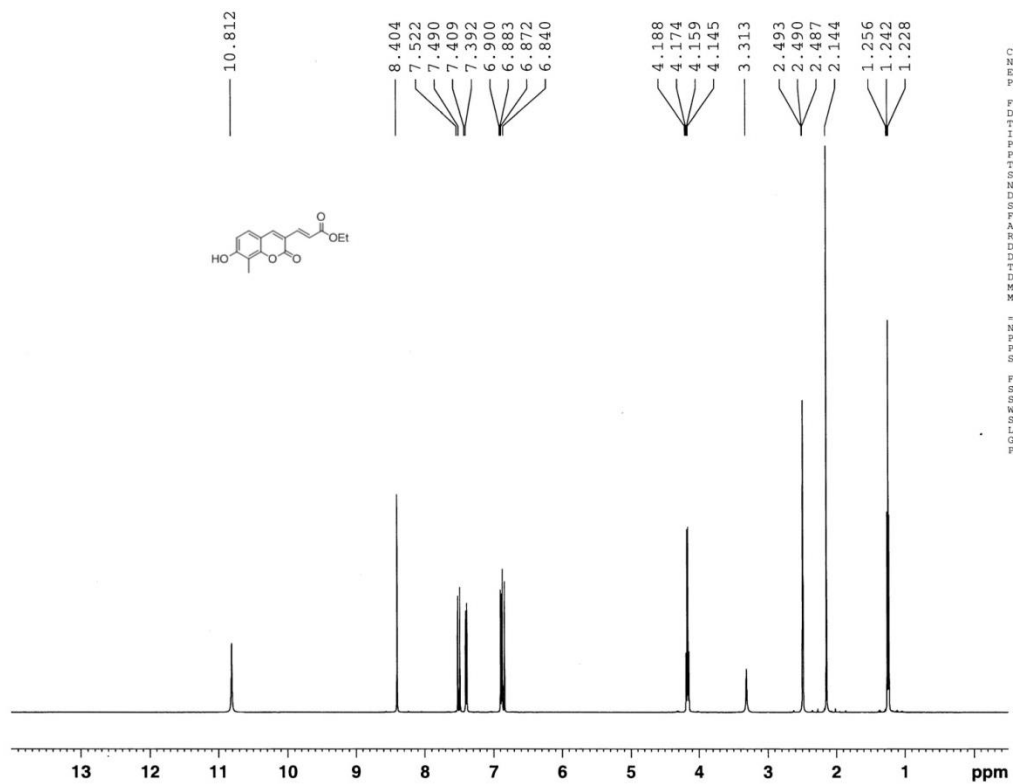
W123456789101112131415161718192021222324252627282930313233343536373839404142434445464748495051525354555657585960616263646566676869707172737475767778798081828384858687888990919293949596979899100

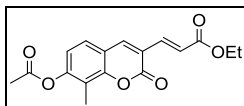


**a:** R<sub>1</sub>, R<sub>2</sub>, R<sub>3</sub> = H; **b:** R<sub>1</sub>, R<sub>2</sub> = H, R<sub>3</sub> = Me; **c:** R<sub>1</sub>, R<sub>2</sub> = Me, R<sub>3</sub> = H; **d:** R<sub>1</sub>, R<sub>2</sub>, R<sub>3</sub> = Me



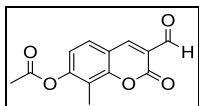
**(53b).** A mixture of 2,4-dihydroxy-3-methylbenzaldehyde (129 mg, 0.541 mmol), diethylglutaconate (1.22 mL, 6.901 mmol), piperidine (0.65 mL, 6.572 mmol), and 20 mL EtOH was stirred in a round bottom flask at 60 °C for 5 h. To the flask was added 3 mL of 1 M HCl followed by removal of the solvent *in vacuo*. Water (20 mL, pH 4) was added to the flask, it was gently swirled, and then vacuum filtered to yield compound **53b** (1.787 g, 99%) as a pale yellow solid (mp 244 °C): <sup>1</sup>H NMR (500 MHz, DMSO) δ 10.81 (s, 1H), 8.40 (s, 1H), 7.51 (d, 1H, *J* = 16.0 Hz), 7.40 (d, 1H, *J* = 8.5 Hz), 6.89 (d, 1H, *J* = 8.5 Hz), 6.86 (d, 1H, *J* = 16.0 Hz), 4.17 (q, 2H, *J* = 7.0 Hz), 2.14 (s, 3H), 1.24 (t, 3H, *J* = 7.0 Hz); <sup>13</sup>C NMR (125 MHz, DMSO) δ 166.3, 160.7, 159.4, 153.3, 146.0, 139.0, 127.7, 119.6, 115.7, 112.9, 111.5, 110.6, 60.0, 14.2, 7.8; IR (neat, cm<sup>-1</sup>) 3240, 1716, 1701, 1617, 1601, 1295, 1199, 977; HRMS calculated for C<sub>15</sub>H<sub>14</sub>O<sub>5</sub> (M + Na<sup>+</sup>): 297.0733. Found: 297.0730.





**(54b)**. Compound **53b** (200 mg, .729 mmol) and Ac<sub>2</sub>O (3.6 mL, 38.155 mmol) were combined in a 25 mL round bottom flask and stirred at room temperature for 10 min. Pyridine (3.6 mL, 44.511 mmol) was added dropwise, then the mixture stirred at room temperature for 23 h. The contents of the flask were poured over ice chips and the white precipitate was vacuum filtered. The remaining solid was purified via column chromatography (3:97 EtOAc/CH<sub>2</sub>Cl<sub>2</sub>) to yield compound **54b** (161.5 mg, 70%) as a white solid (mp 154 °C): <sup>1</sup>H NMR (500 MHz, DMSO) δ 8.54 (s, 1H), 7.61 (d, 1H, *J* = 9.0 Hz), 7.55 (d, 1H, *J* = 16.0 Hz), 7.19 (d, 1H, *J* = 8.5 Hz), 6.95 (d, 1H, *J* = 16.0 Hz), 4.19 (q, 2H, *J* = 7.0 Hz), 2.36 (s, 3H), 2.17 (s, 3H), 1.25 (t, 3H, *J* = 7.0 Hz); <sup>13</sup>C NMR (125 MHz, DMSO) δ 168.6, 166.0, 158.7, 152.3, 152.1, 144.7, 138.1, 127.1, 121.7, 120.1, 119.4, 118.2, 116.7, 60.2, 20.5, 14.1, 8.7; IR (KBr, cm<sup>-1</sup>) 1760, 1731, 1716, 1697, 1694, 1198, 1156; HRMS calculated for C<sub>17</sub>H<sub>16</sub>O<sub>6</sub> (M + Na<sup>+</sup>): 339.0839. Found: 339.0084.

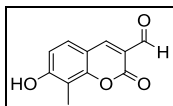




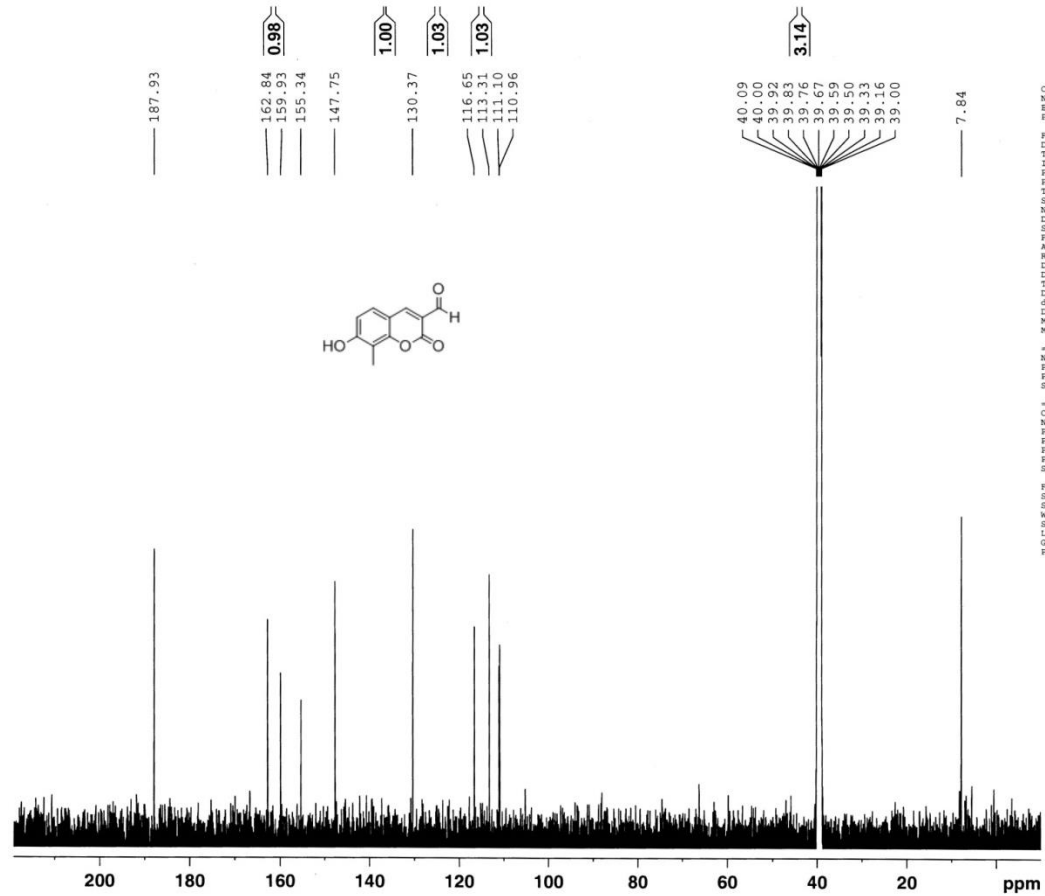
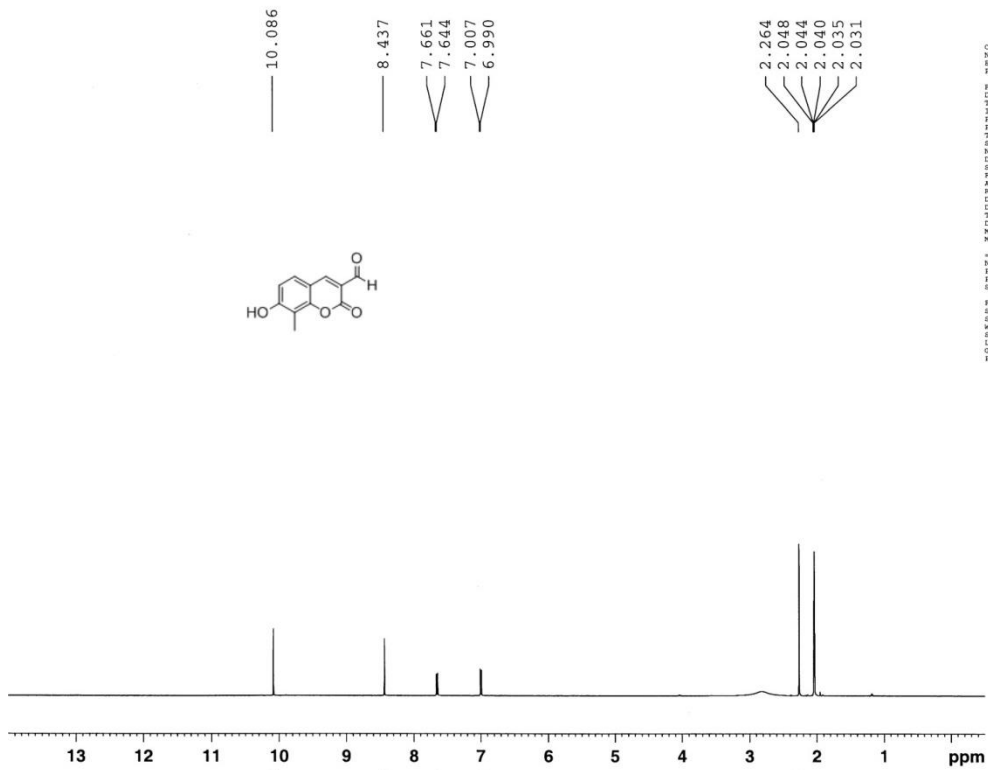
**(55b)**. Compound **54b** (1.00 g, 3.161 mmol) and 87 mL THF were added to a 250 mL flame-dried flask. Added dropwise to the flask was a  $\text{OsO}_4$  (0.87 mL of 4% soln. in water, .3278 mmol). The mixture was stirred at room temperature for 2 h. Sodium periodate (1.487 g, 6.954 mmol) was added and the reaction stirred for 10 days. The solvent was removed in vacuo, water (20 mL, pH 4) was added, and the product was extracted with EtOAc (50 mL x 3). The organic layers were combined, dried over  $\text{MgSO}_4$ , and the solvent was removed *in vacuo*. The diol intermediate was separated from the product via column chromatography (2-50% EtOAc in  $\text{CH}_2\text{Cl}_2$ ) to yield compound **55b** (402.5 mg, 52%) as an off-white solid (mp 169 °C):  $^1\text{H}$  NMR (500 MHz, DMSO)  $\delta$  10.03 (s, 1H), 8.67 (s, 1H), 7.87 (d, 1H,  $J = 8.5$  Hz), 7.23 (d, 1H,  $J = 8.5$  Hz), 2.37 (s, 3H), 2.18 (s, 3H);  $^{13}\text{C}$  NMR (125 MHz, DMSO)  $\delta$  188.0, 168.5, 158.9, 154.0, 153.8, 146.8, 129.3, 120.7, 119.7, 118.6, 116.1, 20.6, 8.7; IR (KBr,  $\text{cm}^{-1}$ ) 2852, 1761, 1720, 1699, 1601, 1569, 1197, 1160, 1078; HRMS calculated for  $\text{C}_{13}\text{H}_{10}\text{O}_5$  ( $\text{M} + \text{Na}^+$ ): 269.0420. Found: 269.0418.





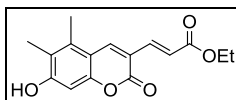


**(56b)**. Compound **55b** (150 mg, .609 mmol), ammonium acetate (610 mg, 7.914 mmol), and 10 mL of a 4:1 MeOH/H<sub>2</sub>O solution were combined in a 25 mL round bottom flask. The mixture was stirred at room temperature for 10 h then poured over ice chips. Water (10 mL, pH 4) was added and the precipitate was vacuum filtered. The crude solid was purified via column chromatography (5:95 EtOAc/CH<sub>2</sub>Cl<sub>2</sub>) to give sensor **56b** (62.1 mg, 50%) as a pale yellow solid (mp 223 °C): <sup>1</sup>H NMR (500 MHz, d-acetone) δ 10.09 (s, 1H), 8.44 (s, 1H), 7.65 (d, 1H, *J* = 8.5 Hz), 7.00 (d, 1H, *J* = 8.5 Hz), 2.26 (s, 3H); <sup>13</sup>C NMR (125 MHz, DMSO) 187.9, 162.8, 159.9, 155.3, 147.8, 130.4, 116.7, 113.3, 111.1, 111.0, 7.8; IR (KBr, cm<sup>-1</sup>) 3269, 1708, 1687, 1604, 1574, 1499, 1320; HRMS calculated for C<sub>11</sub>H<sub>8</sub>O<sub>4</sub> (M + Na<sup>+</sup>): 227.0315. Found: 227.0313.



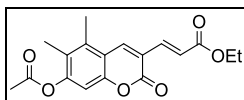
PCORR001 F20K1 M020M0A00000000000000000000

PCORR001 F20K1 M020M0A00000000000000000000

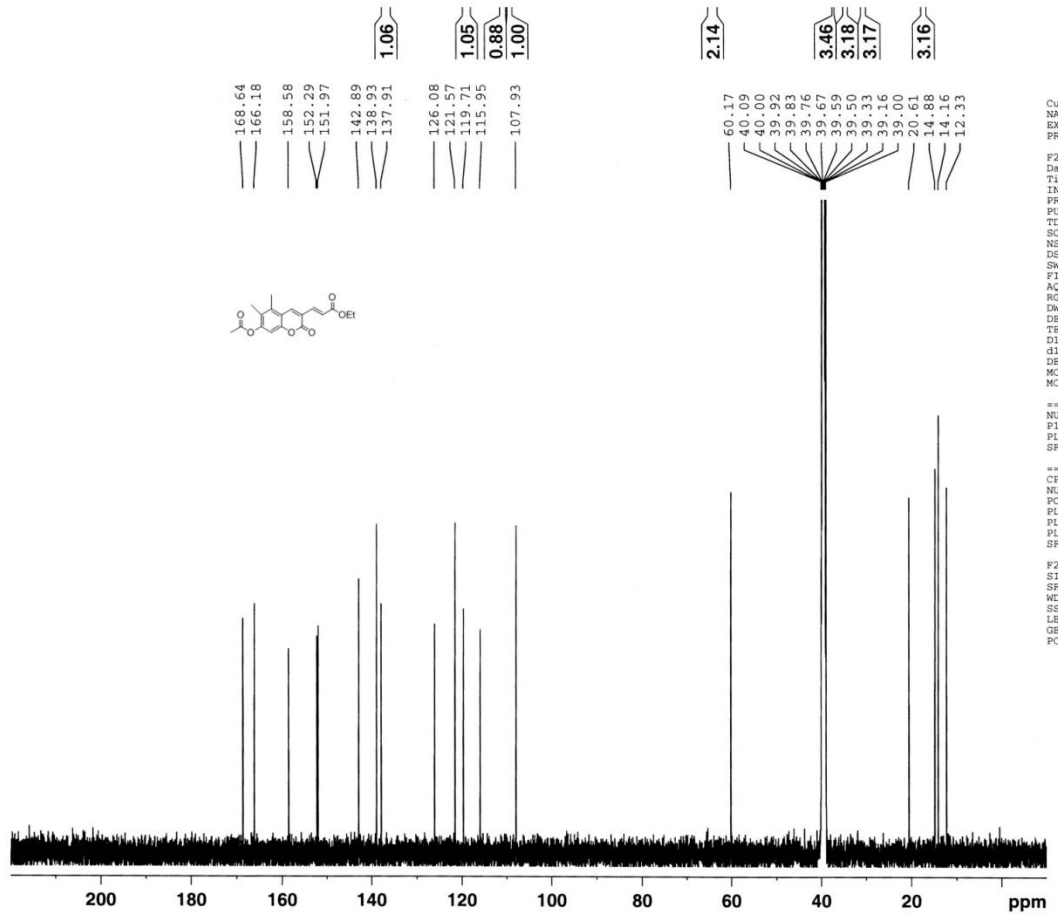
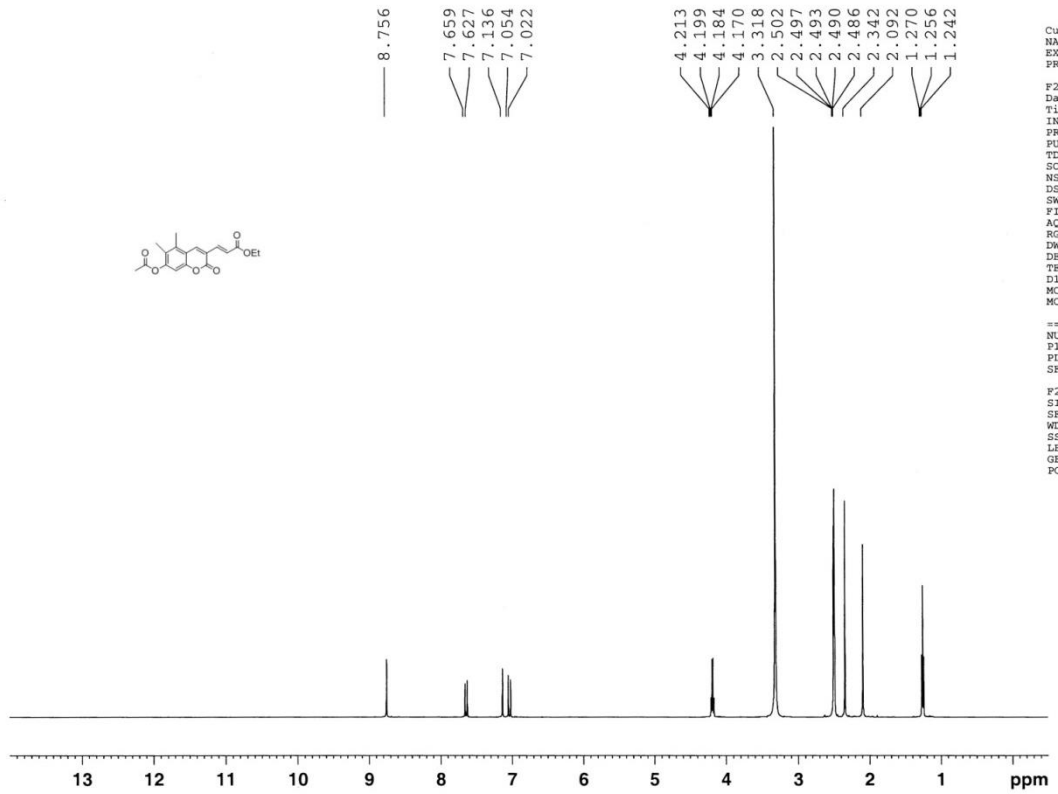


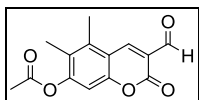
**(53c)**. To a 50 mL round bottom flask were added 4,6-dihydroxy-2,3-benzaldehyde (833 mg, 5.013 mmol), diethylglutaconate (0.93 mL, 5.264 mmol), piperidine (0.5 mL, 5.013 mmol), and 15 mL EtOH. The mixture stirred at 55 °C for 4 h followed by the addition of 4 mL of 1 M HCl. The solvent was removed *in vacuo*. Water (20 mL, pH 4) was added and the solid was vacuum filtered to yield compound **53c** (1.044 g, 72%) as a bright yellow solid (mp 202 °C): <sup>1</sup>H NMR (500 MHz, DMSO) δ 10.86 (s, 1H), 8.64 (s, 1H), 7.61 (d, 1H, *J* = 16.0 Hz), 6.94 (d, 1H, *J* = 16.0 Hz), 6.65 (s, 1H), 4.17 (q, 2H, *J* = 7.0 Hz), 2.43 (s, 3H), 2.11 (s, 3H), 1.25 (t, 3H, *J* = 7.0 Hz); <sup>13</sup>C NMR (125 MHz, DMSO) δ 166.5, 160.7, 159.1, 153.7, 144.1, 139.8, 137.3, 121.3, 119.3, 115.3, 110.7, 99.1, 59.9, 14.6, 14.2, 11.6; IR (KBr, cm<sup>-1</sup>) 3203, 1709, 1699, 1684, 1595, 1567, 1282, 1272, 1213; HRMS calculated for C<sub>16</sub>H<sub>16</sub>O<sub>5</sub> (M + Na<sup>+</sup>): 311.0890. Found: 311.0887.





**(54c).** Compound **53c** (1.044 g, 3.621 mmol) and Ac<sub>2</sub>O (18 mL, 190.773 mmol) were combined in a 50 mL round bottom flask and stirred at room temperature for 10 min. Pyridine (18 mL, 222.554 mmol) was added dropwise to the flask and the mixture was stirred at 50 °C for 1 h then at room temperature for 14 h. The mixture was poured over ice chips and the precipitate was vacuum filtered to yield compound **54c** (944.2 mg, 79%) as a pale yellow solid (mp 201 °C): <sup>1</sup>H NMR (500 MHz, DMSO) δ 8.76 (s, 1H), 7.64 (d, 1H, *J* = 16.0 Hz), 7.14 (s, 1H), 7.04 (d, 1H, *J* = 16.0 Hz), 4.19 (q, 2H, *J* = 7.0 Hz), 2.34 (s, 3H), 2.09 (s, 3H), 1.26 (t, 3H, *J* = 7.0 Hz); <sup>13</sup>C NMR (125 MHz, DMSO) δ 168.6, 166.2, 158.6, 152.3, 152.0, 142.9, 138.9, 137.9, 126.1, 121.6, 119.7, 116.0, 107.9, 60.2, 20.6, 14.9, 14.2, 12.3; IR (KBr, cm<sup>-1</sup>) 3105, 2978, 1762, 1721, 1622, 1310, 1296, 1212, 1166, 1120; HRMS calculated for C<sub>18</sub>H<sub>18</sub>O<sub>6</sub> (M + Na<sup>+</sup>): 353.0996. Found: 353.0991.

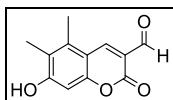




(**55c**). Compound **54c** (902 mg, 2.731 mmol), and 74 mL THF were combined in a flame-dried 200 mL round bottom flask. Added dropwise to the flask was a OsO<sub>4</sub> (0.75 mL of 4% soln. in water, .123 mmol). The mixture was stirred at room temperature for 24 h. Sodium periodate (1.285 g, 6.007 mmol) was added and the mixture stirred at room temperature for 6 days. The solvent was removed *in vacuo*, water (20 mL, pH 4) was added, and the product was extracted with EtOAc (50 mL x 3). The organic layers were combined, dried over MgSO<sub>4</sub>, and the solvent was removed *in vacuo*. The product was purified via column chromatography (5:95 EtOAc/CH<sub>2</sub>Cl<sub>2</sub>) to yield compound **55c** (266.8 mg, 38%) as an off-white solid (decomp 183 °C): <sup>1</sup>H NMR (500 MHz, DMSO) δ 10.03 (s, 1H), 8.75 (s, 1H), 7.21 (s, 1H), 2.53 (s, 3H), 2.36 (s, 3H), 2.11 (s, 3H); <sup>13</sup>C NMR (125 MHz, DMSO) δ 188.2, 168.5, 158.5, 153.9, 153.8, 144.8, 139.9, 126.5, 120.2, 115.2, 108.4, 20.6, 15.0, 12.3; IR (KBr, cm<sup>-1</sup>) 1761, 1732, 1720, 1695, 1601, 1565, 1189, 1119; HRMS calculated for C<sub>14</sub>H<sub>12</sub>O<sub>5</sub> (M + Na<sup>+</sup>): 283.0577. Found: 283.0574.

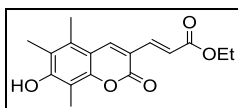




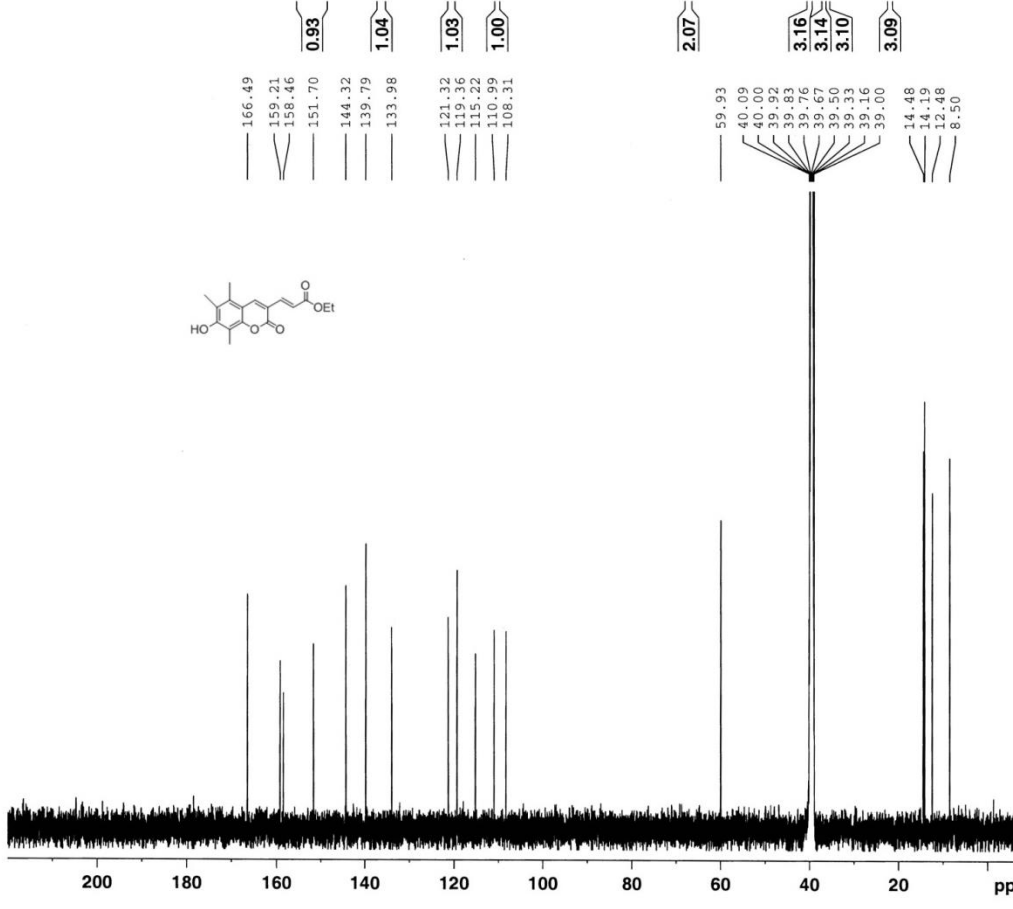
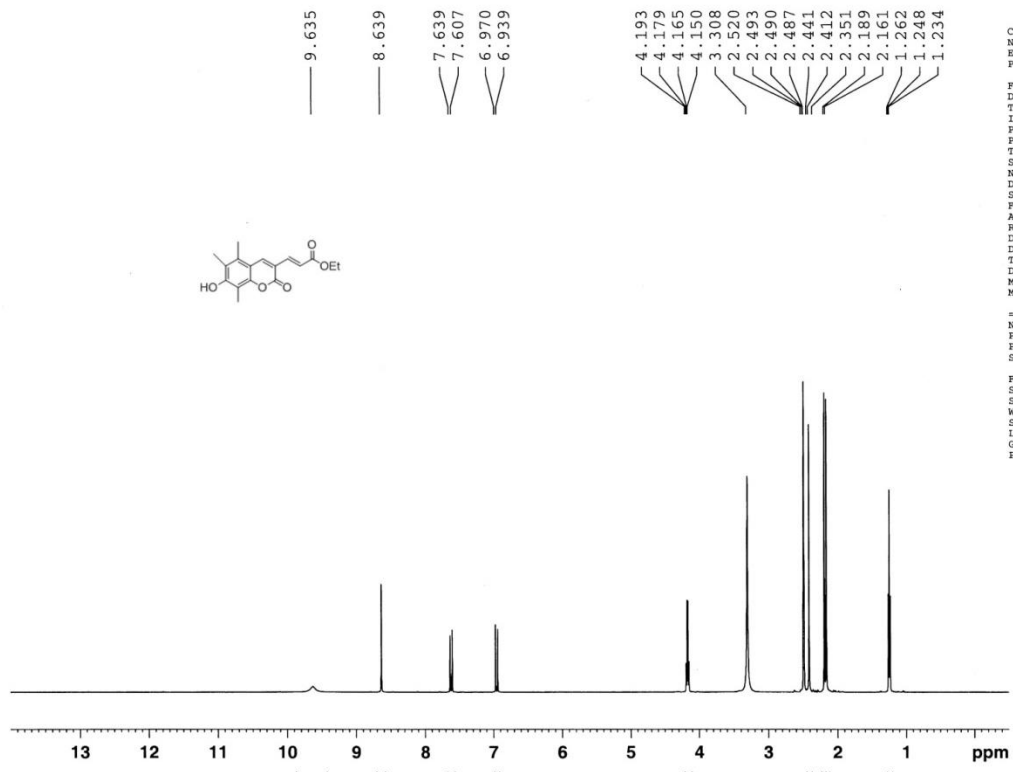


**ES470 (56c).** Compound **55c** (100 mg, .384 mmol), ammonium acetate (610 mg, 7.914 mmol), and 10 mL of a 4:1 MeOH/H<sub>2</sub>O solution were combined in a 25 mL round bottom flask and stirred at room temperature for 13 h. The solvent was removed *in vacuo*, water (10 mL, pH 4) was added, and the product was extracted with EtOAc (15 mL x 3). The organic layers were combined, dried over MgSO<sub>4</sub>, and the solvent was removed *in vacuo*. Purification using column chromatography (10:90 EtOAc/CH<sub>2</sub>Cl<sub>2</sub>) gave sensor ES470 (**56c**) (43 mg, 51%) as a yellow solid (decomp 199 °C): <sup>1</sup>H NMR (500 MHz, DMSO) δ 11.30 (s, 1H), 9.96 (s, 1H), 6.68 (s, 1H), 2.45 (s, 3H), 2.11 (s, 3H); <sup>13</sup>C NMR (125 MHz, DMSO) δ 187.9, 163.0, 159.4, 156.2, 145.2, 139.4, 122.0, 116.0, 110.0, 99.5, 14.7, 11.5; IR (KBr, cm<sup>-1</sup>) 3481, 1724, 1667, 1589, 1377, 1287, 1217, 1168, 764; HRMS calculated for C<sub>12</sub>H<sub>10</sub>O<sub>4</sub> (M + Na<sup>+</sup>): 241.0471. Found 241.0470.

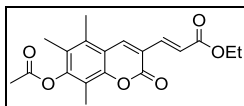




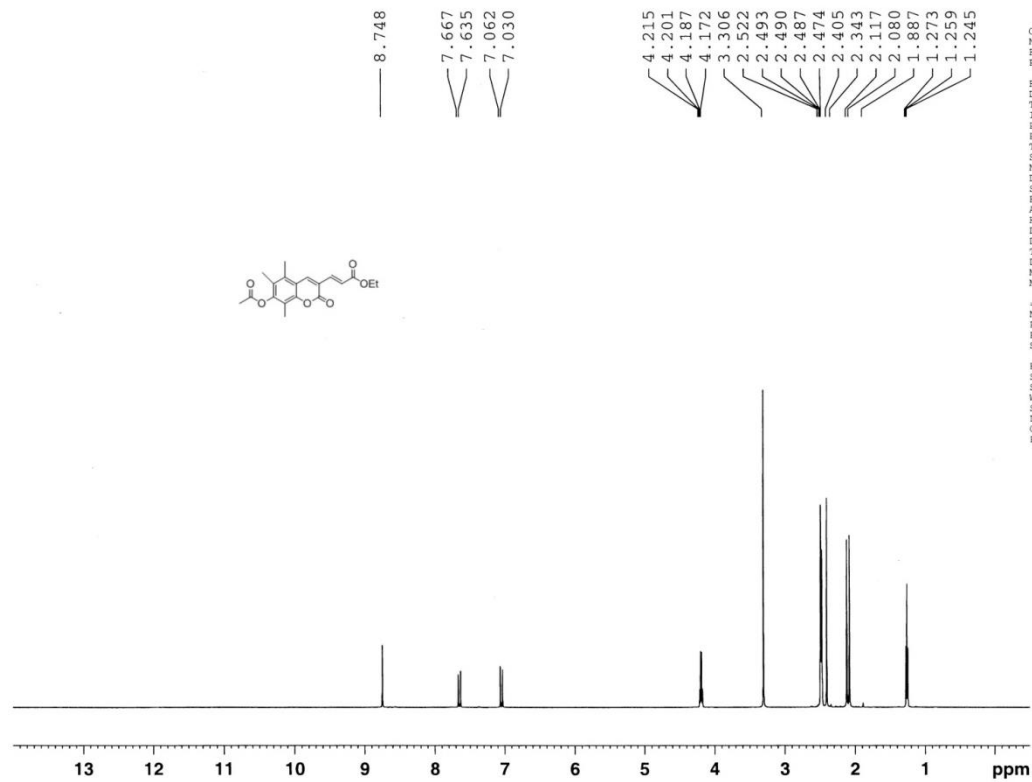
**(53d).** 2,4-Dihydroxy-3,5,6-trimethyl-benzaldehyde (695 mg, 3.857 mmol), diethyl glutaconate (0.72 mL, 4.050 mmol), piperidine (0.38 mL, 3.857 mmol), and 12 mL EtOH were combined in a 50 mL round bottom flask and stirred at 55 °C for 5 h then room temperature for 12 h. The solvent was removed *in vacuo* and 5 mL of 1 M HCl was added. The precipitate was vacuum filtered and rinsed with water (pH 4) to yield compound **53d** (937 mg, 80%) as an orange solid (mp 212 °C):  $^1\text{H}$  NMR (500 MHz, DMSO)  $\delta$  9.64 (s, 1H), 8.64 (s, 1H), 7.62 (d, 1H,  $J = 16.0$  Hz), 6.95 (d, 1H,  $J = 15.5$  Hz), 4.17 (q, 2H,  $J = 7.0$  Hz), 2.41 (s, 3H), 2.19 (s, 3H), 2.16 (s, 3H), 1.25 (t, 3H,  $J = 7.0$  Hz);  $^{13}\text{C}$  NMR (125 MHz, DMSO)  $\delta$  166.5, 159.2, 158.5, 151.7, 144.3, 139.8, 134.0, 121.3, 119.4, 115.2, 111.0, 108.3, 59.9, 14.5, 14.2, 12.5, 8.5; IR (KBr,  $\text{cm}^{-1}$ ) 3420, 1691, 1577, 1283, 1258, 1197, 1152; HRMS calculated for  $\text{C}_{17}\text{H}_{18}\text{O}_5$  ( $\text{M} + \text{Na}^+$ ): 325.1046. Found: 325.1044.



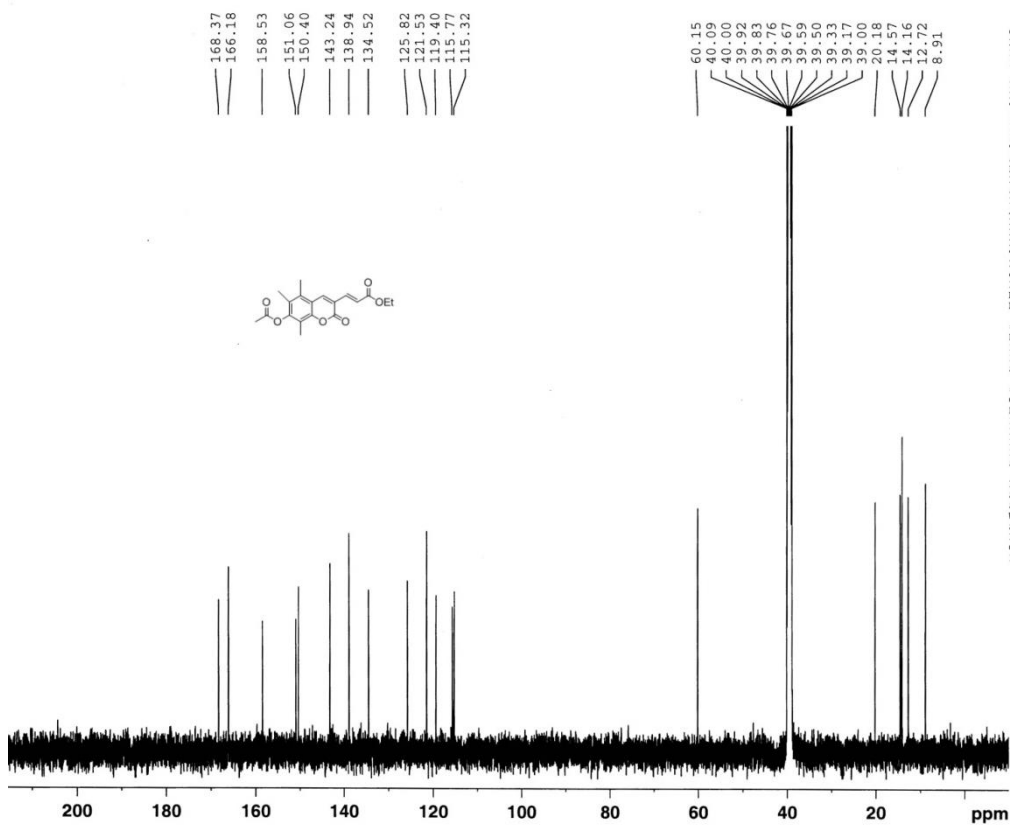
F2 Da T1 IN PR PU TD SO NS DS SW F1 AQ RG DW DE TE D1 C1 DEI MCT MC  
 == NEX P1 PL SF  
 == CFI NEX PCI PL PL PL SF  
 F2 SI SF WIX SSI LB GB PC

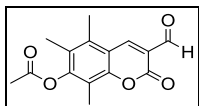


**(54d)**. Compound **53d** (498 mg, 1.647 mmol) and Ac<sub>2</sub>O (8.2 mL, 86.908 mmol) were combined in a 25 mL round bottom flask. Pyridine (8.2 mL, 101.386 mmol) was added dropwise to the flask. The mixture stirred at 55 °C for 1 h then poured over ice chips. The precipitate was vacuum filtered to give compound **54d** (522.5 mg, 92%) as an off-white solid (mp 183 °C): <sup>1</sup>H NMR (500 MHz, DMSO) δ 8.75 (s, 1H), 7.65 (d, 1H, *J* = 16.0 Hz), 7.05 (d, 1H, *J* = 16.0 Hz), 4.19 (q, 2H, *J* = 7.0 Hz), 2.47 (s, 3H), 2.41 (s, 3H), 2.12 (s, 3H), 2.08 (s, 3H), 1.26 (t, 3H, *J* = 7.0 Hz); <sup>13</sup>C NMR (125 MHz, DMSO) δ 168.4, 166.2, 158.5, 151.1, 150.4, 143.2, 138.9, 134.5, 125.8, 121.5, 119.4, 115.8, 115.3, 60.2, 20.2, 14.6, 14.2, 12.7, 8.9; IR (KBr, cm<sup>-1</sup>) 1756, 1729, 1705, 1587, 1312, 1267, 1209, 1175, 1130; HRMS calculated for C<sub>19</sub>H<sub>20</sub>O<sub>6</sub> (M + Na<sup>+</sup>): 367.1152. Found: 367.1148.

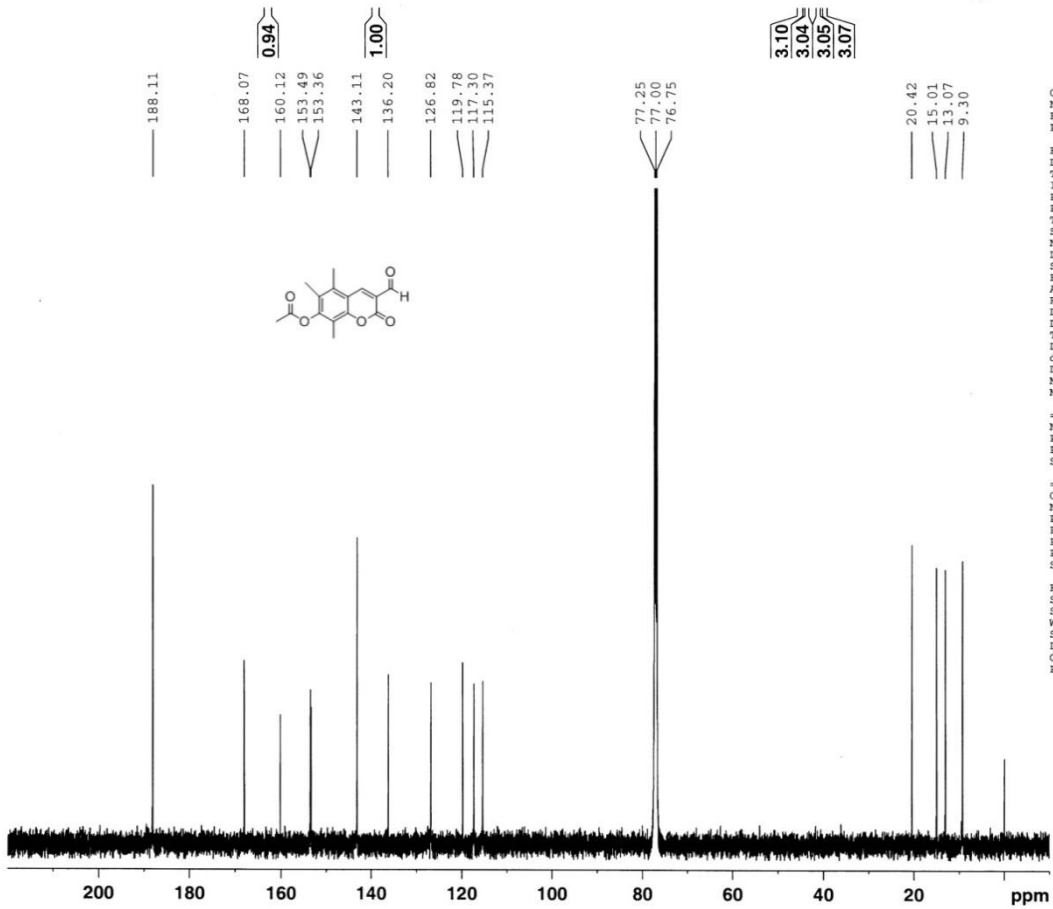
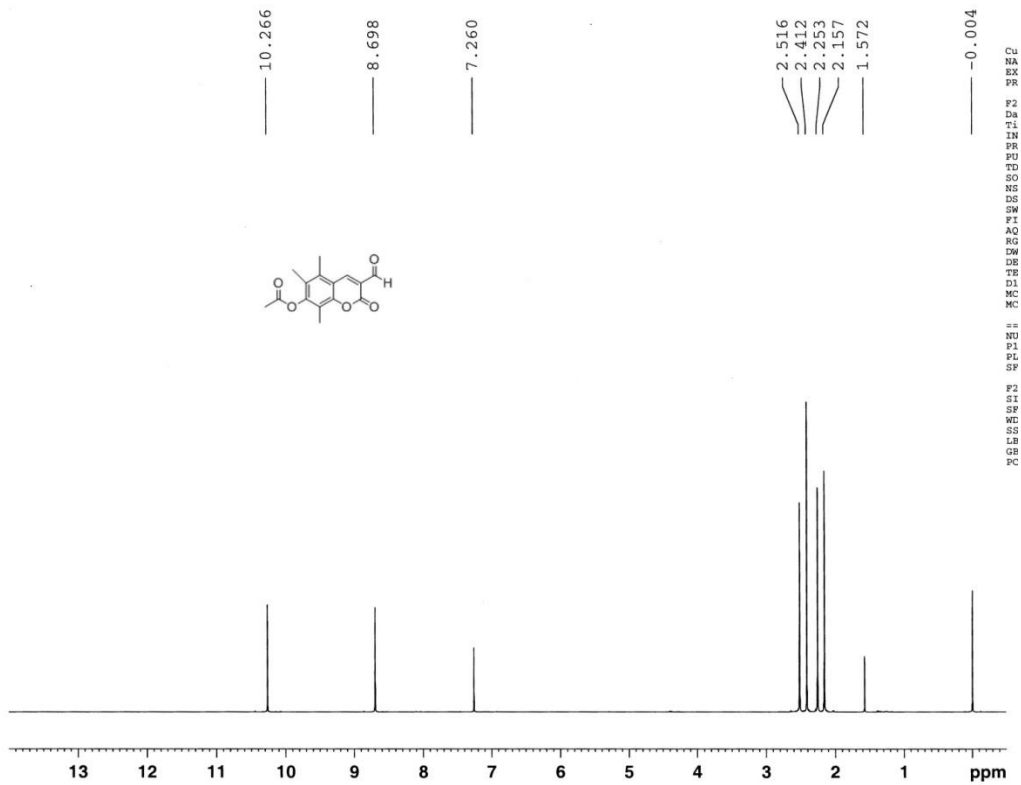


==  
 NU  
 F1  
 PL  
 SF  
 F2  
 S1  
 SF  
 ND  
 SS  
 LB  
 GB  
 PC





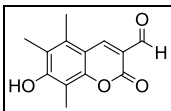
**(55d)**. In a 200 mL round bottom flask, compound **54d** (1133 mg, 3.290 mmol) was dissolved in 80 mL THF. Added dropwise to the flask was a  $\text{OsO}_4$  (0.91 mL of 4% soln. in water, .148 mmol). The mixture was stirred at room temperature for 13 h. Sodium periodate (1.548 g, 7.238 mmol) was added and the mixture stirred at room temperature for 3 days. The solvent was removed *in vacuo*, water (50 mL, pH 4) was added, and the product was extracted with EtOAc (50 mL x 3). The organic layers were combined, dried over  $\text{MgSO}_4$ , and the solvent was removed *in vacuo* to yield compound **55d** (470 mg, 52%) as an off-white solid (mp 172 °C):  $^1\text{H}$  NMR (500 MHz,  $\text{CDCl}_3$ )  $\delta$  10.27 (s, 1H), 8.70 (s, 1H), 2.52, (s, 3H), 2.41 (s, 3H), 2.25 (s, 3H), 2.16 (s, 3H);  $^{13}\text{C}$  NMR (125 MHz,  $\text{CDCl}_3$ )  $\delta$  188.1, 168.1, 160.1, 153.5, 153.4, 143.1, 136.2, 126.8, 119.8, 117.3, 115.4, 20.4, 15.0, 13.1, 9.3; IR (KBr,  $\text{cm}^{-1}$ ) 1753, 1732, 1690, 1573, 1201, 1184, 1128; HRMS calculated for  $\text{C}_{15}\text{H}_{14}\text{O}_5$  ( $\text{M} + \text{Na}^+$ ): 297.0733. Found: 297.0730.



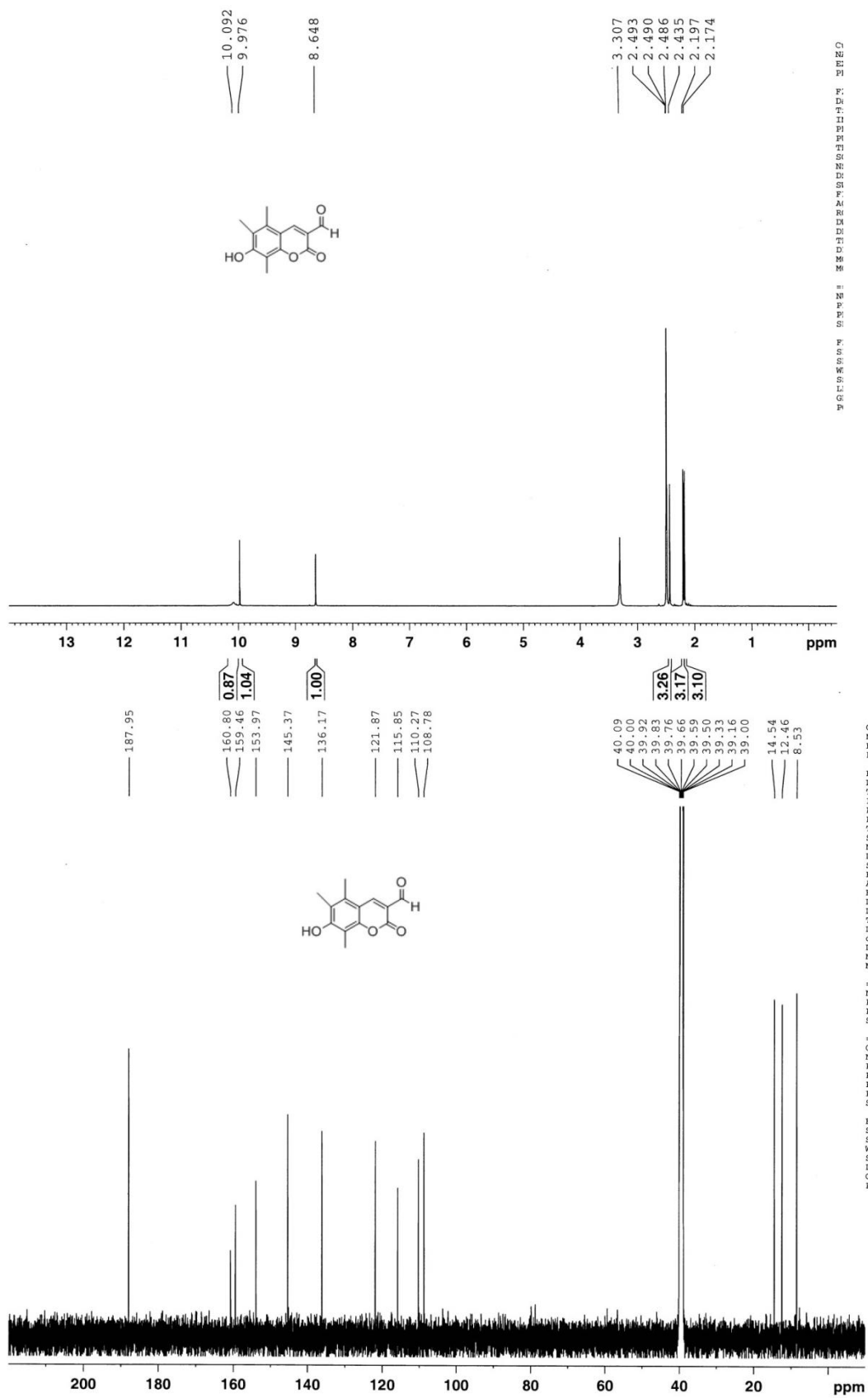
CU  
NA  
EX  
PE  
F2  
Da  
TI  
IN  
FE  
PU  
TD  
SO  
NS  
DS  
SW  
FI  
AQ  
RG  
DM  
DE  
TE  
DI  
MC  
MC  
==  
NU  
PL  
PL  
SF  
F2  
SI  
SF  
ND  
SS  
LB  
GB  
PC

Cur  
NAM  
EXP  
PRO  
F2  
Dat  
Tim  
INS  
PRO  
PUL  
TD  
SOL  
NS  
DS  
SWH  
FID  
AQ  
RG  
DM  
DE  
TE  
DI  
d11  
DEL  
MCR  
MCW  
====  
NUC  
F1  
PL1  
SFO  
====  
CPD  
NUC  
PCP  
PL2  
PL1  
PL1  
PL1  
SFO  
F2  
SI  
SF  
WDW  
SSB  
LB  
GB  
PC





**(56d)**. Compound **55d** (50 mg, .182 mmol), HCl (4 M, 4 mL), AcOH (0.1 mL, 3.274 mmol), and 2 mL H<sub>2</sub>O were combined in a 10 mL round bottom flask and refluxed for 4.5 h. Flask was sonicated as needed to break up solid chunks. The flask was cooled in a 0 °C ice bath followed by vacuum filtration of the precipitate which was rinsed with CH<sub>2</sub>Cl<sub>2</sub> to remove any remaining starting material and yield sensor **56d** (28 mg, 66%) as a yellow/green solid (mp 244°C): <sup>1</sup>H NMR (500 MHz, DMSO) δ 10.09 (s, 1H), 9.98 (s, 1H), 8.65 (s, 1H), 2.44 (s, 3H), 2.20 (s, 3H), 2.17 (s, 3H); <sup>13</sup>C NMR (125 MHz, DMSO) δ 188.0, 160.8, 159.5, 154.0, 145.4, 136.2, 121.9, 115.9, 110.3, 108.8, 14.5, 12.5, 8.5; IR (KBr, cm<sup>-1</sup>) 3391, 1732, 1675, 1565, 1348, 1225, 1193, 1148; HRMS calculated for C<sub>13</sub>H<sub>12</sub>O<sub>4</sub> (M + Na<sup>+</sup>): 255.0628. Found: 255.0626.



P O L S S W S S P F S P P P W I M M D D D D D R R F F S R N R S S S I I P E H I D R F F E E E D

F2  
F1  
T1  
IM  
FR  
PU  
TD  
SO  
NS  
DS  
SW  
FI  
AQ  
RG  
IW  
DE  
TE  
D1  
D1  
DE  
MC  
MC  
MC  
==  
NU  
P1  
PL  
SP  
==  
F2  
S1  
SF  
WD  
SS  
LB  
GB  
PC

## REFERENCES

1. (a) Steed, J. W.; Turner, D. R.; Wallace, K. *Core Concepts in Supramolecular Chemistry and Nanochemistry*. John Wiley & Sons: 2007; (b) Steed, J. W.; Atwood, J. L. *Supramolecular Chemistry*. John Wiley & Sons: 2009.
2. Mohr, G. J. *Anal. Bioanal. Chem.* **2006**, *386*, 1201-1214.
3. Lakowicz, J. R. *Principles of Fluorescence Spectroscopy*. Springer: 2007.
4. Valeur, B. Advanced Techniques in Fluorescence Spectroscopy. In *Molecular Fluorescence*, Wiley-VCH Verlag GmbH: 2001; pp 351-380.
5. Georgakoudi, I.; Jacobson, B. C.; Müller, M. G.; Sheets, E. E.; Badizadegan, K.; Carr-Locke, D. L.; Crum, C. P.; Boone, C. W.; Dasari, R. R.; Van Dam, J. *Cancer Res.* **2002**, *62*, 682-687.
6. Jares-Erijman, E. A.; Jovin, T. M. *Nat. Biotechnol.* **2003**, *21*, 1387-1395.
7. Heyduk, T. *Curr. Opin. Biotechnol.* **2002**, *13*, 292-296.
8. Zlokarnik, G.; Negulescu, P. A.; Knapp, T. E.; Mere, L.; Burren, N.; Feng, L.; Whitney, M.; Roemer, K.; Tsien, R. Y. *Science* **1998**, *279*, 84-88.
9. Mochizuki, N.; Yamashita, S.; Kurokawa, K.; Ohba, Y.; Nagai, T.; Miyawaki, A.; Matsuda, M. *Nature* **2001**, *411*, 1065-1068.
10. Miyawaki, A.; Llopis, J.; Heim, R.; McCaffery, J. M.; Adams, J. A.; Ikura, M.; Tsien, R. Y. *Nature* **1997**, *388*, 882-887.
11. Zhang, X.; Xiao, Y.; Qian, X. *Angew. Chem. Int. Ed. Engl.* **2008**, *47*, 8025-8029.
12. Long, L.; Lin, W.; Chen, B.; Gao, W.; Yuan, L. *Chem. Commun. (Camb)* **2011**, *47*, 893-895.
13. Ueno, T.; Nagano, T. *Nat. Methods* **2011**, *8*, 642-645.
14. Kurishita, Y.; Kohira, T.; Ojida, A.; Hamachi, I. *J. Am. Chem. Soc.* **2010**, *132*, 13290-13299.
15. Bissell, R.; Prasanna de Silva, A.; Nimal Gunaratne, H. Q.; Mark Lynch, P. L.; Maguire, G. M.; McCoy, C.; Samankumara Sandanayake, K. R. A. Fluorescent Pet (Photoinduced Electron Transfer) Sensors. In *Photoinduced Electron Transfer V*, Mattay, J., Ed. Springer Berlin Heidelberg: 1993; Vol. 168, pp 223-264.
16. Myochin, T.; Kiyose, K.; Hanaoka, K.; Kojima, H.; Terai, T.; Nagano, T. *J. Am. Chem. Soc.* **2011**, *133*, 3401-3409.

17. Tang, B.; Yu, F.; Li, P.; Tong, L.; Duan, X.; Xie, T.; Wang, X. *J. Am. Chem. Soc.* **2009**, *131*, 3016-3023.
18. Gabe, Y.; Urano, Y.; Kikuchi, K.; Kojima, H.; Nagano, T. *J. Am. Chem. Soc.* **2004**, *126*, 3357-3367.
19. Koteeswari, R.; Ashokkumar, P.; Malar, E. J.; Ramakrishnan, V. T.; Ramamurthy, P. *Chem. Commun. (Camb)* **2011**, *47*, 7695-7697.
20. Lin, W.; Long, L.; Chen, B.; Tan, W.; Gao, W. *Chem. Commun. (Camb)* **2010**, *46*, 1311-1313.
21. Woo, H.; Cho, S.; Han, Y.; Chae, W. S.; Ahn, D. R.; You, Y.; Nam, W. *J. Am. Chem. Soc.* **2013**, *135*, 4771-4787.
22. Aoki, S.; Sakurama, K.; Matsuo, N.; Yamada, Y.; Takasawa, R.; Tanuma, S.; Shiro, M.; Takeda, K.; Kimura, E. *Chemistry* **2006**, *12*, 9066-9080.
23. Bouffard, J.; Kim, Y.; Swager, T. M.; Weissleder, R.; Hilderbrand, S. A. *Org. Lett.* **2008**, *10*, 37-40.
24. Li, X.; Qian, S.; He, Q.; Yang, B.; Li, J.; Hu, Y. *Org. Biomol. Chem.* **2010**, *8*, 3627-3630.
25. Diwu, Z.; Lu, Y.; Zhang, C.; Klaubert, D. H.; Haugland, R. P. *Photochem. Photobiol.* **1997**, *66*, 424-431.
26. Peng, X.; Du, J.; Fan, J.; Wang, J.; Wu, Y.; Zhao, J.; Sun, S.; Xu, T. *J. Am. Chem. Soc.* **2007**, *129*, 1500-1501.
27. Puri, D. *Elsevier, New Delhi* **2011**.
28. Wu, G. *Amino Acids: Biochemistry and Nutrition*. Taylor & Francis: 2013.
29. Joseph, R.; Chinta, J. P.; Rao, C. P. *J. Org. Chem.* **2010**, *75*, 3387-3395.
30. Ait-Haddou, H.; Wiskur, S. L.; Lynch, V. M.; Anslyn, E. V. *J. Am. Chem. Soc.* **2001**, *123*, 11296-11297.
31. Leung, D.; Folmer-Andersen, J. F.; Lynch, V. M.; Anslyn, E. V. *J. Am. Chem. Soc.* **2008**, *130*, 12318-12327.
32. Hortala, M. A.; Fabbriizzi, L.; Marcotte, N.; Stomeo, F.; Taglietti, A. *J. Am. Chem. Soc.* **2003**, *125*, 20-21.
33. Dean, K. E.; Klein, G.; Renaudet, O.; Reymond, J. L. *Bioorg. Med. Chem. Lett.* **2003**, *13*, 1653-1656.

34. Rosete-Luna, S.; Medrano, F.; Bernal-Uruchurtu, M. I.; Godoy-Alcántar, C. *J. Mex. Chem. Soc.* **2009**, *53*, 209-219.
35. Lu, G.; Grossman, J. E.; Lambert, J. B. *J. Org. Chem.* **2006**, *71*, 1769-1776.
36. Tsubaki, K.; Tanima, D.; Nuruzzaman, M.; Kusumoto, T.; Fuji, K.; Kawabata, T. *J. Org. Chem.* **2005**, *70*, 4609-4616.
37. Tsubaki, K.; Kusumoto, T.; Hayashi, N.; Nuruzzaman, M.; Fuji, K. *Org. Lett.* **2002**, *4*, 2313-2316.
38. Famulok, M. *J. Am. Chem. Soc.* **1994**, *116*, 1698-1706.
39. Shao, J.; Guo, H.; Ji, S.; Zhao, J. *Biosens. Bioelectron.* **2011**, *26*, 3012-3017.
40. Lu, J.; Sun, C.; Chen, W.; Ma, H.; Shi, W.; Li, X. *Talanta* **2011**, *83*, 1050-1056.
41. Hortalá, M. A.; Fabbrizzi, L.; Marcotte, N.; Stomeo, F.; Taglietti, A. *J. Am. Chem. Soc.* **2003**, *125*, 20-21.
42. Kwon, H.; Lee, K.; Kim, H. *J. Chem. Commun. (Camb)* **2011**, *47*, 1773-1775.
43. Jung, H. S.; Ko, K. C.; Kim, G. H.; Lee, A. R.; Na, Y. C.; Kang, C.; Lee, J. Y.; Kim, J. S. *Org. Lett.* **2011**, *13*, 1498-1501.
44. Huo, F. J.; Sun, Y. Q.; Su, J.; Yang, Y. T.; Yin, C. X.; Chao, J. B. *Org. Lett.* **2010**, *12*, 4756-4759.
45. Zhou, Y.; Yoon, J. *Chem. Soc. Rev.* **2012**, *41*, 52-67.
46. Hettie, K. S.; Liu, X.; Gillis, K. D.; Glass, T. E. *ACS Chem. Neurosci.* **2013**, *4*, 918-923.
47. Secor, K.; Plante, J.; Avetta, C.; Glass, T. *J. Mater. Chem.* **2005**, *15*, 4073-4077.
48. Feuster, E. K.; Glass, T. E. *J. Am. Chem. Soc.* **2003**, *125*, 16174-16175.
49. (a) Zhou, X.-b.; Yip, Y.-W.; Chan, W.-H.; Lee, A. W. *Beilstein J. Org. Chem.* **2011**, *7*, 75-81; (b) Nonokawa, R.; Yashima, E. *J. Am. Chem. Soc.* **2003**, *125*, 1278-1283; (c) Hu, M.; Fan, J.; Li, H.; Song, K.; Wang, S.; Cheng, G.; Peng, X. *Org. Biomol. Chem.* **2011**, *9*, 980-983.
50. Malenka, R. *Intercellular Communication in the Nervous System*. Elsevier Science: 2010.
51. Riveros, N.; Fiedler, J.; Lagos, N.; Munoz, C.; Orrego, F. *Brain Res.* **1986**, *386*, 405-408.

52. Burger, P. M.; Mehl, E.; Cameron, P. L.; Maycox, P. R.; Baumert, M.; Lottspeich, F.; De Camilli, P.; Jahn, R. *Neuron* **1989**, *3*, 715-720.
53. Bruns, D.; Jahn, R. *Nature* **1995**, *377*, 62-65.
54. Borges, R.; Pereda, D.; Beltran, B.; Prunell, M.; Rodriguez, M.; Machado, J. D. *Cell Mol. Neurobiol.* **2010**, *30*, 1359-1364.
55. Camacho, M.; Machado, J. D.; Alvarez, J.; Borges, R. *J. Biol. Chem.* **2008**, *283*, 22383-22389.
56. Jankowski, J. A.; Schroeder, T. J.; Ciolkowski, E. L.; Wightman, R. M. *J. Biol. Chem.* **1993**, *268*, 14694-14700.
57. Mikula, S.; Binding, J.; Denk, W. *Nat. Methods* **2012**, *9*, 1198-1201.
58. Tapia, J. C.; Kasthuri, N.; Hayworth, K. J.; Schalek, R.; Lichtman, J. W.; Smith, S. J.; Buchanan, J. *Nat. Protoc.* **2012**, *7*, 193-206.
59. Wu, J. S.; Luo, L. *Nat. Protoc.* **2006**, *1*, 2110-2115.
60. Antanitus, D. S.; Choi, B. H.; Lapham, L. W. *Brain Res.* **1975**, *89*, 363-367.
61. (a) Betz, W. J.; Mao, F.; Bewick, G. S. *J. Neurosci.* **1992**, *12*, 363-375; (b) Betz, W. J.; Bewick, G. S. *Science* **1992**, *255*, 200-203; (c) Gaffield, M. A.; Betz, W. J. *Nat. Protoc.* **2006**, *1*, 2916-2921.
62. (a) Yuste, R.; Miller, R. B.; Holthoff, K.; Zhang, S.; Miesenbock, G. *Methods Enzymol.* **2000**, *327*, 522-546; (b) Burrone, J.; Li, Z.; Murthy, V. N. *Nat. Protoc.* **2006**, *1*, 2970-2978; (c) Miesenbock, G. *Cold Spring Harb. Protoc.* **2012**, *2012*, 213-217.
63. (a) Gubernator, N. G.; Zhang, H.; Staal, R. G.; Mosharov, E. V.; Pereira, D. B.; Yue, M.; Balsanek, V.; Vadola, P. A.; Mukherjee, B.; Edwards, R. H.; Sulzer, D.; Sames, D. *Science* **2009**, *324*, 1441-1444; (b) Lee, M.; Gubernator, N. G.; Sulzer, D.; Sames, D. *J. Am. Chem. Soc.* **2010**, *132*, 8828-8830; (c) Rodriguez, P. C.; Pereira, D. B.; Borgkvist, A.; Wong, M. Y.; Barnard, C.; Sonders, M. S.; Zhang, H.; Sames, D.; Sulzer, D. *Proc. Natl. Acad. Sci. U S A* **2013**, *110*, 870-875.
64. Carrera, V.; Sabater, E.; Vilanova, E.; Sogorb, M. A. *J. Chromatogr. B* **2007**, *847*, 88-94.
65. Deng, Y. H.; Wang, H.; Zhang, H. S. *J. Sep. Sci.* **2008**, *31*, 3088-3097.
66. Heien, M. L.; Johnson, M. A.; Wightman, R. M. *Analyt. Chem.* **2004**, *76*, 5697-5704.
67. Ferry, Y.; Leech, D. *Electroanalysis* **2005**, *17*, 113-119.

68. Staal, R. G.; Mosharov, E. V.; Sulzer, D. *Nat. Neurosci.* **2004**, *7*, 341-346.
69. (a) Hires, S. A.; Zhu, Y.; Tsien, R. Y. *Proc. Natl. Acad. Sci. U S A* **2008**, *105*, 4411-4416; (b) Brun, M. A.; Tan, K. T.; Griss, R.; Kielkowska, A.; Reymond, L.; Johnsson, K. *J. Am. Chem. Soc.* **2012**, *134*, 7676-7678; (c) Masharina, A.; Reymond, L.; Maurel, D.; Umezawa, K.; Johnsson, K. *J. Am. Chem. Soc.* **2012**, *134*, 19026-19034.
70. (a) Secor, K. E.; Glass, T. E. *Org. Lett.* **2004**, *6*, 3727-3730; (b) Jang, Y. J.; Jun, J. H.; Swamy, K.; Nakamura, K.; Koh, H. S.; Yoon, Y. J.; Yoon, J. *Bull. Kor. Chem. Soc.* **2005**, *26*, 2041.
71. de Silva, A. P.; Gunaratne, H. Q. N.; McVeigh, C.; Maguire, G. E. M.; Maxwell, P. R. S.; O'Hanlon, E. *Chem. Commun.* **1996**, 2191-2192.
72. Phillips, P. E.; Wightman, R. M. *TrAC Trends in Analyt. Chem.* **2003**, *22*, 509-514.
73. Okumoto, S.; Looger, L. L.; Micheva, K. D.; Reimer, R. J.; Smith, S. J.; Frommer, W. B. *Proc. Natl. Acad. Sci. U S A* **2005**, *102*, 8740-8745.
74. Tsien, R. Y. *FEBS Lett.* **2005**, *579*, 927-932.
75. Keighron, J. D.; Ewing, A. G.; Cans, A. S. *Analyst* **2012**, *137*, 1755-1763.
76. Murthy, V. N.; Stevens, C. F. *Nature* **1998**, *392*, 497-501.
77. Sankaranarayanan, S.; De Angelis, D.; Rothman, J. E.; Ryan, T. A. *Biophys. J.* **2000**, *79*, 2199-2208.
78. Allersma, M. W.; Wang, L.; Axelrod, D.; Holz, R. W. *Mol. Biol. Cell* **2004**, *15*, 4658-4668.
79. Miesenbock, G.; De Angelis, D. A.; Rothman, J. E. *Nature* **1998**, *394*, 192-195.
80. Mahon, M. J. *Adv. Biosci. Biotechnol. (Print)* **2011**, *2*, 132.
81. Gaffield, M. A.; Tabares, L.; Betz, W. J. *J. Neurosci.* **2009**, *29*, 15308-15316.
82. Tremblay, M. S.; Halim, M.; Sames, D. *J. Am. Chem. Soc.* **2007**, *129*, 7570-7577.
83. Chen, Y.; Guillemin, G. J. *Int. J. Tryptophan Res.* **2009**.
84. Chen, Y.; Stankovic, R.; Cullen, K. M.; Meininger, V.; Garner, B.; Coggan, S.; Grant, R.; Brew, B. J.; Guillemin, G. J. *Neurotox. Res.* **2010**, *18*, 132-142.
85. Mezrich, J. D.; Fechner, J. H.; Zhang, X.; Johnson, B. P.; Burlingham, W. J.; Bradfield, C. A. *J. Immunol.* **2010**, *185*, 3190-3198.

86. Stone, T. W.; Forrest, C. M.; Darlington, L. G. *FEBS J.* **2012**, *279*, 1386-1397.
87. Prendergast, G. C. *Nature* **2011**, *478*, 192-194.
88. Opitz, C. A.; Litzenburger, U. M.; Sahm, F.; Ott, M.; Tritschler, I.; Trump, S.; Schumacher, T.; Jestaedt, L.; Schrenk, D.; Weller, M.; Jugold, M.; Guillemin, G. J.; Miller, C. L.; Lutz, C.; Radlwimmer, B.; Lehmann, I.; von Deimling, A.; Wick, W.; Platten, M. *Nature* **2011**, *478*, 197-203.
89. Notarangelo, F. M.; Wu, H. Q.; Macherone, A.; Graham, D. R.; Schwarcz, R. *Anal. Biochem.* **2012**, *421*, 573-581.
90. Vaarmann, A.; Kask, A.; Mäeorg, U. *J. Chromatogr. B* **2002**, *769*, 145-153.
91. Guillemin, G. J.; Cullen, K. M.; Lim, C. K.; Smythe, G. A.; Garner, B.; Kapoor, V.; Takikawa, O.; Brew, B. J. *J. Neurosci.* **2007**, *27*, 12884-12892.
92. Krcmova, L.; Solichova, D.; Melichar, B.; Kasparova, M.; Plisek, J.; Sobotka, L.; Solich, P. *Talanta* **2011**, *85*, 1466-1471.
93. (a) Li, H.; Tian, J.; Wang, L.; Zhang, Y.; Sun, X. *Journal of Materials Chemistry* **2011**, *21*, 824; (b) Varghese, N.; Mogera, U.; Govindaraj, A.; Das, A.; Maiti, P. K.; Sood, A. K.; Rao, C. N. *ChemPhysChem* **2009**, *10*, 206-210.
94. Reeves, R. L.; Smith, W. F. *J. Am. Chem. Soc.* **1963**, *85*, 724-728.
95. Kayser, R.; Pollack, R. *J. Am. Chem. Soc.* **1977**, *99*, 3379-3387.
96. Boyd, B. W.; Witowski, S. R.; Kennedy, R. T. *Anal. Chem.* **2000**, *72*, 865-871.
97. Burchfield, J. G.; Lopez, J. A.; Mele, K.; Vallotton, P.; Hughes, W. E. *Traffic* **2010**, *11*, 429-439.
98. Felmy, F. *Traffic* **2007**, *8*, 983-997.
99. Steyer, J.; Horstmann, H.; Almers, W. *Nature* **1997**, *388*, 474-478.
100. Omiatek, D. M.; Dong, Y.; Heien, M. L.; Ewing, A. G. *ACS Chem. Neurosci.* **2010**, *1*, 234-245.
101. Chang, H.-T.; Yeung, E. S. *Anal. Chem.* **1995**, *67*, 1079-1083.
102. Kristensen, H. K.; Lau, Y. Y.; Ewing, A. G. *J. Neuroscience Meth.* **1994**, *51*, 183-188.
103. Kennedy, R. T.; Oates, M. D.; Cooper, B. R.; Nickerson, B.; Jorgenson, J. W. *Science* **1989**, *246*, 57-63.



104. Leszczyszyn, D. J.; Jankowski, J. A.; Viveros, O. H.; Diliberto, E. J., Jr.; Near, J. A.; Wightman, R. M. *J. Biol. Chem.* **1990**, *265*, 14736-14737.
105. Ponchon, J. L.; Cespuaglio, R.; Gonon, F.; Jouvet, M.; Pujol, J. F. *Anal. Chem.* **1979**, *51*, 1483-1486.
106. Li, L.; Garden, R. W.; Sweedler, J. V. *Trends Biotechnol.* **2000**, *18*, 151-160.
107. Ge, S.; Koseoglu, S.; Haynes, C. L. *Anal. Bioanal. Chem.* **2010**, *397*, 3281-3304.
108. Sreejith, S.; Ajayaghosh, A. *Indian J. Chem. A* **2012**, *51*, 47.
109. de Silva, A. P.; Uchiyama, S. Molecular Logic Gates and Luminescent Sensors Based on Photoinduced Electron Transfer. In *Luminescence Applied in Sensor Science*, Springer: 2011; pp 1-28.
110. De Silva, A. P. Molecular Logic Gates. In *Supramolecular Chemistry: From Molecules to Nanomaterials*, Gale, P. A.; Steed, J. W.; Anzenbacher, P., Eds. Wiley-Blackwell: 2012; Vol. 7, pp 2497-2506.
111. Zenisek, D.; Steyer, J. A.; Feldman, M. E.; Almers, W. *Neuron* **2002**, *35*, 1085-1097.
112. Chen, Y. A.; Scheller, R. H. *Nat. Rev. Mol. Cell Biol.* **2001**, *2*, 98-106.
113. Wolfbeis, O. S.; Baustert, J. H. *J. Heterocyclic Chem.* **1985**, *22*, 1215-1218.
114. Rousseaux, C. G. *J. Toxicol. Pathol.* **2008**, *21*, 25-51.
115. Huidobro-Toro, J. P.; Lorca, R. A.; Coddou, C. *Eur. Biophys. J.* **2008**, *37*, 301-314.
116. (a) Brady, S. T.; Siegel, G. J.; Albers, R. W.; Price, D. L. *Basic Neurochemistry: Principles of Molecular, Cellular and Medical Neurobiology*. Elsevier Academic Press: 2012; (b) Bitanhirwe, B. K.; Cunningham, M. G. *Synapse* **2009**, *63*, 1029-1049.
117. Frederickson, C. J.; Hershfinkel, M.; Giblin, L. J. The Gluzineric Synapse: Who's Talking and Who's Listening? In *Synaptic Plasticity and Transsynaptic Signaling*, Springer: 2005; pp 123-137.
118. Paoletti, P.; Vergnano, A. M.; Barbour, B.; Casado, M. *Neuroscience* **2009**, *158*, 126-136.
119. Sun, X. Y.; Wei, Y. P.; Xiong, Y.; Wang, X. C.; Xie, A. J.; Wang, X. L.; Yang, Y.; Wang, Q.; Lu, Y. M.; Liu, R.; Wang, J. Z. *J. Biol. Chem.* **2012**, *287*, 11174-11182.

120. Sensi, S. L.; Paoletti, P.; Bush, A. I.; Sekler, I. *Nat. Rev. Neurosci.* **2009**, *10*, 780-791.
121. Klockow, J. L.; Hettie, K. S.; Glass, T. E. *ACS Chem. Neurosci.* **2013**.
122. Ottersen, O. P.; Laake, J. H.; Reichelt, W.; Haug, F. M.; Torp, R. *J. Chem. Neuroanat.* **1996**, *12*, 1-14.
123. Ottersen, O. P.; Zhang, N.; Walberg, F. *Neuroscience* **1992**, *46*, 519-534.
124. Wu, J.; Sheng, R.; Liu, W.; Wang, P.; Zhang, H.; Ma, J. *Tetrahedron* **2012**, *68*, 5458-5463.
125. Xie, L.; Takeuchi, Y.; Cosentino, L. M.; McPhail, A. T.; Lee, K.-H. *J. Med. Chem.* **2001**, *44*, 664-671.
126. Hettie, K. S.; Glass, T. E. *Chem. Eur. J.* **2014**, in review.
127. (a) Frederickson, C. J. *Int. Rev. Neurobiol.* **1989**, *31*, 145-238; (b) Frederickson, C. J.; Suh, S. W.; Silva, D.; Frederickson, C. J.; Thompson, R. B. *J. Nutr.* **2000**, *130*, 1471S-1483S; (c) Frederickson, C. J.; Bush, A. I. *Biometals* **2001**, *14*, 353-366.
128. Bruns, D.; Riedel, D.; Klingauf, J.; Jahn, R. *Neuron* **2000**, *28*, 205-220.
129. Yang, Y.; Craig, T. J.; Chen, X.; Ciufu, L. F.; Takahashi, M.; Morgan, A.; Gillis, K. D. *J. Gen. Physiol.* **2007**, *129*, 233-244.
130. Moro, M. A.; Lopez, M. G.; Gandia, L.; Michelena, P.; Garcia, A. G. *Anal. Biochem.* **1990**, *185*, 243-248.
131. Liu, X.; Barizuddin, S.; Shin, W.; Mathai, C. J.; Gangopadhyay, S.; Gillis, K. D. *Anal. Chem.* **2011**, *83*, 2445-2451.
132. Defeng, Z.; Zhuoshu, L.; Jinghai, X. *Chinese. J. Chem. Eng.* **2000**, *8*, 366-373.

## VITA

Jessica Klockow was born and raised in Columbia, MO. She attended Rock Bridge High School where she amassed a myriad of interests. After graduation, she promptly began her undergraduate career at the University of Missouri – Columbia. She focused concurrently on language and sciences classes and in 2008, she graduated *magna cum laude* with a B.A. in Spanish

Subsequent enrollment in the chemistry graduate program at MU led to research in fluorescent chemical sensing under the direction of Dr. Timothy E. Glass. After years of blood, sweat, and synthesis, she obtained her doctorate in 2014 and went on to Stanford University to commence postdoctoral research. She desires to pursue a career in academia in order to inspire young scientists and conduct independent research.